HIGH-ENERGY SEDIMENTARY PROCESSES IN KLUANE LAKE, YUKON TERRITORY

by

Sarah Crookshanks

A thesis submitted to the Department of Geography

In conformity with the requirements for

the degree of Master of Science

Queen's University

Kingston, Ontario, Canada

(May, 2008)

Frontispiece: Kluane Lake and Slims River delta, July, 2007 (Photograph: S. Crookshanks).

Abstract

A lacustrine sedimentary process study was undertaken at Kluane Lake, which is a large, glacier-fed, alpine lake in the southwestern corner of Yukon Territory. Data from moored instruments, sediment traps, water column profiling, and high-resolution sub-bottom acoustic surveys were collected over the peak melt seasons of 2006 and 2007 in order to document the spatial and temporal lacustrine sedimentation patterns. A river monitoring station was also established to continuously record the inflow variations of Slims River, which drains meltwater from Kaskawulsh Glacier. Kluane Lake receives sediment-laden (up to 5 g l^{-1}) water from Slims River, which varies diurnally in terms of both discharge and suspended sediment concentration. While evidence of seasonal sediment exhaustion is present within the system, the diurnal hysteresis relationship between discharge and suspended sediment is either insignificant or more commonly counterclockwise. The high suspended sediment load delivered by Slims River produces continuous, diurnally fluctuating turbidity currents with maximum velocities in excess of 0.6 m s^{-1} at delta-proximal locations, although velocities between 0.2 and 0.4 m s^{-1} are more typical. During peak flow conditions, variations in current velocity can be traced to the deepest portion of the lake, over 4 km from the point of inflow. The longitudinal changes in the vertical concentration profiles, suspended sediment load, and mass accumulation rates suggest that the flow structure of the turbidity currents changes rapidly along the first several kilometres of flow. Sedimentation in the Kluane Lake basin is dominated by turbidity currents; overflows occur intermittently and contribute less than 2% to sediment accumulation along the lake bed. The highest rate of deposition occurs approximately 1 km from the delta and is consistent with an accumulation of approximately 0.4 m a^{-1}; closer to the delta, high current velocities appear to inhibit sediment deposition. The sediment in Kluane Lake is dominated by silt-size particles and contains virtually no sand except in small amounts very close to the delta. The diurnal pattern of

turbidity current activity produces daily rhythmites in sediment traps deployed near the lake bottom, but these laminations do not occur consistently over time or space.

Acknowledgements

First, I would like to thank Dr. Robert Gilbert. His commitment and passion for earth system science and specifically limnology have been a source of inspiration throughout the past few years. His thoughtful insights and constant encouragement have been instrumental to my academic growth and the development of this project in particular.

I would also like to acknowledge NSERC and the Northern Scientific Training Program who supplied funding for this project. The Arctic Institute of North America provided logistical assistance in the field. Without their support, this research would not have been possible.

The pleasures (and challenges) of field work were shared with Laura Duncanson and Tim Philpott, who were unfailingly cheerful and energetic no matter what the Yukon threw their way. Their willingness to get their hands dirty – literally and figuratively – is much appreciated.

Dr. Scott Lamoureux generously provided access to various pieces of equipment and lab space. Also, thanks to Dr. Ana da Silva and Andrew Binns for their assistance in operating the flume in the Civil Engineering Department. Mark Publicover was exceedingly helpful in various construction projects and Kathy Hoover, Joan Knox, Sheila MacDonald, and Sharon Mohammed cheerfully answered my various questions whenever I wandered into the departmental office.

Fellow geography graduate students have made the day-to-day both entertaining and enjoyable. Specifically, thanks to Dana McDonald and Paul Lewkowicz for the mid-day squash games and Suzanne Mills for the lunchtime runs; these activities cleared my head and were a welcome interruption to sitting at my computer. Kyle Hodder has provided invaluable guidance throughout my time here at Queen's. Many other students, including Krys Chutko, James Fletcher, Kasey Kathan, Claire Kaufman, Emil Laurin, and Jess Tomkins, have offered much-appreciated advice and many diversions.

Despite the distance, my family's support has been incredibly important to me over these past two years. The unconditional love and encouragement of my parents, Helen Irwin and Grant Crookshanks, have given me the confidence to believe in myself and what more could a daughter ask for? My sister, Rebecca, was always just a phone call away and her thoughtful advice and good humour have been a constant source of reassurance and laughter. Finally, thanks to Nick Grahn who has patiently listened to me talk about mud in lakes, provided a variety of welcome distractions, and fed me lots of apples.

I know that I am just a grain of sand
meeting water at the land
We could make our castles here
and sweep them all away
I know that I am just a drop of water
frozen into ice on the stormy earth
who gave us birth over and over
in cycles, lovely cycles

-T. Dekker (2005)

Table of Contents

List of Figures

List of Tables

List of Symbols

d	Flow thickness
D	Typical flow dimension
f_i	Friction coefficient from the fluid interface
f_o	Friction coefficient from the bed
fl	Falling limb
Fr	Froude number
Fr_d	Densiometric Froude number
g	Acceleration due to gravity
HI	Hysteresis index
MAR	Mass accumulation rate
PSD	Particle size distribution
Q	Discharge
R	Hydraulic radius
Re	Reynolds number
Ri	Richardson number
rl	Rising limb
SSC	Suspended sediment concentration
SSL	Suspended sediment load
u	Flow velocity
U	Average flow velocity
β	Slope angle
δρ	Density difference between the lake and the turbidity current
μ	Dynamic viscosity

ρ	Density
ρ_w	Density of the ambient water
υ	Kinematic viscosity
υ_s	Particle fall velocity constant

Chapter 1

Introduction

Lacustrine sedimentation is influenced by the interaction of a variety of physical, chemical, and biological processes characteristic of the lake itself as well as the surrounding regional environment. The delivery of material from the catchment is particularly significant for sedimentation in glacial lakes, because the large volume of glacially-derived sediment dominates the lacustrine environment (Sturm, 1979). Consequently, the regional hydroclimatology and catchment processes have considerable influence on the accumulation of sediment in a glacial lake. Of equal importance, however, are the processes that distribute the sediment once it enters the lake.

Past research on sedimentation in glacial lakes has emphasized the importance of lacustrine sedimentary records in paleoenvironmental reconstruction. Because lake sedimentation responds to various controlling factors, a wide range of environmental variables may be preserved in the sediment depending on the sensitivity of a particular lake. A lake serves as a sediment trap for its entire catchment; therefore, it ideally provides a continuous record of climatic and catchment conditions. Numerous studies have attempted to derive a direct relationship between climate and annual sediment accumulation in glacial lakes (e.g. Desloges, 1994; Leemann and Niessen, 1994; Lamoureux and Gilbert, 2004; Menounos et al., 2005). However, it is becoming increasingly accepted that in order to accurately interpret past environmental conditions from lacustrine sediment, the processes that control both the delivery of sediment to a lake basin and the distribution of sediment within that basin must be more fully understood. Hodder et al. (2007) argue that many of the processes that control the transfer of the hydroclimatic signal to a lacustrine varved record are non-linear in nature and may be part of a feedback system. By

simply bundling the catchment, lacustrine, and climatic processes into a "black box" and applying a linear regression, valuable hydroclimatic information may be lost. Other studies have also emphasized that process work is important to validate the use of lake sediment as a hydroclimatic proxy, particularly in regions where long-term climate data are not readily available (Bradley et al., 1996; Gilbert et al., 1997b; Lewis et al., 2002). Sediment delivery is influenced not only by external processes such as specific climatic controls, but also by physical lake processes. Temporally or spatially variable sedimentary processes can complicate paleoenvironmental interpretations or introduce uncertainty to the dating of annually resolved sediments (Stihler et al., 1992; Lamoureux, 1999; Francus et al., 2002; Lewis et al., 2002). An understanding of modern sedimentary processes allows more accurate and detailed interpretations of past environmental conditions to be derived from lacustrine sedimentary records.

This thesis further explores the sediment transfer processes in proglacial lakes, by presenting data collected from Kluane Lake, a large proglacial lake in Yukon Territory. Kluane Lake receives a large amount of sediment from Kaskawulsh Glacier, and consequently is a highly dynamic sedimentary environment. In a proglacial environment, the fluvial system releases a large volume of meltwater and glacially-eroded sediment into the prodelta area of a lake. This region forms the boundary between the fluvial and lacustrine systems; therefore, the processes that occur in this area are critical to the delivery of sediment to the wider lake basin. The prodelta system is highly complex because of the influence of both the river and lake environments, the components of which vary over multiple timescales.

The occurrence of turbidity currents throughout the peak melt season in Kluane Lake provides a unique opportunity to obtain direct measurements of mid-scale turbidity currents. The hydraulic complexity of turbidity currents, particularly those that form in response to large-scale, infrequent catastrophic events, are of great interest to many marine geologists because of the

association between turbidity currents and hydrocarbon reserves (Shanmugam and Moiola, 1985). However, direct measurements of marine turbidity currents are notoriously difficult to obtain because of their large scale and inaccessibility. While experimental and numerical models can successfully explain some aspects of turbidity current dynamics, the models are a simplified and idealized form of reality. As such, it has been suggested that further development in this field is dependent on the monitoring of mid-size turbidity currents in the natural environment (Middleton, 1993). Intermediate-scale lakes and fjords are analogous to deep-sea environments, yet allow sampling at a higher spatial resolution and present more manageable logistics (Gilbert and Crookshanks, in press).

Previous studies of lacustrine turbidity currents have generally measured flow characteristics at one or several points in the lake, employing limited spatial analysis (Gilbert, 1975; Lambert et al., 1976; Chikita and Okumara, 1990; Best et al., 2005). The most spatially-extensive study of turbidity currents in a glacilacustrine environment to date involved the deployment of an instrumentation network in a small, glacial lake in the Purcell Mountains of British Columbia (Weirich, 1986a). However, a similarly spatially-distributed and temporally-extensive study has yet to be attempted in a large, high-energy glacial lake environment. Flow velocities of turbidity currents in lakes typically vary on the order of several cm s^{-1} to several tens of cm s^{-1}, but can reach speeds in excess of 100 cm s^{-1} (Lambert et al., 1976; Weirich, 1986a). Because of the diurnal nature of glacial meltwater production, turbidity current activity often occurs periodically at approximately the same time every day (Gilbert, 1975; Weirich, 1986a); however, turbidity currents have been observed to flow continuously for several days in response to flood events in both glacial and non-glacial lakes (Gilbert, 1975; Lambert et al., 1976; Chikita and Okumura, 1990).

Turbidity currents are an important mechanism in the transfer of sediment to alpine lake basins. They carry large volumes of relatively coarse material along the lake bottom and form significant deposits that would not be otherwise found at deep, distal locations (Gilbert, 1975; Weirich, 1985; Weirich, 1986a; Desloges and Gilbert, 1994). Furthermore, because turbidity currents in lakes often form in response to high-density river inflow, they directly mediate the transfer of a hydroclimatic signal to the sedimentary record. Turbidity currents are, therefore, significant to the development of high-resolution lacustrine sedimentary records.

The primary objective of this study is to characterize the sedimentary processes within a large, dynamic proglacial lake during the peak melt season by:

1. evaluating how changes in river discharge and sediment transport affect the spatial and temporal patterns of sedimentation within the prodelta region;
2. obtaining direct measurements of lacustrine turbidity currents in order to document the flow behaviour of lacustrine turbidity currents in a natural environment; and
3. relating the observed sedimentary processes to the modern patterns of sedimentation.

Chapter 2

Literature Review

In order to understand the sedimentary environment in the delta-proximal region of a high-energy glacial lake, both the inputs to the system and lake processes must be considered, including: (i) the transfer of water and sediment from glacial to lacustrine environments by the proglacial fluvial system; (ii) the physical lake processes that influence the river inflow once it has entered the lake; (iii) the behaviour of turbidity currents; and (iv) the resulting patterns of sedimentation.

2.1 Proglacial fluvial hydrology and suspended sediment transport

Glaciers are effective physical weathering agents and produce large amounts of erodible debris. Because most of the fine sediment is eventually carried away from glaciers by meltwater, proglacial streams are often very turbid and export a high load of sediment away from ice margins. While the majority of the coarser sediment accumulates as fluvial and delta deposits, a large volume of fine sediment is maintained in suspension by the turbulent nature of the flow and thus transported the length of the river to be deposited in lacustrine or marine basins. The variations of discharge and sediment concentration in a proglacial fluvial system require interannual, seasonal, diurnal, and sub-diurnal scales of analysis in order to fully understand the temporal complexity of sediment delivery to glacial lakes.

2.1.1 Discharge

Discharge in glacial streams is highly seasonal because of its dependence on the annual pattern of snow and ice melt. The annual hydrograph from a typical mid-latitude alpine glacier exhibits a nival peak, followed by a late-summer maximum in discharge associated with high

glacier melt. During the breakup period in early spring, snow at the surface begins to melt, but most of the water refreezes within the snowpack. The nival period occurs once a large interconnected system of drainage establishes along the proglacial system, thereby allowing the release of the stored meltwater at flows in excess of the daily melt rate. Because ice has a lower albedo than snow, melt production per unit of solar energy is enhanced during the late summer when the snow cover has melted and the ice surface is exposed. During this time, the melting rate and discharge are more closely related to each other with fewer anomalous high discharge events and less delay between meltwater production and discharge (Smith, 1985). Freezeback in autumn marks the end of glacial meltwater production; however, some water may continue to flow as the glacial channels drain and the groundwater table drops. At higher latitudes, the lower air temperatures and lower annual radiation receipt cause a shorter melt season and reduced annual runoff variability. Glacial runoff also exhibits considerable interannual variability because of changes in climate and glacier hydrology (Willis, 2005).

The diurnal discharge pattern is typically highly periodic for glacial systems, because of the changing melt production over the course of the daily cycle of solar radiant energy. At a glacier proximal location, the meltwater flow is characteristically low in the morning, increases suddenly in the late afternoon or early evening, after which it gradually declines through the night. However, some larger glacial systems with more complex drainage systems exhibit a subdued diurnal signal, and in some cases in southeast Alaska no diurnal variations whatsoever are detected (Boothroyd and Ashley, 1975; Gustavson, 1975).

The nature of the diurnal hydrograph changes both temporally and spatially. The diurnal pattern is most distinct in late summer when glacial meltwater contributes the largest proportion of the flow. Early in the melt season when the snowpack slows and partially reabsorbs the meltwater throughflow, the diurnal flow pattern has a reduced amplitude and peaks at a later time

(Clifford et al., 1995). The nature of the diurnal discharge cycle is also a function of the location within the drainage basin; as the monitoring distance from the glacier terminus increases, the hydrograph has a dampened amplitude and lagged peak discharge (Smith, 1985).

Because snow and ice melt is weather dependent, discharge is also closely linked to variations in local weather conditions. Sunny periods are associated with high meltwater production, particularly in late summer when low albedo ice is exposed over most of the glacier. Rainfall has varying effects on the discharge depending on its duration, intensity, distribution, the air temperature, and time of year (Smith, 1985). In rainfall-dominated systems in coastal Alaska, precipitation-induced discharge peaks are very common in the late summer when the drainage pathways through the glacier are open and the glacier surface is bare (Gustavson and Boothroyd, 1987). At other sites, however, rainy periods, which are associated with cloud cover and lower air temperature, result in lower discharge levels (Hammer and Smith, 1983; Röthlisberger and Lang, 1987; Sawada and Johnson, 2000).

An anomalous discharge event may occur when a volume of water that is stored within or near the glacier suddenly drains. This meltwater outburst can trigger large flood events, termed jökulhlaups (Icelandic for glacier burst), and transport extremely high sediment loads of often coarse particles (Willis, 2005). Ice-marginal lakes, crevasse ponds, englacial or subglacial water-filled cavities, slush ponds, or dammed stream channels may all serve as sources of water for these flood events.

Non-stationarity in discharge is observed not only between diurnal cycles, but also at a subdiurnal time-scale. Small-scale fluctuations in discharge have been attributed to the tapping of water storage reservoirs by englacial flow within the glacier (Fahnestock, 1963; Röthlisberger and Lang, 1987). Minor discharge variations have also been explained by water surges created by the collapse of ice cliffs and transient ice and slush dams near the glacial terminus (e.g.

Church and Gilbert, 1975; Ballantyne and McCann, 1980; Russell et al., 1995; Stott and Grove, 2001). Other possible mechanisms for subdiurnal discharge fluctuations include the temporary blockage of subglacial conduits (Warburton and Fenn, 1994) and diurnal changes in the channelized englacial or subglacial reservoirs (Collins, 1979; Clifford et al., 1995; Willis et al., 1996). Recent technological advances in instrumentation have allowed the measurement of high-frequency variations in velocity. For example, Clifford et al. (1995) measured high-frequency velocity fluctuations with a periodicity of less than 10 seconds, which is similar to the characteristics of fluid turbulence.

2.1.2 Suspended sediment transport

In proglacial streams, the suspended sediment concentration (SSC) is usually very high, ranging between 0.2 – 10 kg m^{-3}, and varies over multiple time scales (Gurnell, 1987). A river at high discharge typically carries sediment in higher concentrations than at low discharge; therefore, the suspended sediment concentration (SSC) patterns would be expected to reflect the seasonal, diurnal, and sub-diurnal variations in discharge. While this behaviour is generally observed, additional variables such as hysteresis, sediment supply, rainfall patterns, local hydrology, and recent discharge history tend to complicate the sediment response to changes in flow.

Since the transport of suspended sediment depends on the flow velocity, suspended sediment rating curves (SSC versus water discharge) have been historically used to predict the sediment yield from a basin (e.g. Collins, 1979); however, the exact relationship between SSC and discharge is often more complex, which leads to large scatter and a weak correlation in suspended sediment rating curves (Østrem, 1975; Collins, 1979; Bogen, 1980; Klein, 1984; Richards, 1984; Williams, 1989; Hodgkins, 1996). Østrem (1975) concludes that valid curves may be established for sub-periods within a season, but that "the relationship between discharge

and transport is changing more or less continuously during a runoff season and from year to year."

The effect of hysteresis on suspended sediment transport has been discussed in great detail. When plotted in time sequence, the discharge-suspended sediment curve for glacial systems most often shows a diurnal clockwise hysteresis loop, in which the suspended sediment concentration at a given discharge is greater for the rising hydrograph limb (Østrem, 1975; Collins, 1979; Bogen, 1980; Willis et al., 1996; Hodgkins, 1999). The shape of a hysteresis curve may be discussed in terms of both sediment supply and sediment source area, but in proglacial rivers, hysteresis is more often explained through sediment exhaustion effects. For example, a typical interpretation of clockwise hysteresis in a proglacial river involves sediment deposition during low flow because of loss of competence. During the following period of increasing discharge, the sediment is remobilized and subsequently exhausted, leading to hysteresis (Church, 1972; Collins, 1979; Bogen, 1980; Willis, 1996). The suspended sediment concentration at any given time, therefore, is a function of not only the existing hydrological conditions, but also the recent discharge history of the stream and the prevalence of sediment exhaustion. In non-glacial fluvial systems, the shape of the hysteresis curve is also commonly explained with reference to the location of the sediment source area. If the sediment is farther from the main channel or has a greater travelling time, the sediment pulse is relatively more important later in the discharge event and counterclockwise hysteresis may dominate the system (Fig. 2.1; Williams, 1989).

The weak correlation between SSC and discharge can be explained by hysteresis that occurs over not only diurnal time scales, but also longer time periods, such as an ablation season. Early season flushing typically releases a larger amount of suspended sediment than expected, whereas late season sediment exhaustion effects are commonly observed (Nanson, 1974; Østrem, 1975; Hammer and Smith, 1983; Fenn et al., 1985). As such, a discharge event that occurs early

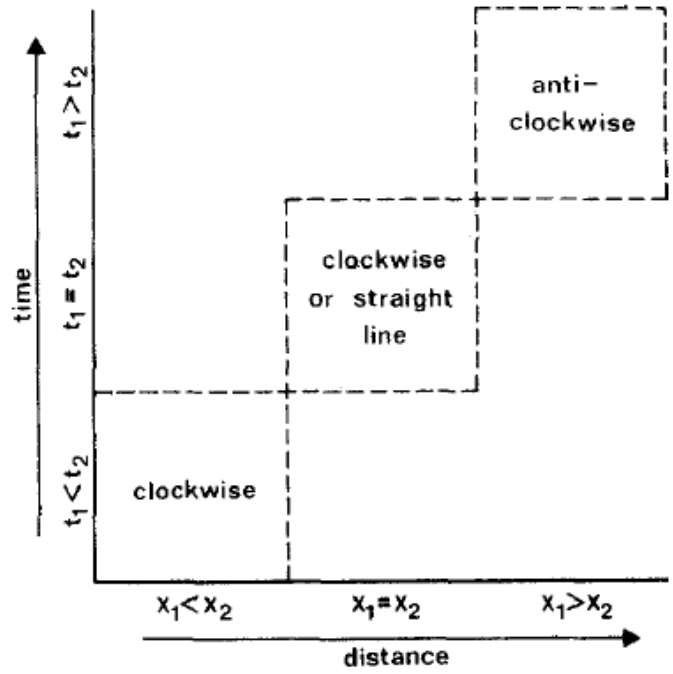

Figure 2.1 The hysteresis shape for the Q-SSC relationship as a function of travelling time and distance from the source areas, where x_1 is the distance from the centre of gravity of the sediment source area to the basin outlet, x_2 is the distance from the centre of gravity of the water contributing area to basin outlet, t_1 is the travelling time from the centre of gravity of the sediment source area to basin outlet, and t_2 is the time from the centre of gravity of water contributing area to basin outlet (source: Klein, 1984).

in the melt season will generally be associated with a higher SSC than an equal discharge event later in the year.

In addition to hysteresis, variations in local sediment supply and precipitation events also contribute to scatter on sediment rating curves. An increase in local sediment supply in the proglacial zone in response to mass movement events, channel marginal events, or bank collapses have been found to increase SSC independently from a change in discharge (Lliboutry et al., 1977; Hammer and Smith, 1983; Richards, 1984; Gurnell and Warburton, 1990). Many studies

have also suggested that subglacial sediment evacuation may be an important control on sediment availability in proglacial streams (e.g. Østrem, 1975; Bogen, 1980; Thayyen et al., 1999; Bogen and Bonsnes, 2003). However, subglacial processes have been only recently directly linked to sediment transport dynamics. In a study of sub-seasonal variations in suspended sediment transport at Haut Glacier d'Arolla, Switzerland, Swift et al. (2005) document variations in the efficiency of subglacial sediment evacuation in response to changes in the structure of the subglacial drainage system. This variability, in turn, changes the proglacial sediment supply over the course of a melt season. Rainfall events that vary in duration and intensity are also thought to change the relationship between discharge and SSC (Church, 1972; Richards, 1984).

Glacial meltwater outbursts, or jökulhlaups, have been found to transport sediment at higher concentrations than what may be predicted from a suspended sediment rating curve. Very few SSC records exist for meltwater outbursts because of the rare and unpredictable nature of these events. One measurement record at the Tsidjiore Nouve glacier in the Alps showed that two outburst events in 1981 accounted for over 50% of the suspended sediment transport and only 20% of the discharge volume over just 15% of the 3-month monitoring period (Beecroft, 1983; Gurnell, 1987).

High-frequency variations in suspended sediment concentration form a substantial component of the overall sediment transport regime, which highlights the importance of continuous, or at least frequent, monitoring of suspended sediment (Østrem, 1975; Bogen, 1980). For example, a study at the Glacier de Tsidjoire Nouve and Bas Glacier d'Arolla in Switzerland, found that high-frequency, short-duration flushes of SSC contributed 36% and 47% of the total sediment load respectively (Gurnell and Warburton, 1990).

Despite its importance, not much is known about the patterns or mechanisms of high-frequency variation in suspended sediment. Since the main control on SSC is discharge, many

short-term SSC variations are associated with small-scale changes in discharge (Stott and Grove, 2001). Bogen (1980) explains microfluctuations in SSC by the temporary patchy deposition of sediment in rivers shortly followed by erosion at a higher discharge. This process results in multiple sediment "clouds" flowing downstream and appearing as irregular fluctuations at a fixed monitoring station. Clifford et al. (1995) identified multiple scales of subdiurnal SSC cycles with periodicities of 10-20 minutes, 2-5 minutes, and < 1 minute. The longer "pseudo-periodic" fluctuations were associated with channel bank and bed migration, whereas the high-frequency variations were attributed to turbulent velocity fluctuations.

Proglacial fluvial storage and release of suspended sediment are important controls on the transfer of sediment from glacial to lacustrine environments. In a study of the Small River Glacier basin in the Canadian Rockies, up to 80% of the sediment load is derived from the proglacial area, not from contemporary glacial erosion (Orwin and Smart, 2004). Others have found that sediment eroded from the proglacial zone comprises 16 – 50% of the sediment load, and up to 95% during large-magnitude flood events (Maizels, 1979; Hammer and Smith, 1983; Warburton, 1990).

Sediment storage in a proglacial fluvial environment is thought to be primarily controlled by the runoff regime during a given year. Episodic periods of high meltwater discharge have been found to be the dominant control on the release of sediment from proglacial storage, transporting sediment loads comprised of up to 95% of formerly proglacially stored sediment (Warburton, 1990; Hodgkins et al., 2003). Depending on the hydrological regime, the proglacial area can function as both a source and a sink of sediment during a particular melt season or period within a melt season (Hodgkins et al., 2003).

2.2 Lacustrine physical processes

While lakes do not exhibit the dynamic variability of rivers, the seasonal and diurnal changes in the physical lake environment are also important in determining the sedimentation patterns.

2.2.1 Thermal stratification

Glacier-fed lakes are commonly dimictic; thermal stratification is present during the summer, bounded by periods of overturn in early spring and late fall. In summer, solar heating and wind-induced mixing of the surface water result in a characteristic stable temperature distribution with depth. This thermal structure is often complicated by variations in wind strength and direction, solar radiation, inflowing water, precipitation, chemical stratification, and morphology, which can result in complex spatial and temporal thermal variations within a lake.

2.2.2 Inflow behaviour

As a river enters a lake, the flow undergoes 2 or 3-dimensional expansion, turbulent mixing, and an exponential lakeward decrease in velocity. The primary control on the behaviour of this plume is the density difference between the river inflow and lake water and the vertical density profile in the lake (Smith and Ashley, 1985). Water density is a function of suspended sediment concentration, temperature, and dissolved ion concentration. Suspended sediment concentration is generally the most important factor in determining the density of glacial streams, because it varies more rapidly and over a wider range than the other variables.

Three spatial patterns of inflow-lake interactions are generally observed in glacial lakes: overflows, interflows, and underflows. An overflow occurs when the inflowing water is less dense than the ambient lake water, whereas an underflow occurs when the inflowing water is

denser than the lake water. If the lake is stratified, an interflow may occur where the inflowing water is less dense than the bottom water, yet denser than the surface water.

In proglacial lakes, overflows are generally considered to be the most insignificant of the three inflow processes because of the high sediment production rates of glaciers (Smith and Ashley, 1985). They are usually observed during times of low sediment input when thermal properties control the density difference between the two water masses (Sturm and Matter, 1978; Pickrill and Irwin, 1982). Currents created by wind or inflow are important in influencing the behaviour of overflow patterns (Gilbert, 1975).

When interflows or underflows occur, the diffusing river plume proceeds only slightly beyond the top of the foreset beds of the delta to a position called the plunge line, where it sinks until the density of the inflowing water equals that of the lake water and proceeds as an interflow or, in the case of high-density water, continues as an underflow. The turbulence at the margins of the sinking plume entrains ambient water, causing further flow expansion as well as inducing a shoreward surface current to replace the entrained water. A distinct contact line between turbid inflow and lake water forms where the reverse surface current meets the plunging inflow.

Interflows are the dominant inflow process occurring in certain glacial lakes with low fine-sediment input (Smith, 1978; Pharo and Carmack, 1979). In thermally stratified proglacial lakes with a high sediment input, periods of interflow often alternate on diurnal or seasonal time-scales with underflows (Gilbert, 1975; Gustavson, 1975; Sturm and Matter, 1978; Pickrill and Irwin, 1982). The Coriolis effect causes interflows and overflows to bend to the right and flow along the right-hand shoreline in the northern hemisphere (Hamblin and Carmack, 1978; Smith, 1978; Sturm and Matter, 1978; Pharo and Carmack, 1979; Pickrill and Irwin, 1983).

Underflows are widely recognized as the principal mechanism of sediment distribution in proglacial lakes (Smith and Ashley, 1985). Also known as turbidity currents, density currents or

hyperpycnal flows, turbid underflows can be generated in glacial lakes by either high-density river inflow or subaqueous slope failure. River-inflow generated underflows can be distinguished by their quasi-continuous nature (Smith and Ashley, 1985), correlation with river discharge variations (Pharo and Carmack, 1979), and temperature deviations associated with the initial river water temperature (Gilbert, 1975). Underflows tend to occur when thermal stratification is weak (Pharo and Carmack, 1979) or when the suspended sediment concentration of the inflowing water is particularly high (Gilbert, 1975). Even for lakes in which they are rare, underflows may still deliver the largest volume of sediment to the basin because of their tendency to form during times of high sediment input (Smith and Ashley, 1985).

2.2.3 Delta control on sediment delivery

Since deltas form at the boundary between fluvial and lacustrine environments, they are an important control on sediment delivery to the deeper lake environment. Where a river enters a body of standing water, the slope of the water surface decreases to the slope of the lake at some distance from the point of inflow. The shape of this slope, termed the backwater surface, is a function of the total energy relation of the river and is quantified by the derivative of the Bernoulli equation (Henderson, 1966). As the water slope decreases, the depth of the flow increases to a value greater than what is associated with uniform flow, resulting in an overall decrease in flow velocity. Additional flow expansion in a lateral direction compounds the flow deceleration. Deposition of the coarser sediment, including much of the bedload, occurs along the length of the backwater surface, reaching a maximum at the break in slope (Church and Gilbert, 1975). Some fine sediment may be deposited in the delta region, but a large portion is transported in suspension into the basin. Sediment distribution over the delta front occurs through avalanching, suspension fallout, underflowing river water, and gravity induced

deformation. Once deposited, sediment may be redistributed along the shallow delta front shoreline by wave action and wind currents.

2.2.4 Wind and currents

The movement of water in lakes is primarily caused by the wind. Wind-induced water circulation is difficult to model because of the geometrical complexity of lake basins as well as the stochastic variations in wind strength and direction (Csanady, 1978). In the simplest case, wind stress is applied in a spatially uniform manner to a closed lake basin with homogenous water. In this situation, closed topographic gyres are created, where the upwind streamlines follow the deepest water and the downwind streamlines are found in the two shore zones. If a steady wind blows over a lake, a setup of the lake's surface occurs, where the downwind end is higher than the upwind end. When the wind stops, lake level oscillations, known as seiches, are produced. In reality, however, spatial variations in water density (e.g. thermal stratification), complex lake morphometry, and variations in wind character significantly affect the pattern of water currents. In the case of a simple set-up, currents in the epilimnion cause a set-up along the thermocline in the opposite direction, which leads to the development of internal seiche unrelated to the surface seiche. The Coriolis effect is also important to lake circulation, particularly with respect to internal waves. If the Coriolis effect is balanced by the force of gravity, then a standing wave, referred to as a Kelvin wave, rotates around the basin along the thermocline and contributes to significant mixing, which has implications for the distribution of energy and particulates within the water column.

2.3 Turbidity current dynamics

Turbidity currents are particle-laden underflows that travel along the lake or ocean bed. They deliver a significant volume of relatively coarse sediment to alpine lake basins; therefore, in order to understand the sedimentation patterns within such lakes, the dynamics of turbidity current flow must first be understood. Since turbidity currents involve the transport of water and sediment, they can be classified as both fluid and sediment gravity flows. In a fluid context, turbidity currents are considered to be stratified gravity currents (or density currents) in which flow takes place above, below, or between the ambient fluid(s) because of the minor difference in unit weight between the two water masses (Middleton, 1993). Stratified flows can result from differences in density because of temperature, salinity, or composition. In a sedimentary context, turbidity currents are classified as a type of sediment gravity flow in which the sediment is held in suspension primarily by fluid turbulence, and thus cannot exceed a flow concentration of 9% by volume (Bagnold, 1962; Kneller and Buckee, 2000).

2.3.1 Mechanisms and environments of formation

In the lacustrine environment, turbidity currents most often form in response to high-density river inflow and sediment slumping on an oversteepened subaqueous slope (Smith and Ashley, 1985), whereas in the ocean, the suspended sediment concentration of river water is only rarely large enough for the inflow density to exceed that of seawater (Wright et al., 1988). Surging turbidity currents that form in response to subaqueous slumping or other rapid disturbance situations are short-lived, episodic, and unsteady, whereas turbidity currents that form in response to high density river inflow can flow for hours or sometimes days at a time and are consequently often described as quasi-continuous (Smith and Ashley, 1985).

2.3.2 Hydraulics

The early studies of the mechanics of turbidity currents employed parametric models that relied on geometric or statistical methods (e.g. Middleton, 1966a, 1966b). As the understanding of flow mechanics improved, complex process-based models derived from first-principles have become increasingly important (e.g. Parker et al., 1987; Akiyama and Fukushima, 1985; Zeng and Lowe, 1997). However, no one model accurately describes the full range of turbidity current flow processes and sediment deposition. The consideration of the results of several numerical models is, therefore, important in gaining an understanding of fluid and sediment motion in turbidity currents.

2.3.2.1 Flow parameterization

Gravity flows theoretically exhibit both laminar and turbulent flow regimes. The transition from laminar to turbulent flow is delineated by the Reynolds number (Re), which is a dimensionless number proportional to the ratio of the inertial forces to the viscous forces. The transition between flow regimes in turbidity currents occurs at $2000 < \mathrm{Re} < 3000$ (Liu and Mei, 1990). The Reynolds number is given by the relationship:

$$\mathrm{Re} = \frac{\rho UD}{\mu} = \frac{UD}{\upsilon} \tag{2.1}$$

where D is a typical flow dimension, U is the average flow velocity, μ is the dynamic viscosity, and υ is the kinematic viscosity. Laminar flow occurs very rarely in nature and never in the main flow of natural turbidity currents, because turbulent flow is, by definition, the mechanism by which the sediment is suspended in the fluid. The Reynolds number is additionally employed as a measure of the magnitude of flow, since it accounts for both the flow dimensions and velocity of the current.

The Froude number (Fr) can also be used for scaling turbidity current flows, but it is more commonly used to define supercritical (Fr > 1) and subcritical (Fr < 1) flow. The densiometric Froude number (Fr_d) is a dimensionless number proportional to the square root of the ratio of inertial to reduced gravity forces and is given by the expression:

$$Fr_d = \frac{U}{\sqrt{\left(\frac{\delta\rho}{\rho}\right)gD}} \tag{2.2}$$

where U is the average flow velocity, D is a typical flow dimension such as flow thickness, g is the acceleration because of gravity, δρ is the density difference between the lake and the turbidity current, and ρ is the density of the ambient water.

2.3.2.2 Flow structure

A turbidity current is often described as being composed of a front or head advancing into an ambient fluid, followed by the main body of the current. The governing hydraulic equations for the head are considerably different from those for the main body, because the head must displace the ambient fluid, which significantly changes its flow dynamics. While the flow of the body is often assumed to be steady and quasi-uniform, the flow of the head is highly unsteady and non-uniform (Graf, 1998). Because lacustrine turbidity currents in glacial lakes more commonly form in response to quasi-continuous high-density inflow, the flow dynamics of the head are not as important and will not be fully discussed here.

The vertical concentration structure of turbidity currents is a critical factor in understanding flow and sediment dynamics. Because limited data are available from natural turbidity current systems, existing models are largely derived from theoretical and experimental understanding. Two-layer models, which are based on visual observations, subdivide a flow into a dense lower part and an overlying, low-concentration plume (Middleton, 1969, 1993; Mulder et

al., 1997). These concentration profiles describe a near-uniform concentration in the lower layer, which is divided from the upper layer by a major inflection point (Fig. 2.2a). The models conventionally define the height of a turbidity current as the height from the bed to the inflection point of the vertical sediment concentration profile (Middleton, 1993). However, measurements of experimental currents indicate that the sediment concentration typically continuously decreases with height for equilibrium subcritical flows, supercritical currents on low slopes, and weakly depositional subcritical flows (Fig. 2.2b; Garcia, 1994; Altinakar et al., 1996; Peakall et al., 2000). In some cases, a prominent step in the vertical concentration profile is observed, which is associated with purely erosional currents and/or currents with a high rate fluid entrainment (i.e. flows along steep slopes; Fig. 2.2c; Garcia, 1993; Garcia and Parker, 1993). The vertical concentration profile also exhibits significant stratification in terms of grain size. Fine-grained material is typically more uniformly distributed, whereas coarse-grained material is more concentrated near the bed (Fig. 2.2d; Garcia, 1994).

The turbidity current may be divided into inner and outer regions by the level above the bed at which the velocity reaches a maximum (Fig. 2.3). In the inner region, turbulence is created by the bed, whereas in the outer region, turbulence is created by the friction and entrainment of the ambient fluid (Graf, 1998). The height of the velocity maximum is a function of the ratio of the drag forces at the upper and lower boundaries (Middleton, 1966b) and in many experimental currents, has been found to occur at 0.2 to 0.3 of the height of the current (Altinakar et al., 1996, Kneller et al., 1999).

2.3.2.3 Uniform flow of the body

The steady, uniform flow of the body can be modeled using a simple Chézy type law for open channel-flow with an additional factor to quantify the frictional resistance at the upper fluid

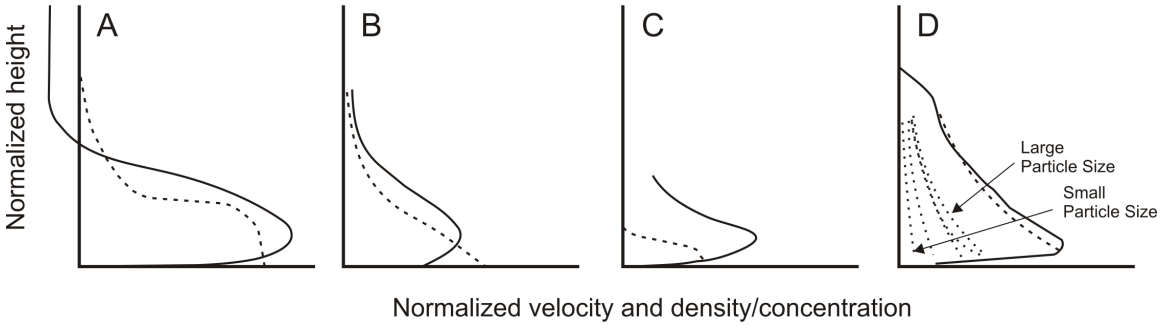

Figure 2.2 Schematic diagrams showing various characteristic density or concentration profiles (dashed lines) and velocity profiles (solid lines) in gravity currents: (A) a two-layer model type concentration profile; (B) a smooth profile, characteristic of weakly depositional flows; (C) A stepped concentration profile observed in erosional flows; (D) a Rouse-type vertical distribution of sediment grain-sizes (modified from Kneller and Buckee, 2000).

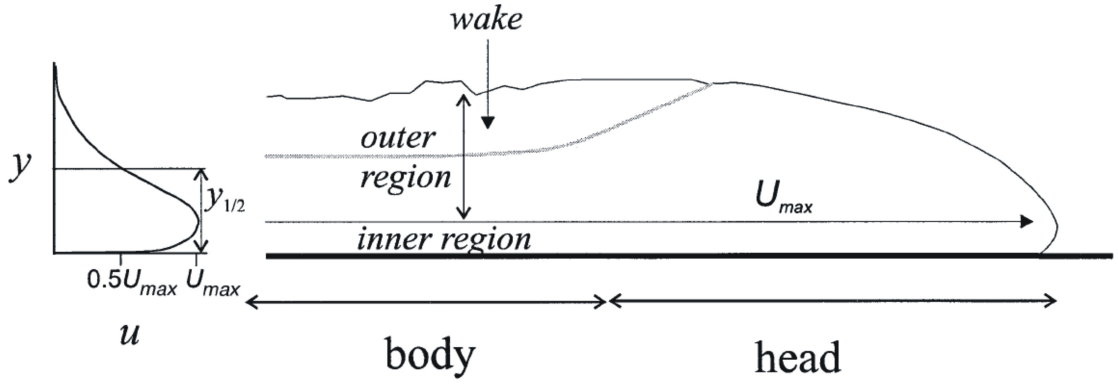

Figure 2.3 The vertical structure of the head and body of a turbidity current, where y is the height from the bed and u is the velocity (source: Kneller and Buckee 2000).

interface. The average velocity (U) of a uniformly flowing turbidity current is given by (Middleton, 1966b):

$$U = \sqrt{\frac{8g\frac{\delta\rho}{\rho}}{f_i + f_o} R\beta} \tag{2.3}$$

where g is the acceleration because of gravity, $\delta\rho$ is the density difference between the lake and the turbidity current, ρ is the density of the lake water, R is the hydraulic radius, β is the bottom slope, and f_i and f_o are the Darcy-Weisbach friction coefficients at the upper and lower boundaries of the current, respectively.

Bed friction (f_o) is related to Re where the bed is smooth and can be estimated using the Moody diagram for rough channels (Middleton, 1966b). The quantification of friction at the fluid interface (f_i), however, is much more difficult and is a function of the densiometric Froude number (Middleton, 1966b). If $Fr_d < 1$, there will be relatively little mixing and thus a low value of f_i; however, as Fr_d increases above 1, the frictional resistance at the fluid interface also increases. Middleton (1966b) found that f_i may be predicted only semi-quantitatively.

2.3.2.4 Fluid entrainment and mixing

Entrainment of the ambient fluid into a turbidity current is a major control on the evolution of the suspended sediment concentration. Fluid entrainment essentially occurs because of the Bernoulli equation; the static pressure in the motionless ambient fluid is larger than the pressure of the moving current. The resultant pressure gradient between the two fluid masses causes fluid penetration from the ambient fluid into the turbidity current. The Froude number is known to be an important control on fluid interface stability and thus water entrainment (Ellison and Turner, 1959). While less mixing occurs along the body of a turbidity current relative to the head, Ellison and Turner (1959) observed large irregular eddies at the upper boundary of the body

of experimental currents. Internal gravity waves can also form along the stable fluid interface, when the flow is turbulent and the velocity is large compared to the kinematic viscosity (Turner, 1973). Because of the occurrence of continuous water entrainment along the length of the turbidity current, theoretical models require that the flow volume progressively increases in the downslope direction (Komar, 1973; Stacey and Bowen, 1988; Dade et al., 1994). The suspended sediment concentration, therefore, becomes progressively diluted in the downflow direction, reducing the density difference and thus the flow velocity.

2.3.2.5 Sediment dynamics

Suspended sediment dynamics within a turbidity current is difficult to parameterize, because of the highly complex feedback process between turbulence and suspended sediment (Kneller and Buckee, 2000). The sediment changes the turbulent structure of the flow and the turbulent structure is important in determining the rate of fluid mixing at the upper fluid interface as well as the vertical distribution of velocity and sediment. These factors are in turn responsible for changing the concentration of sediment via erosion or deposition at the bed and dilution of the current through the incorporation of ambient fluid into the flow. The suspended sediment concentration affects the flow properties of a current in several ways. A higher suspended sediment concentration increases a) the effective flow density and thus the driving force of fluid motion, and b) the apparent flow viscosity, which increases the resistance to flow and sediment motion (Zeng and Lowe, 1997).

Bagnold (1962) was the first to propose the condition of autosuspension, in which the magnitude of gravitational energy acting on the turbidity current is just sufficient to sustain the turbulence necessary to keep the sediment in suspension and to overcome friction at the upper and lower interface. Because the suspended sediment provides the gravitational energy that drives the flow of a turbidity current, the suspended sediment in effect creates the turbulence that

is responsible its own suspension (i.e. autosuspension). The relationship derived from a simple energy balance was found to be (Bagnold, 1962):

$$\frac{v_s}{U} \leq \sin\beta \tag{2.4}$$

where v_s is the constant fall velocity of the particles, U the mean transport velocity of the particles that is approximated by the mean flow velocity, and β is the slope angle. If the slope exceeds v_s/U, then the excess gravitational force is able to overcome the friction at the bed. An efficiency coefficient is often added to the downslope velocity term, in order to account for vertical variations in the turbidity current's velocity and concentration (e.g. Stacey and Bowen, 1990).

2.3.3 Direct measurements of lacustrine turbidity currents

Turbidity currents have been detected in glacier-fed lakes using a variety of indirect and direct methods. The inflowing river water is often warmer than the ambient lake water, yet its high sediment concentration causes it to plunge to the lake bottom and flow along the lake bottom. Because this water is both warmer and contains more sediment than the overlying water, the underflow can be detected by both temperature sensors (Gilbert, 1975; Lambert and Giovanoli, 1988; Lewis et al., 2002) and transmissivity probes (Weirich, 1986a; Gilbert and Butler, 2004). Flow velocities of lacustrine turbidity currents have been measured using current meters and typically vary on the order of several cm s^{-1} to several tens of cm s^{-1}, although velocities exceeding 100 cm s^{-1} have been reported on occasion (Table 2.1).

Underflows in lakes may flow essentially continuously for extended periods, sometimes up to days at a time, in response to high river discharges (Gilbert and Shaw, 1981; Lambert et al., 1976; Lewis et al., 2002). Because of the diurnal nature of glacial discharge patterns, it is very common to see turbidity current activity occurring for several hours at approximately the same time every day during the period of peak water inflow (Weirich, 1984). High discharge in

Table 2.1 Velocity measurements of turbidity currents in lakes

Location	Maximum Velocity (cm s^{-1})	Comments	Reference
Lake Malaspina, Alaska	18	• SSC = 1.55 g l^{-1}	Gustavson (1975)
Walensee, Switzerland	30	• Pulsating flow • Current direction reversals	Lambert et al. (1976)
Lake Superior, Ontario	58	• Human induced currents • Pulsating flow • Hydraulic jump inferred • Estimated SSC = 1.01 g l^{-1}	Normark and Dickson (1976)
Peyto Lake, Alberta	13		Vendl (1978)
Walensee, Switzerland	60		Lambert and Hsü (1979)
Sunwapta Lake, British Columbia	32	• SSC > 1.4 g l^{-1}	Gilbert and Shaw (1981)
Lake Constance, Switzerland	120		Lambert (1982)
Small alpine lake, Purcell Mountains, British Columbia	110	• Possibly still influenced by river inflow	Weirich (1986a)
Lake Geneva, Switzerland	>50		Lambert and Giovanoli (1988)
Katsurazawa Reservoir, Japan	31	• SSC = 0.4 g l^{-1}	Chikita and Okumara (1990)
Bear Lake, Devon Island, Nunavut	20		Lewis et al. (2002)
Meziadin Lake, British Columbia	5-10	• Velocity calculated after Middleton (1966b) • SSC = 0.75 g l^{-1}	Gilbert and Butler (2004)
Lillooet Lake, British Columbia	58	• Pulsating flow	Best et al. (2005)

response to storm-induced flooding (Lambert et al., 1976) or spring meltwater runoff (Chikita and Okumara, 1990) has also been found to follow a diurnal pattern over short time periods.

Turbidity currents of shorter duration have been documented in glacial lakes independent of an increase in river discharge and are thought to be a response to a sudden input of sediment to the stream or slumping on the delta front (Gilbert, 1975; Gilbert and Shaw, 1981; Weirich, 1986b).

Since turbidity currents have been compared to underwater rivers, some studies have suggested that unconfined turbidity currents may meander like their subaerial counterparts. While several field observations suggest that meandering may occur, this behaviour has been verified in neither the natural environment nor the laboratory. Gilbert and Shaw (1981) recorded several flow interruptions on the order of 10 minutes in length during a turbidity current event in Sunwapta Lake, which were hypothesized to be caused by the current temporarily shifting away from the location of the meters. In Walensee, Switzerland, low-velocity (< 5 cm s^{-1}) turbidity currents also exhibited periodic changes in current direction from westward to eastward (Lambert et al., 1976).

Several records document rapid underflow velocity fluctuations that do not correspond to variations in the river discharge. Weirich (1986a) measured pulsations with a frequency of 3 to 6 cycles per minute in turbidity currents in a small glacial lake. Longer pulsations were observed in underflows in Walensee, Switzerland with a period ranging from 15 to 20 minutes (Lambert et al. 1976). The velocity changes were asymmetrical, increasing rapidly to a maximum, followed by a gradual decrease. Anthropogenic turbidity currents in Lake Superior were found to exhibit velocity fluctuations with a period of 1 to 2.5 hours, as well as short-term velocity oscillations with a 6.5-minute period (Normark and Dickson, 1976). More recently, Best et al. (2005) used an acoustic Doppler profiler in Lillooet Lake to observe pulsing velocity flow independent of river inflow or wave effects with the most distinct periods between 4 and 8 minutes.

The cause of these pulsations is not known, but several theories have been proposed. Both rapid pulsations (3 to 6 per minute) as well as longer pulsations (15 to 20-minute period) have been suggested to occur because of supercritical flow conditions (Lambert et al., 1976; Weirich, 1986a). However, underflows in Lake Superior and Lillooet Lake were calculated to be subcritical during the period of pulsations. In Lake Superior, the weight of rapid sedimentation

on the steep delta slope was hypothesized to cause repacking and the periodic expulsion of pore water and fine particles, which would subsequently lead to irregular increases in flow density and thus current velocity (Normark and Dickson, 1976). It was also proposed that the current meters were located near the upper edge of the flow, and therefore measured the passage of an irregular upper flow surface. Best et al. (2005) explain the pulsations in Lillooet Lake by the lateral and longitudinal movement of the sediment-laden inflow, which is hypothesized to cause spatial variations in the turbidity current flow pattern.

2.3.4 Hydraulic jumps

Hydraulic jumps in turbidity currents have been reproduced experimentally (e.g. Garcia and Parker, 1989) and inferred from the marine geologic record (e.g. Komar, 1971). A hydraulic jump involves the transition from swift and shallow supercritical flow ($Fr > 1$) to slow and deep subcritical flow ($Fr < 1$) (Fig. 2.4). The deceleration and thickening of the flow at a hydraulic jump sets up a gravitationally unstable surface; therefore, the thicker flow tries to move down the interface slope in the opposite direction of the main current. However, the underlying flow prevents the wave's movement "downslope" until the wave propagation speed equals the flow speed. The jump in flow thickness and the transition from supercritical to subcritical flow occurs at the point where the two velocities are equal (Hand, 1974).

In the marine environment, hydraulic jumps are thought to commonly occur at the slope transition between a submarine canyon and alluvial fan (Komar, 1971; Hand, 1974; Garcia and Parker, 1989). Hydraulic jumps are of significant geomorphic importance, because the rapid deceleration results in a sudden increase in sedimentation rates because of loss of flow competence. Substantial mixing can also occur at a hydraulic jump, as confirmed by the energetic secondary currents that have been observed experimentally (Komar, 1971; Weirich, 1989).

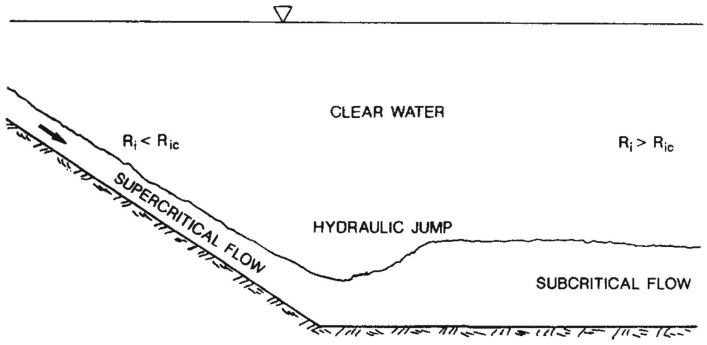

Figure 2.4 Transition from supercritical flow to subcritical flow through a hydraulic jump. R_{ic} indicates the critical Richardson number that is near unity, such that $R_i<R_{ic}$ corresponds to supercritical flow and $R_i>R_{ic}$ corresponds to subcritical flow (source: Garcia, 1993).

Hydraulic jumps have only rarely been inferred from observations of lacustrine turbidity currents. Normark and Dickson (1976) propose that a hydraulic jump was occurring in an anthropogenically induced turbidity current in Lake Superior. The flow was calculated to change from supercritical flow on the delta slope to subcritical flow on the fan, which was accompanied by a 3-fold decrease in density. Supercritical flow conditions have also been documented in several other lakes, though no accompanying hydraulic jumps were directly observed (Lambert et al., 1976; Weirich, 1986a; Chikita and Okumara, 1990; Best et al., 2005).

2.4 Lacustrine sedimentation

As a river enters a lake, the velocity dramatically decreases and the sediment begins to settle from suspension as a function of the settling velocity. The sediment dispersal process, whether that be via overflows, interflows, underflows, or homopycnal mixing, is important in determining the nature of the deposits. In high-energy glacilacustrine environments, the delivery of sediment to the lake bottom is largely by turbidity currents; this delivery has important

implications for the sedimentation pattern within the basin, the sedimentary record, and the creation of bedforms.

2.4.1 Sedimentation from quasi-steady turbidity currents

When sediment is distributed by quasi-steady underflows, the turbulence of the current maintains particles in suspension, allowing coarser sediment to be transported further into the lake basin. A schematic diagram of the longitudinal variations in density and velocity is shown in Fig. 2.5. The velocity often reaches a maximum at the base of the delta slope, and then gradually decreases away from the source of inflow. This longitudinal decline in velocity is a response to the loss of sediment from suspension, fluid entrainment, turbulent mixing, and friction with the upper and lower flow boundaries. Deposition from turbidity currents occurs when the fluid and suspended sediment move down the shear velocity gradient, which is generally equivalent to a velocity gradient. Deposition can occur when the velocity decreases along a spatial transect (in response to a decrease in slope, flow expansion, or a reduced sediment load), over time (in response to variations in sediment supply), or both (Kneller and McCaffrey, 2003). Therefore, the amount of sediment deposited on the lake bottom typically decreases away from the point of inflow, except in situations where the currents are blocked or inhibited by bottom topography that may cause localized enhanced deposition (e.g. Gilbert and Desloges, 1987). A longitudinal decrease in grain size is also commonly observed, because the coarser particles have a greater fall velocity and thus settle out more rapidly than finer material (Pickrill and Irwin, 1983).

In an experimental study of quasi-steady density currents, Alexander and Mulder (2002) attempted to assess the importance of the proximal slope and various inflow characteristics on the nature of the distribution of sediment deposits. First, the authors found that the runout distance of the current depends on the discharge and the proportion of fine-grained sediment within the flow.

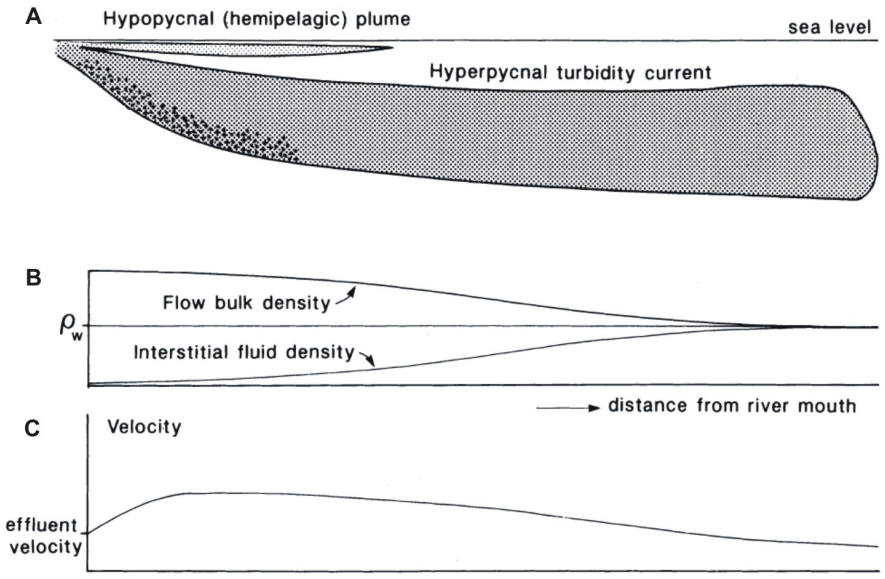

Figure 2.5 A conceptual diagram of the flow of a quasi-steady turbidity current into a basin (A) and the accompanying longitudinal variations in flow bulk density and interstitial fluid density (B) and velocity (C) (modified after Kneller and Buckee, 2000).

Secondly, although the total mass of the deposit is related to the discharge, the maximum mass per unit area (i.e. bed thickness) is not, because the distance over which the particles are deposited increases at higher discharges. Finally, the slope angle is important in determining both the longitudinal variation of deposit mass as well as the bed thickness.

Mulder and Alexander (2001) suggest that the longitudinal and vertical structure of a sedimentary deposit from a quasi-steady turbidity current depends on the shape of its hydrograph (i.e. temporal variations in flow) as well as the spatial variations in flow structure. The authors identify three representative sedimentary sequences that may be created depending on the degree of erosion experienced at proximal locations (Fig. 2.6). In the case of a flash flood, a steep delta slope, or channelized flow, the turbidity current velocity may be high enough on the rising limb

of a flood that deposition becomes insignificant and the flow is able to rework its own deposits at delta-proximal areas (Fig 2.6C).

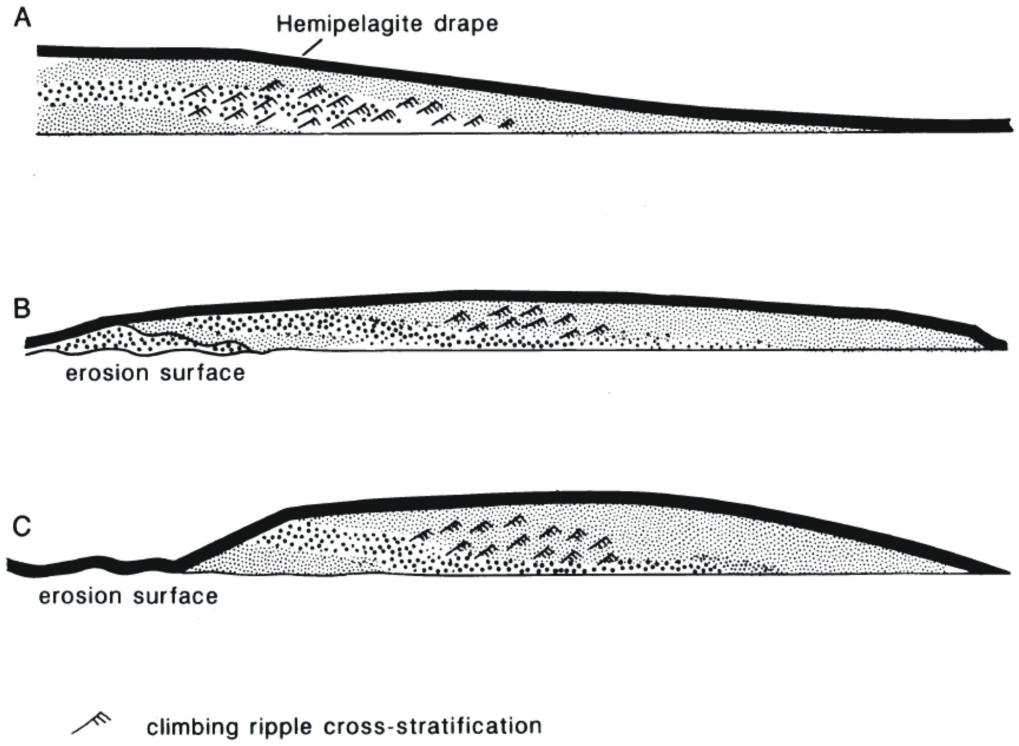

Figure 2.6 A schematic representation of turbidites deposited by quasi-steady turbidity currents shown in a flow-parallel section, where the inflow from the left. The three diagrams represent the deposits of quasi-steady turbidity currents with (A) no erosion, (B) moderate erosion, and (C) high erosion. The size of stipple relates to the relative grain size (source: Kneller and Buckee, 2000).

At more distal locations, the flow is depletive and sediments can be deposited and preserved, possibly as an inversely-graded unit. As the flood continues to rise, deposition progrades and the zone of erosion moves further into the basin so that areas that were initially depositional may become erosional. The site of maximum deposition begins to retreat back

towards the point of inflow during the waning portion of the flood, which creates a fining-upward profile within the sedimentary record.

2.4.2 Sedimentary record

2.4.2.1 Varves

The highly seasonal nature of sediment delivery to proglacial lakes often results in the formation of varves, which are defined as sediment that has been deposited in seasonal layers over the course of one year (Renberg, 1981; O'Sullivan, 1983). Classic glacial varves are composed of a basal layer of coarse material (sand or silt) that fines upward and an upper layer composed of fine, often clay-sized, material (de Geer, 1912). The coarser material is deposited during the peak melt season, whereas the finer material is deposited during the winter as the fine material settles out from suspension.

Because of their annual resolution, glacial varves have been widely used to develop chronologies in paleoenvironmental reconstruction. However, periodic laminations within a sedimentary record may not necessarily represent a true chronology, either because the laminations are not annual in nature (e.g. Lambert and Hsü, 1979; Stihler et al., 1992) or erosional discontinuities and/or changes in sedimentary processes cause interruptions in the varve record (e.g. Francus et al., 2002). Multiple dating methods or multiple core sites may be used to verify the accuracy of a varve chronology (Lamoureux, 1999; Tomkins and Lamoureux, 2005).

2.4.2.2 Hydroclimatic inferences

The delivery of sediment to a lake basin is largely controlled by the regional hydroclimatology. As such, many paleoenvironmental studies have successfully related lacustrine sedimentary records to variables such as temperature, precipitation, and runoff (e.g. Hicks et al., 1990; Desloges, 1994; Leemann and Niessen, 1994; Hardy et al., 1996). Varve

thickness has been commonly used as a climate proxy in paleoclimatic reconstruction, because the amount of sediment that accumulates on the lake floor can be linked to regional hydroclimatic processes. For some lakes, however, the complexity of the sediment delivery process may prevent the identification of a simple relationship between climate and sediment delivery. For example, at a proglacial lake in the Northwest Territories, Tomkins and Lamoureux (2005) found significant correlations between sedimentation and multiple climate controls related to temperature, rainfall, and snowfall, which suggests that the calibration of a single climate variable to a sedimentary record may not be realistic in some cases. Furthermore, geomorphic processes relating to the geologic, fluvial, or glacial systems may affect sediment availability and complicate the supposedly simple relationship between climate and lake sedimentation (Hodder et al., 2007).

2.4.2.3 Subannual sedimentary record

Subannual laminae represent discrete episodes of sediment deposition that can be visually distinguished within the sedimentary record. These laminae are typically coarse-grained and may be identified through the visual examination of the sediment or through the microscopic examination of thin sections. The presence of subannual laminae within a sedimentary record suggests a complex sediment delivery process and consequently requires more detailed analysis. In proglacial Lillooet Lake, British Columbia, two different mechanisms responsible for subannual laminae were identified: extreme hydroclimatic events such as rainstorms and geomorphic events such as subaqueous slumps (Desloges and Gilbert, 1994). Lamoureux (2000) also identified rainfall-induced subannual laminae in the sedimentary record of a high arctic lake, which allowed inferences to be made regarding synoptic climate conditions over the past 500 years. Similarly, Cockburn and Lamoureux (2007a) classified subannual sedimentary events in a

glacial lake as either nival-glacial or rainfall-induced, allowing the reconstruction of major late-summer rainfall events for the northern Coast Mountains.

Subannual textural variations, as opposed to varve thickness, may be more directly associated with hydrological processes, such that a more realistic relationship may be developed between the regional hydrometeorology and sediment characteristics. For example, by studying the microstructural and textural parameters of a sedimentary record from a varved arctic lake, Francus et al. (2002) was able to establish a significant relationship between certain particle size fractions and snowmelt intensity despite a poor overall correlation between climate and varve thickness. The particle size distribution of the sediment that is deposited at a given location on a lake floor can also be theoretically linked to streamflow competence and thus maximum flow velocity; therefore, the temporal changes in grain size distributions within a sedimentary unit can potentially be used to reconstruct flow conditions during deposition (Sundborg and Calles, 2001). However, recent work suggests that intra-annual grain size hysteresis must also be considered when interpreting flow conditions from lacustrine sedimentary records, as the grain size becomes biased towards finer material later in the melt season (Cockburn and Lamoureux, 2007b). Furthermore, if the sediment was deposited by an underflow, recent work suggests that the loss of flow capacity may be more important in controlling deposition from turbidity currents (Hiscott, 1994; Kneller and McCaffrey, 2003), which would negate the relationship between particle size and flow velocity.

These studies and others indicate that valuable information regarding hydrometeorological and catchment events can be obtained from subannual sedimentary properties. The subannual signal can be used to reconstruct the frequency and/or magnitude of a subannual event such as rainfall or snowmelt (Lamoureux, 2000; Francus et al., 2002; Cockburn and Lamoureux, 2007a). Alternatively, the underlying thermal-sediment relationship can be

improved by identifying and removing the subannual component (Desloges, 1994). However, the order and timing of hydroclimatological events is potentially important in interpreting the subannual sedimentary record. For example, sediment hysteresis is widely documented in glacial sedimentary systems from diurnal to seasonal time scales (Østrem, 1975; Hammer and Smith, 1983; Fenn et al., 1985) and must be considered when interpreting the sedimentary record. In Lillooet Lake, sediment supply hysteresis appears to occur as the melt season progresses, resulting in fewer and thinner subannual laminae later on in the season (Desloges and Gilbert, 1994). The seasonal development of the thermal structure in Lillooet Lake also appears to influence the transfer of sediment down-lake (Desloges and Gilbert, 1994).

2.4.3 Sediment waves

Sediment waves have been documented in a variety of marine settings (see reviews by Wynn et al., 2000c; Lee et al., 2002), yet have not been observed in lakes until recently, when they were discovered in Kluane Lake (Fig. 2.7; Gilbert and Crookshanks, in press). They cover large areas up to hundreds of square kilometres and individual waves typically have wavelengths from 0.6 to 7 km and waveheights from 2 to 70 m (Wynn and Stow, 2002). The crests of the waves are oriented roughly parallel to the slope and the wave dimensions usually decrease downslope. Upslope migration is commonly observed, where individual beds are thicker and coarser grained on the upslope wave flank (Lee et al., 2002). Sediment waves preferentially form in fine material (silt and clay) on low slopes that range from 0.1 to 7°. Relative to typical marine sediment waves, those in Kluane Lake occur in shallower water (10-65 m depth) and are smaller (mean wavelength 129.4 m; mean wave height 2.3 m), although their internal structure is remarkably similar.

Sediment waves are most often associated with turbidity currents, but have also been observed in areas that experience other bottom currents. Sediment waves generated by turbidity

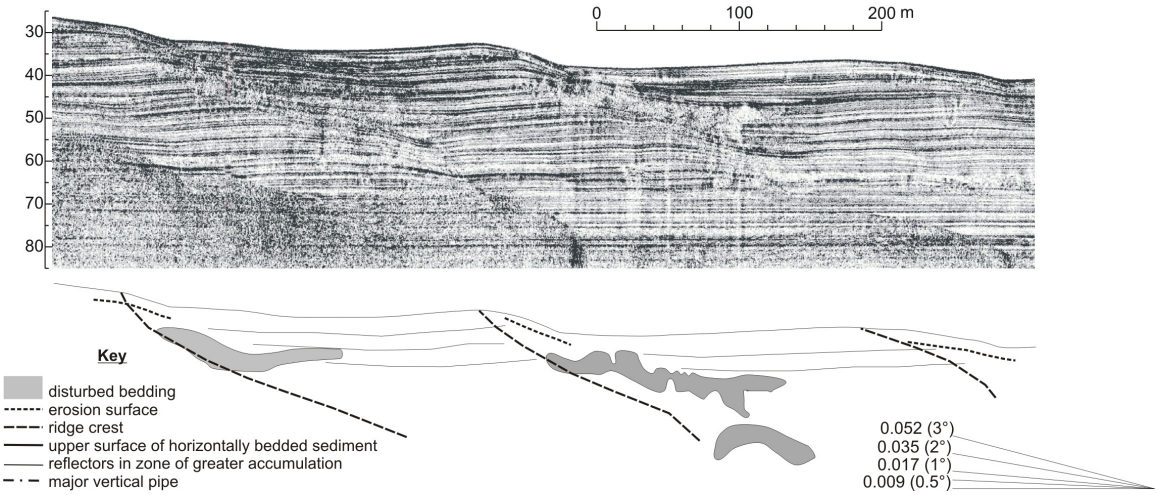

Figure 2.7 Portion of a sub-bottom acoustic record of sediment waves in Kluane Lake showing the internal structure of the sediment waves (source: Gilbert and Crookshanks, in press).

currents have been found on the backslopes of channel levees (e.g. Normark et al., 1980, Nakajima et al., 1998), in turbidity current channels (e.g. Wynn et al., 2000a), in association with unchannelized flow on the slopes of volcanic islands (Wynn et al., 2000b) and the continental slope and rise (Wynn et al., 2000a; Wynn et al., 2000c; Lee et al., 2002). The large dimensions and prolonged existence of sediment wave fields suggest that they are generally in equilibrium with the turbidite system (Wynn and Stow, 2002).

Because they are commonly found in deep water (up to 4900 m), the processes that generate marine sediment waves have been inferred from the geologic record and remote imaging techniques such as side-scan sonar or seismic reflection. As a result of the indirect nature of these field measurements, much debate regarding the origin of these bedforms has taken place and several models have been proposed. The lee-wave model, which was first suggested by Flood (1988), involves a weakly stratified water mass flowing over an initial seafloor perturbation,

which initiates the development of lee waves within bottom current flow. The more generally accepted mechanism of sediment wave formation is the antidune model. Hand et al. (1972) first suggested that large-scale antidunes could form in response to the occurrence of surface waves at the interface between a turbidity current and the ambient water. This model predicts values of sediment concentration and flow thickness that are very similar to field measurements (Stow and Bowen, 1980; Piper and Savoye, 1993).

2.5 Conclusions

The transport of sediment from glacifluvial to glacilacustrine environments is highly complex, varying over multiple temporal and spatial scales. An important component of this system is the prodelta region, which mediates the transfer of sediment from the river to the basin. Both the river inflow and physical lake characteristics control the method of sediment distribution and are thus important in determining the pattern of sedimentation. One of the most dynamic processes in a high-energy glacial lake is the transport of water and sediment by turbidity currents along the delta slope and beyond. While experimental and modeled results provide a theoretical basis for understanding the flow structure, velocity, and suspended sediment dynamics, direct measurements of turbidity currents in the natural environment also offer valuable insights with respect to flow behaviour. By observing the sedimentary processes that are occurring within a lake, the patterns of sedimentation, sedimentary structures, and sedimentary bedforms may be more fully understood.

Chapter 3

Study Area

3.1 General characteristics

Kluane Lake is located on the Yukon Plateau in southwestern Yukon Territory, bordering the eastern margin of the St. Elias Mountains (Fig. 3.1). It is the largest lake in the territory with a surface area of 432 km^2 and a maximum depth of 78 m. Slims River, which flows from Kaskawulsh Glacier, is the primary source of water and sediment for Kluane Lake. This glacier is one of the major valley glaciers that flow out of the Icefield Ranges, which are located within the St. Elias Mountains and are part of the most extensive non-polar icefield in the world. Because Kaskawulsh Glacier lies on the hydrological divide between the Yukon River system (via Slims River, Kluane Lake, and Kluane River) and the Alsek River system (via Kaskawulsh River), it is not possible to determine the precise division of the watershed. This study assumes that the watershed boundary is along the midline of the glacier; therefore, the lake's total drainage area can be calculated as 5373 km^2. These and other physical characteristics of Kluane Lake and its watershed are summarized in Table 3.1.

Table 3.1 The physical characteristics of Kluane Lake and its watershed

Elevation	777 m
Length	65 km
Average width	4 km
Surface area	432 km^2
Maximum depth	78 m
Maximum watershed relief	1783 m
Watershed area	5373 km^2
Glaciated area	492 km^2 (9.2%)
Watershed area to lake area ratio	12.44

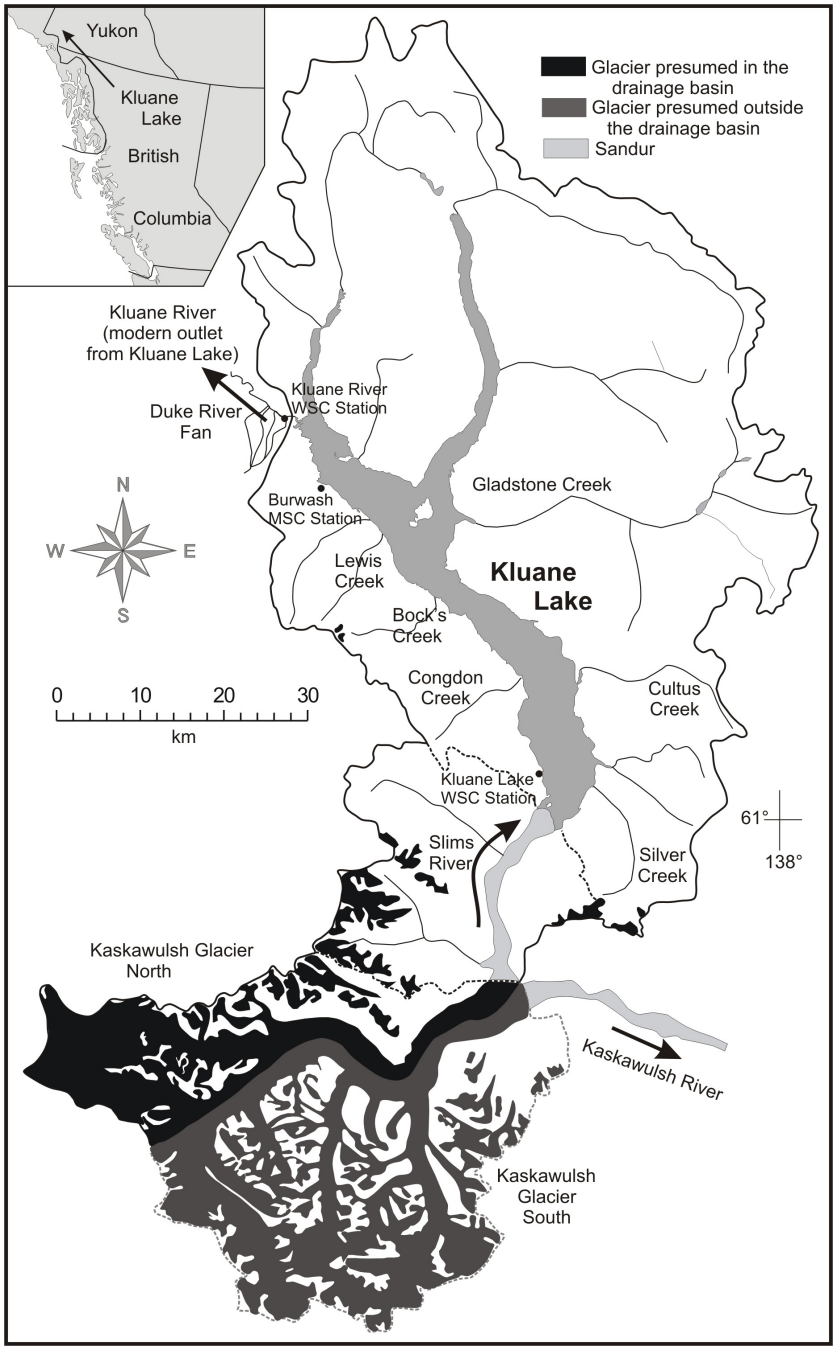

Figure 3.1 Map of the drainage basin of Kluane Lake, showing the assumed hydrological division of Kaskawulsh Glacier, major rivers, Burwash Meteorological Service of Canada (MSC) station, Horseshoe Bay Water Survey of Canada (WSC) station, and tributary streams. Inset map shows the location of Kluane Lake in Yukon Territory (modified after Gilbert and Crookshanks, in press).

3.2 Existing hydrological and meteorological data sources

The Water Survey of Canada monitors the lake level in Horseshoe Bay at 15-minute intervals and has done so since 1952. A gauging station was in operation on Kluane River from 1952, but was discontinued in 1995. The Meteorological Service of Canada operates a station at Burwash Landing (MSC Stn Burwash A), which is located approximately 50 km from the study area, and has done so since 1962. The location and characteristics of these hydrological and meteorological stations are shown in Table 3.2.

Table 3.2 Climate and water survey stations near Kluane Lake operated by the Meteorological Survey of Canada and the Water Survey of Canada

Station	Code	Latitude	Longitude	Elevation	Duration
Kluane River	09CA002	61° 25’	139° 03’	n/a	1952 to 1995
Kluane Lake	09CA001	61° 03’	138° 30’	n/a	1952 to present
Burwash A	2100182	61° 22’	139° 03’	806.80 m	1966 to present

3.3 Post-glacial history

The post-glacial history of Kluane Lake has been highly dynamic and a matter of speculation since Bostock (1969) originally proposed a reversal in drainage direction from Kluane Lake. The late Holocene drainage history of Kluane Lake has been extensively explored using both geomorphological and geochemical methods (Clague et al., 2006; Brahney et al., in press). Kluane Lake is thought to have originally drained southward through the Slims, Kaskawulsh, and Alsek valleys to the Pacific Ocean. The advance of the Kaskawulsh Glacier during the Little Ice Age blocked the southward drainage and caused the aggradation of outwash

near the former southern outlet of the lake. Meltwater from Kaskawulsh Glacier caused the water level of the lake to rapidly rise to 12 m above the present level. The lake water eventually overflowed its northern boundary at the Duke River fan, thus establishing the current drainage outlet of Kluane Lake via the Kluane River and Yukon River systems. The lake fell to its current level before 1800 AD and has not fluctuated more than several metres over the past 200 years. Several studies have proposed that with the further retreat of Kaskawulsh Glacier, its meltwater may become almost completely diverted to the Kaskawulsh River system due to its steeper gradient, thus effectively discontinuing the major water source to Kluane Lake (Bryan, 1974c; Clague et al., 2006).

3.4 River hydrology and sediment delivery

Slims River is the most significant source of both water and sediment to Kluane Lake. Slims River derives 70-90% of its flow from the meltwater of Kaskawulsh Glacier, with the remainder originating from the tributary streams that enter the Slims River farther downstream (Sawada and Johnson, 2000). The river flow fluctuates both diurnally and seasonally, following the temporal discharge pattern of other glacially controlled meltwater river systems (Bryan, 1974c). The Slims River discharge varies from zero in the winter up to 566 m^3s^{-1} in the late summer (Fahnestock, 1969) and published values of maximum suspended sediment concentrations range widely from 11.83 g l^{-1} (Sawada and Johnson, 2000), to 15 g l^{-1} (Johnson, 1991), and up to 25 g l^{-1} (Pharo and Carmack, 1984). Because Kaskawulsh Glacier feeds two hydrological systems, its meltwater may be directed primarily through only one of these river systems in a given year (Barnett, 1974; Bryan, 1974b, 1974c; Sawada and Johnson, 2000). Complications to the discharge record may also exist even within a given season; a dramatic decrease in the Slims River discharge was observed at the beginning of August 1970, which was

attributed to shifting glacial drainage between the two river systems (Barnett, 1974; Bryan, 1974a).

Slims River transports large amounts of glacially scoured, fine-grained material from Kaskawulsh Glacier, material that is subsequently deposited in Kluane Lake. Along the Slims River valley, numerous alluvial fans have formed along both sides of the sandur. These fans deliver significant quantities of gravel, sand, and finer materials to the sandur; coarser gravel is deposited further up the fans, never reaching the river (Fahnestock, 1969).

While the main source of water is Slims River, numerous small high-gradient creeks flow out of the Kluane Ranges over alluvial fans into the south end of Kluane Lake. Several creeks that are incised in drift-filled valleys flow into the north end of the lake (Terrain Analysis and Mapping Services, 1978). Most of the drainage areas of these small streams do not contain any glaciers because of the intense rain shadow of the St. Elias Mountains. Exceptions include the small cirque glaciers that are found at the headwaters of Bock's Creek and Lewis Creek on the west side of Kluane Lake and Silver Creek on the south side of Kluane Lake. Silver Creek in particular may contribute a significant amount of sediment to the lake, since several measurements indicate that the suspended sediment concentration may reach values up to 35 g l^{-1}. However, despite its high sediment load and large fan, Silver Creek does not appear to play a significant role in Slims River delta processes, as CTD casts do not document any plume entering the lake.

The thick raised lacustrine sedimentary sequences along the perimeter of the lake, particularly on the east side, may also potentially supply sediment to the lake basin, although their contribution is likely minimal relative to the Slims River inflow (Terrain Analysis and Mapping Services, 1978). Along the west side of the lake, large Holocene alluvial and colluvial fans emerge from the Kluane Ranges, the easternmost range of the St. Elias Mountains (Clague,

1981). Storms or earthquakes may cause debris flows or torrents to occur along the high-gradient streams that cross these alluvial fans; however, in recent years a large number of these streams have been artificially constrained to a single channel with the hope of reducing the flooding and debris flow risk. Multiple landslides have occurred in the Kluane Ranges near the south end of Kluane Lake, although none have occurred since Kluane Lake reached its present extent. The most recent and spectacular of these landslides is the Sheep Mountain rockfall avalanche, which formed as a result of two separate failures between 500 and 1950 radiocarbon years ago (Clague, 1981). In 2007, highway construction was underway along the southwestern shore of the lake for the majority of the summer and added an unknown amount of sediment to the lake.

Dust storms are relatively frequent in the Kluane Lake region. They acquire material by eroding the fine, dry sediment along the Slims River sandur and delta (Nickling, 1978). The storms have been hypothesized to contribute to sedimentation in the southern end of the lake (Terrain Analysis and Mapping Services, 1978), although no study has been undertaken with regards to this subject.

3.5 Kluane Lake hydrology and sediment distribution

The water level of Kluane Lake is primarily controlled by the Slims River discharge (Fig. 3.2), although the water level appears to be influenced by other factors as well. Water inflow from other stream tributaries, evaporation from the lake, precipitation events, and groundwater fluxes all likely have an impact on seasonal variations in lake level. The modern outlet of Kluane Lake is via Kluane River, which flows along the eastern edge of the Duke River fan, a 80 km^2 complex of alluvial and colluvial material, eventually reaching the Yukon River system. The Kluane River discharge is well correlated with the water level of Kluane Lake (Fig. 3.3), likely because of the morphological control of the Duke River fan.

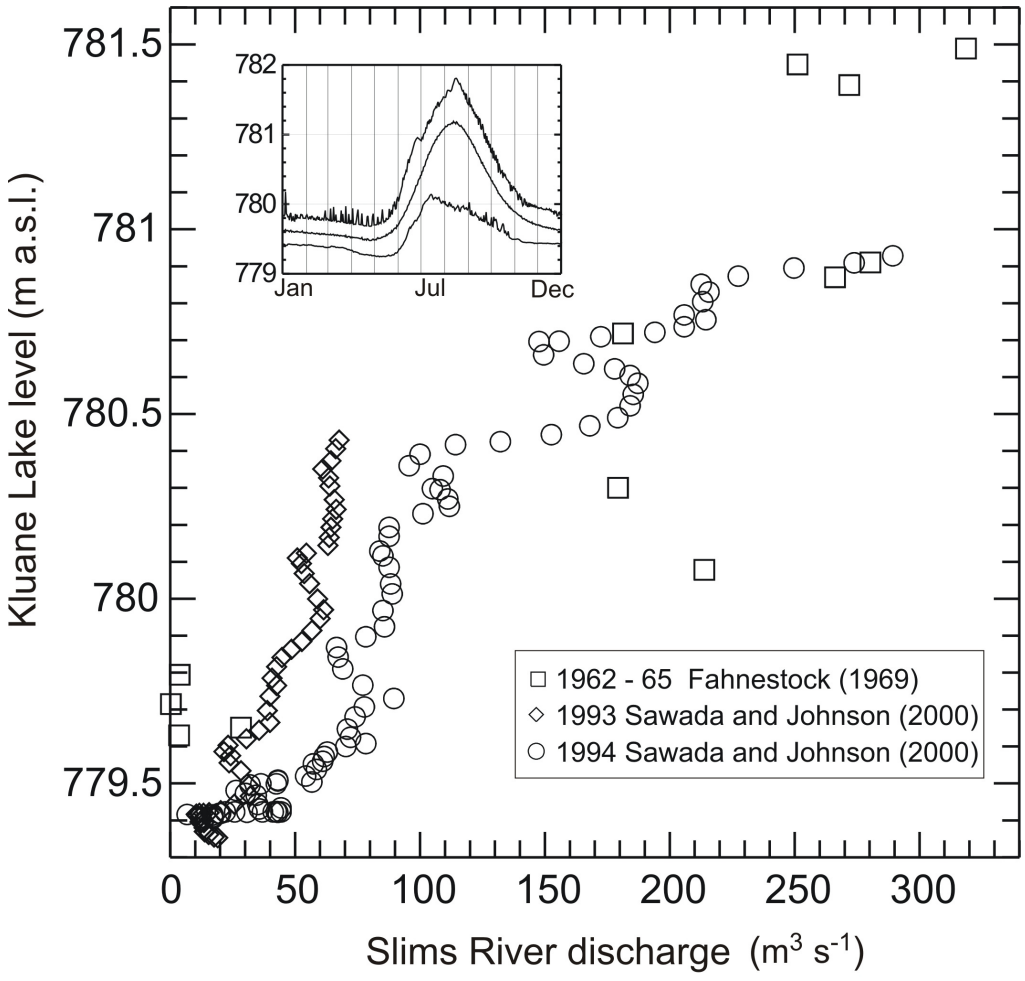

Figure 3.2 Relation between discharge in Slims River and the water level in Kluane Lake. Inset is the annual hydrograph of Kluane Lake, showing the mean daily, maximum daily, and minimum daily levels for the period 1953 to 2004. Slims River data are from Sawada and Johnson (2000) and Fahnestock (1969). Kluane Lake data are from the Water Survey of Canada station 09CA001 (source: Clague et al., 2006).

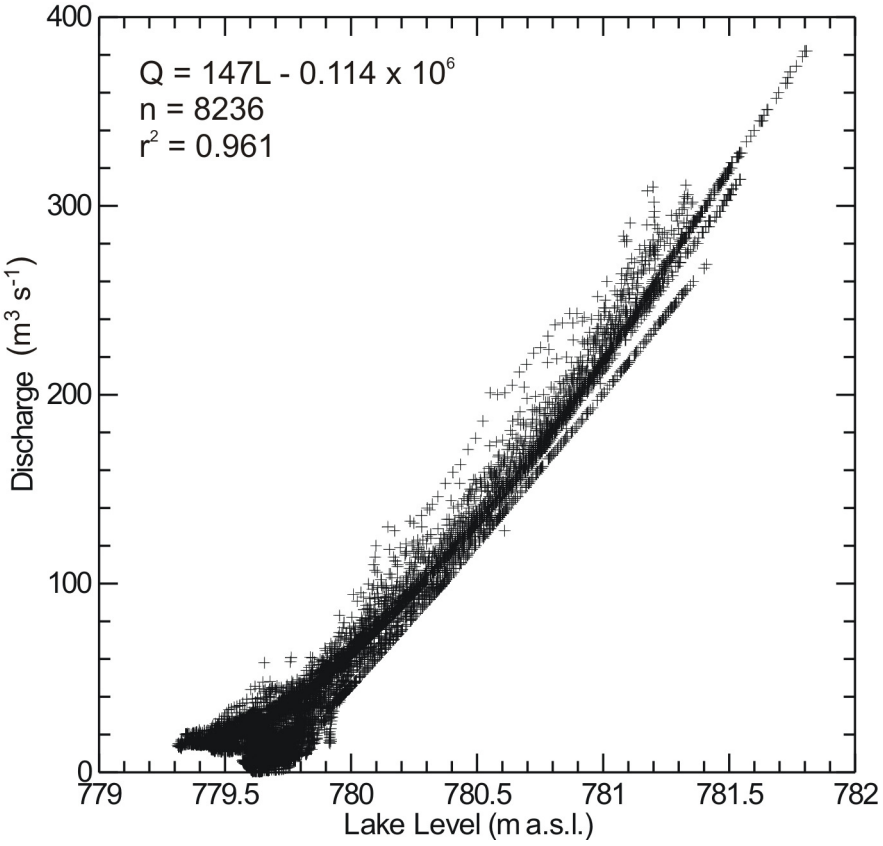

Figure 3.3 Relation between water level (L) for Kluane Lake and mean daily discharge (Q) for Kluane River for the data available from the Water Survey of Canada stations 09CA001 and 09CA002, respectively, between 1952 and 1995 (source: Gilbert, pers. comm. 2008).

The majority of sediment deposited in Kluane Lake comes out of suspension from the Slims River inflow (Terrain Analysis and Mapping Services, 1978). Underflows directly off the subaqueous Slims River delta front, interflows at 30 m depth and overflows have been observed in density profiles (Bryan, 1974a, 1974d). Kluane Lake sedimentation rates are at a maximum at the Slims River delta, decreasing to approximately 2 – 3 mm a^{-1} in the area of the Congdon Creek and Cultus Creek (Terrain Analysis and Mapping Services, 1978).

3.6 Sandur and delta morphology

The Slims River sandur currently extends just over 20 km from Kaskawulsh Glacier to Kluane Lake, covering the majority of the valley floor except where large alluvial fans have formed along the valley edges. The sandur has formed over the last 400 years since the drainage reversal of Slims River, and thus developed remarkably quickly. The average rate of delta advance has decreased from 74 m a^{-1} during the period between 1899 and 1913 (Bostock, 1952), to 27 m a^{-1} between 1947 and 1970 (Bryan, 1974c), and to approximately 18 m a^{-1} between 1970 and 2006. This dramatic decline in delta advance may be partially a response to the construction of the modern Alaska Highway across the sandur in 1942 and the relocation of the bridge 3 km downstream to the delta in 1956. The modern bridge confines the river's flow to two artificially narrowed channels and likely traps most of the sand and gravel upstream, slowing the rate of delta growth. Another reason for this decline may be that increasingly more water and sediment are being diverted away from Slims River and into the Kaskawulsh River system.

While Slims River has a braided morphology upstream of the bridge, the river forms a single channel that periodically undergoes avulsion on the delta downstream of the bridge. Satellite images, air photographs and hand-held photographs from small aircraft and the mountain sides from 22 of the years between 1944 and 2007 show that during 18 (82%) of those years, flow was directed to the centre or right-hand (east) side of the delta, while during the remaining four years (1970-71 and 2006-07), flow was directed more toward the left (west). As a result, the eastern portion of the delta front has advanced more rapidly than the western.

The subaqueous morphology of the Slims delta is unlike most other glacilacustrine deltas, which commonly exhibit a Gilbert-type delta morphology. The Slims delta has neither distinct topset, foreset, and bottomset beds nor any sharp break in slope. The slope is particularly gradual (1°) on the east side of the island, where the river flow has been directed in the majority of

previous years. On the west side of the island, the slope is, on average, slightly steeper (4.5°), but decreases to near zero 5 km offshore where the lake reaches a maximum depth of 78 m. The wedge of sediment that has been deposited in front of the advancing Slims River sandur has a maximum thickness of more than 50 m close to the delta, decreasing to less than 1 m by 7 km from the delta (Clague et al., 2006).

Submerged, small, irregular channels and levees in front of the Slims River delta have been documented in several acoustic surveys of the area (Bryan, 1974b; Gilbert and Crookshanks, in press) and were likely eroded by turbidity currents. Step-like features have also been observed in front of Silver Creek and Slims River (Bryan, 1974b; Gilbert and Crookshanks, in press). These steps are not faults because acoustic reflectors beneath can be traced under the scarps without offset. They probably instead represent minor surface-layer detachments and downslope sediment flows in the weak muddy deposits off the river mouth (cf. Prior and Coleman, 1978).

Turbidity currents have created a field of sediment waves in fine-grained sediment on the prodelta slope. These sediment waves are analogous to those of marine systems, but previously not reported from lakes (Gilbert and Crookshanks, in press). These bedforms have a mean wavelength of 130 m (range 16 – 440 m) and mean amplitude of 2.3 m (range 0.1 – 9.0 m). They are migrating up-slope and their internal architecture is consistent with a sedimentary record formed by turbidity currents with variable flow that facilitates localized areas of enhanced and reduced deposition (Fig. 2.6).

Chapter 4
Methods

Field data were collected at Kluane Lake in 2006 (July 14 - July 25) and 2007 (June 27 – July 29) during the peak melt season.

4.1 Meteorology

Air temperature was measured with an Onset Hobo temperature logger at a height of 2 m from the ground at the Alaska Highway crossing of Slims River between July 12 and July 29, 2007. An hourly temperature record is also available from the Burwash Meteorological Survey of Canada (MSC) Station, which is located approximately 50 km from the study area. A comparison of the overlapping records from the Hobo logger and the Burwash MSC station indicates only a weak correlation ($r^2 = 0.45$, $p<0.001$; Appendix A). General comparisons between meteorology and hydrology are based on the record from the Burwash MSC station to ensure consistency over the entire monitoring period. Data from the Burwash MSC Station were also used to calculate daily precipitation values for the study area. In 2007, an anemometer (Davis Standard Industrial Anemometer) that records both wind speed (Omega pulse data logger) and direction (Hobo H8 logger) was deployed 4 m above the ground on the Slims River delta (Fig. 4.1).

4.2 River hydrology and suspended sediment

Hydrological and sediment data from Slims River were collected in 2007 at the Alaska Highway bridge, which is 19 km downstream from Kaskawulsh Glacier and 1.7 km upstream from where the river enters the lake (Fig. 4.1).

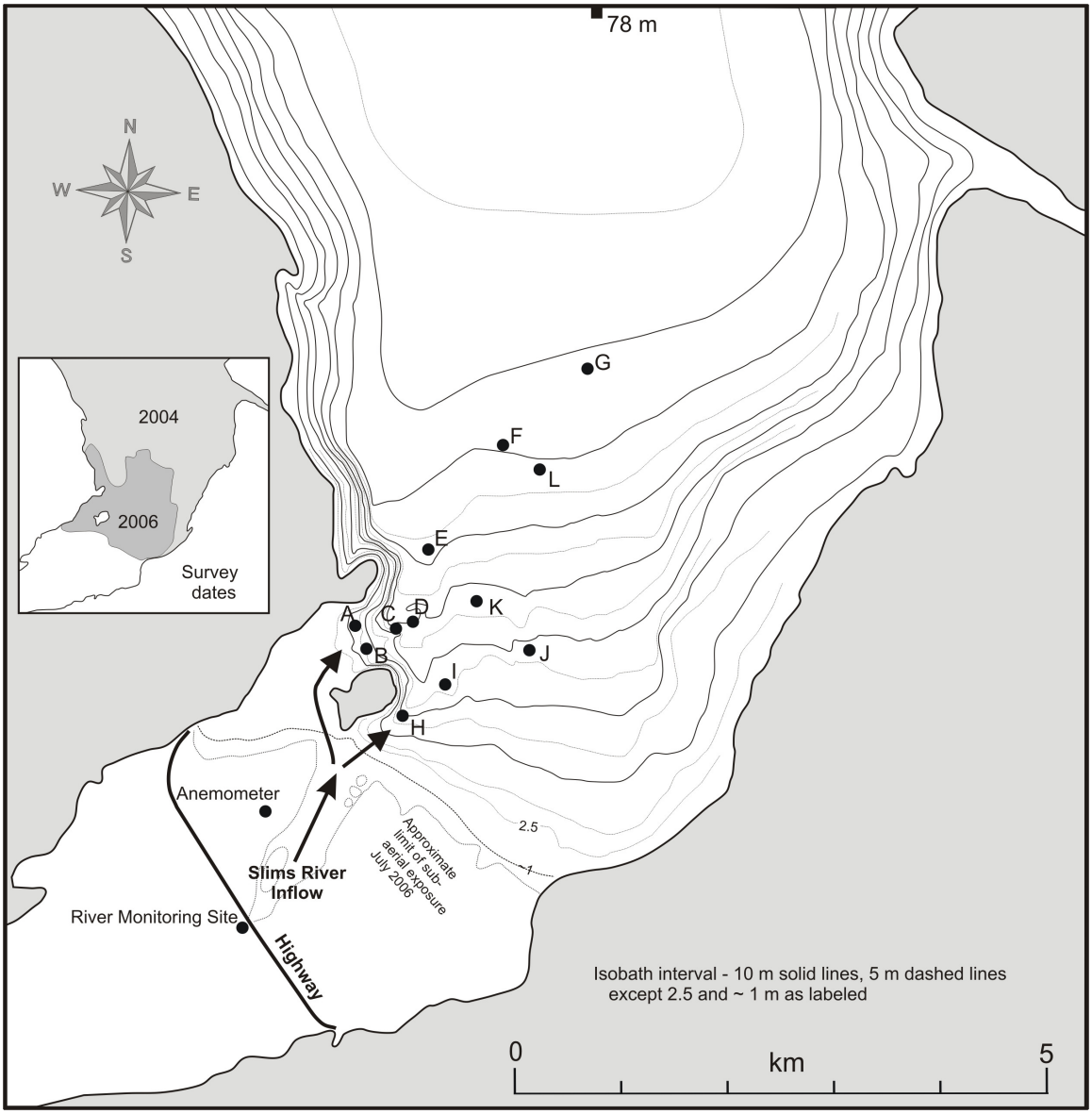

Figure 4.1 Bathymetric map of the prodelta region of Kluane Lake, indicating the river monitoring site, anemometer position, and mooring locations (A to L). The direction of river inflow is indicated by the arrows. Modified from Gilbert and Crookshanks (in press).

Stage was measured at 15-minute intervals with a Global Water WL16 Logger that was placed in a large stilling well. Discharge was successfully measured on five occasions using an Ott C31 current meter, but instrumental failure prevented any further attempts. At the Alaska Highway bridge, the river bottom is armoured with large rocks that were installed during bridge construction. At this site, the river also becomes constricted, which increases the velocity and prevalence of large eddies in the channels. The river cross-sectional profile, therefore, remains consistent after mid-June once the river exceeds approximately 100 m3/s (Appendix B; Sawada, 1996). The lack of bed accretion and erosion in Slims River during the peak melt season allows the rating curve developed for the same site by Sawada and Johnson (2000) to be applied to the 2007 data with reasonable confidence. Because the discharge measurements performed in 2007 occur only over a small range, the stage measurements are associated with the same datum as was used by Sawada and Johnson by averaging the discharge measurements and floating that point on to the rating curve. Considerable scatter occurs around the rating curve because minor backwater conditions, fast flow conditions, and large eddies influence current measurements. There are also old wooden pilings along the river bed from an earlier bridge that affect velocity measurements. However, a river monitoring station at the Alaska Highway bridge is preferable for several reasons. If a monitoring station had been constructed upstream or downstream of the bridge, the station would have been not only a considerable financial investment, but also a significant challenge to operate because of the shifting channels, transient bars, and quick-sand that are present along the sandur and delta.

Turbidity was measured at one-minute intervals with an Analite Turbidity Probe 9500 and the 15-minute average was recorded by a Starlog Data Logger. Dip samples of water were taken daily from the river in order to analyze the fluvial grain size and determine the suspended sediment concentration (SSC). While depth-integrated sampling from the river surface to the bed

is the standard method for determining SSC (Guy and Norman, 1970), the available equipment was not suitable to use in Slims River because of the river's large scale. The water samples were filtered with Millipore 0.45 μm polycarbonate filters, which were then transported to the laboratory, dried for 24 hours at 45°C, and weighed. SSC values are well correlated with turbidity measurements (Fig. 4.2; 28 dip samples; $r^2 = 0.85$, $p<0.001$), which allows the conversion of the 15-minute turbidity record to SSC.

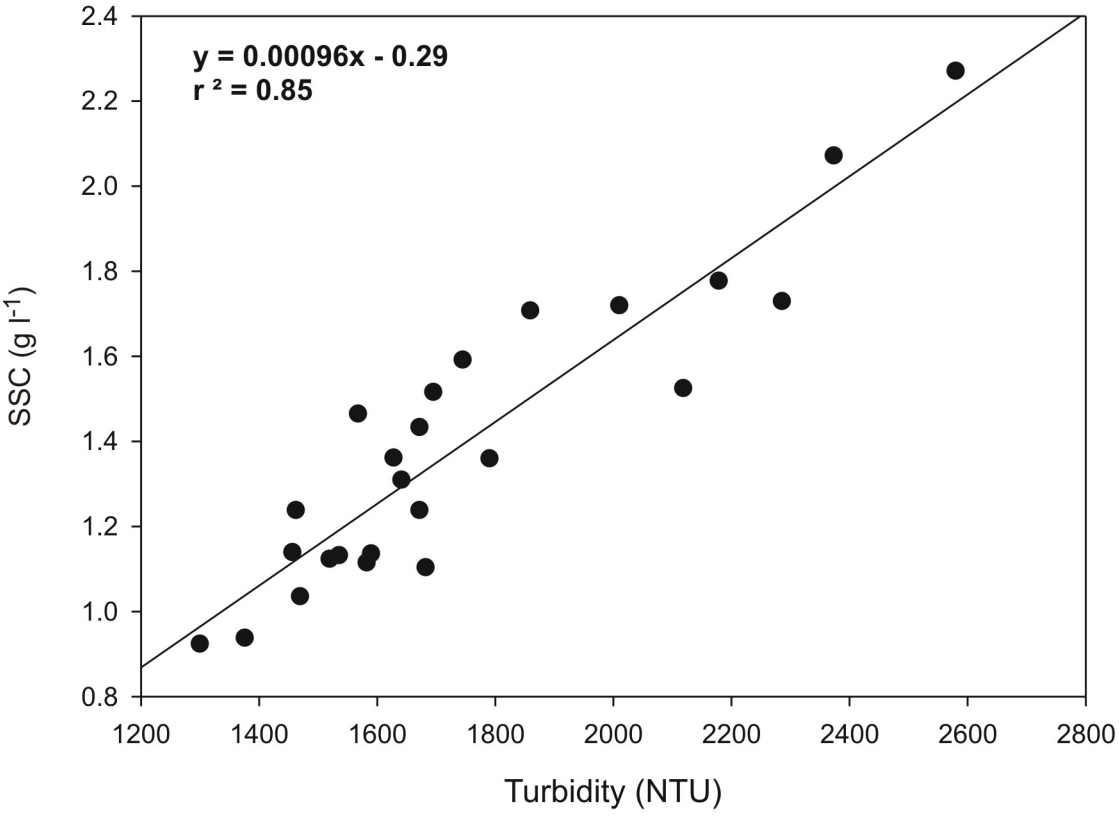

Figure 4.2 Calibration curve between suspended sediment concentration (SSC) and turbidity for the Analite Turbidity Probe 9500. Curve was developed by taking dip samples from Slims River throughout the monitoring period and comparing the SSC of each sample with the 15-minute averaged turbidity reading from the Analite probe.

While turbidometers allow high-frequency data collection, the conversion from turbidity to SSC introduces some uncertainty, which can be observed in the scatter in the relationship between turbidity and SSC. Instantaneous dip samples may not be directly comparable to the logged turbidity, which is averaged over 15 minutes. Furthermore, other studies have observed significant intrinsic variance in the SSC of dip samples (Johnson, 1992; Brasington and Richards, 2000). Turbidity depends on not only the SSC, but also the particle size, organic matter content, and mineral composition of the sediment (Brasington and Richards, 2000; Orwin and Smart, 2004); therefore, variations in these characteristics may introduce some uncertainty to the SSC record.

Water temperature was recorded with a Hobo Stowaway Tidbit temperature logger at 15-minute intervals. River bottom sediment was sampled immediately downstream from the bridge using a 1.5 L bucket dredge operated from the river bank.

4.3 Lake monitoring

Moorings were deployed in Kluane Lake at 6 locations in 2006 and 11 locations in 2007 in order to continuously record lake water characteristics with a variety of instruments (Fig. 4.1). Water temperature was monitored with Onset Hobo Stowaway Tidbits and Watertemp Pros. Turbidity current velocity was recorded by an Alec electromagnetic (EM) current meter and tilting current meters, which are described below. The EM current meter was moved from mooring B to mooring A on July 8, 2007 in order to situate the meter in the middle of the main flow. When analysis of the entire record is required, the velocity values prior to July 8 are adjusted by assuming that the average velocity at moorings A and B remained constant over the time required to relocate the meter (30 minutes). Both laboratory and field tests confirm that the current direction measurements by the EM current meter consistently deviated by 39°E; therefore, a correction was applied to all measurements in order to account for this instrumental error.

Suspended sediment concentration was monitored with a Yellow Springs Instrument turbidometer in 2006; however, the instrument malfunctioned in 2007 and did not record accurate data. Cylindrical sediment traps (2.5 height to width ratio) were placed 0.7 m off the lake bottom and funnel sediment traps (5.95 concentration ratio) were placed at the top of each mooring at 1-m depth in order to collect sediment falling from suspension or deposited by turbidity currents. Cylindrical traps with a height to width ratio of greater than 2.3 have been found to trap a representative mass of sediment relative to the lake bottom in environments with a significant horizontal velocity component (Gardner, 1980; Bale, 1998).

Tilting current meters were constructed based on meters developed by Hendricks (1985), albeit with significant modifications. A full description of the construction and calibration process is provided in Appendix C. A Hobo Pendant G logger was secured within a finned waterproof case that was able to tilt freely in a rectangular metal frame. This apparatus was then fastened to a mooring line with two swivels. The fins on the waterproof case were glued to the case such that the meter could orient itself into the flow. The logger recorded the tilt of the waterproof case at 2-minute intervals. The tilt data were then averaged over 10 minutes to remove instantaneous velocity fluctuations and smooth the entire record. The current meters were individually calibrated in a flume to allow the conversion between tilt and velocity. Using the method of least squares, third degree polynomial regression models were derived for the relationship between tilt and velocity for all current meters (s_{est} =1.90 – 2.45; r^2 = 0.905 – 0.948, $p<0.001$). The detection limit of the meters ranges from 0.04 to 0.09 m s^{-1} depending on the individual meter; therefore, tilting meter velocity records often have interruptions that may represent a velocity greater than zero. The calibration curves are generally consistent with each other (Appendix C); however, individual calibration data were used for each current meter

because of the small variations between curves. A representative calibration curve with 95% confidence intervals is shown in Fig. 4.3.

CTD casts were performed daily or on alternate days with a Hydrolab Datasonde-3 at every mooring site and other locations within 5 km of the delta in order to document changes in temperature, SSC, and conductivity in the water column. The turbidity probe on the Hydrolab Datasonde was calibrated to SSC in the laboratory using lake sediment samples from Kluane Lake (Fig. 4.4; $r^2 = 0.99$, $p<0.001$).

Surface sediment samples were collected from the lake floor with an Ekman box corer; however, the extremely underconsolidated sediment near the delta prevented the preservation of short cores from the Ekman corer or the recovery of long cores by conventional gravity coring or vibra coring.

4.4 Sub-bottom acoustic survey

Sub-bottom acoustic surveys using a Benthos CAP-6600 Chirp profiler were conducted for Kluane Lake in July of 2004 and 2006. In 2006, the acoustic survey was performed at a higher spatial resolution (200-m transect line spacing) and limited to the area within 4 km of the Slims River delta. GPS data accurate to about 5 m were logged at 3-second intervals. Bathymetric and sub-bottom data are based on sound velocity of 1430 m s^{-1}, which is appropriate for the temperature of the water at the time of survey, and are corrected to 781.0 m above sea level, the average elevation of the water surface in mid-summer. All isobaths on the bathymetric map were plotted by hand based on the sub-bottom acoustic survey data (Fig. 4.1). The 1-m isobath was determined by marking points with a GPS echo sounder (accurate to 5 m) and interpolating between the points. The limit of the subaerial delta front was determined by marking points along the waterline using a hand-held Garmin Etrex GPS (accurate to 5 m) and, once again, interpolating between the points.

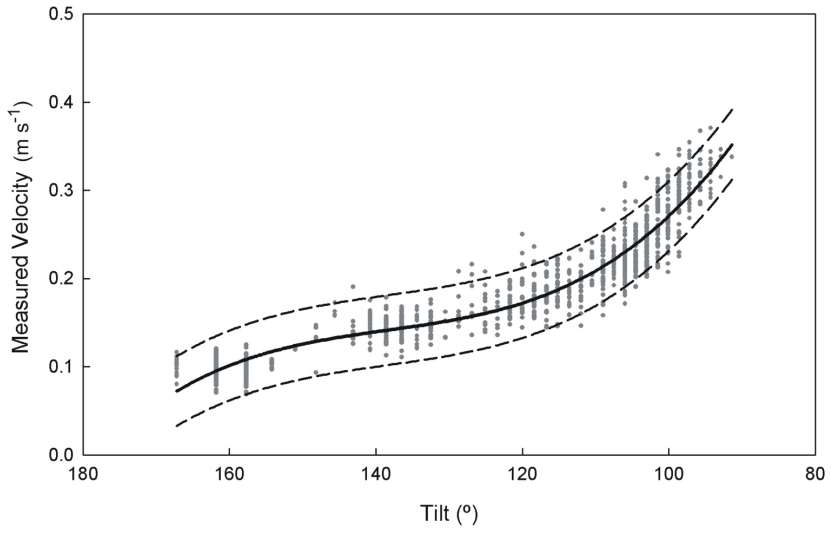

Figure 4.3 An example of a tilting current meter calibration curve used to convert tilt values to velocity values. The solid black line represents the mean value and the dashed lines represent the 95% confidence intervals.

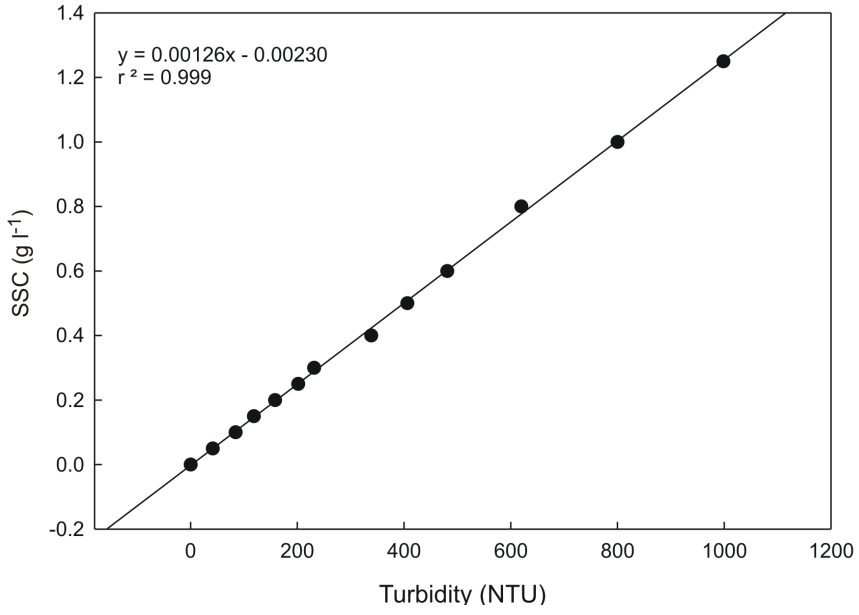

Figure 4.4 Calibration curve between suspended sediment concentration (SSC) and turbidity for the Hydrolab Datasonde-3. Curve was developed in the laboratory using sediment samples from the Kluane Lake bed.

4.5 Laboratory and data analysis

In the laboratory, the sediment traps were split, dried, and photographed. Sediment samples (7 x 1.5 x 1 cm) to be used for thin section analysis were removed from the sediment by pressing aluminum trays into the smooth core face and removing the trays, producing slabs of sediment of equal dimensions. The sediment slab samples were freeze-dried and vacuum embedded in epoxy using standard procedures (Lamoureux, 2001). The cured samples were then cut and ground to produce thin sections. Thin sections were photographed using a Polaroid camera attached to an optical microscope. Water content, bulk density, and loss on ignition were determined by oven-drying samples at 105°C and combusting the organic material present in the samples at 550°C (Heiri et al., 2001).

Grain size analysis was performed on the river samples, lake samples, and sediment trap material with a Beckman Coulter LS 200 particle size analyzer equipped with a fluid module. Samples were pre-treated with 35% hydrogen peroxide to remove organic matter and Calgon containing sodium hexa meta-phosphate, which acts as a dispersant. The samples underwent three successive 60-second measurement runs using sonication to break up aggregated particles. The third run of each sample was used for analysis to ensure complete disaggregation of particles.

Daily current run, which is analogous to wind run, is calculated as the total distance that the turbidity current travels past a measuring point during a 24-hour period. Where tilting current meters were deployed, the meter detection limit is approximately 0.07 m s^{-1}. During these times, the velocity is assumed to be zero; therefore, the current run does not take into account any velocity variations below that value.

Chapter 5
Results and Discussion

5.1 Results

5.1.1 Slims River hydrology and sediment transport

In 2007, the Slims River discharge increased from 200 $m^3 s^{-1}$ on June 27 to a maximum of 300 $m^3 s^{-1}$ on July 24 (Fig. 5.1). The discharge exhibits strong diurnal variation, generally peaking between 2:30 and 5:30 in the morning and reaching a minimum approximately 12 hours later. The significant lag (>12 hours) between the time of maximum daily solar heating and the peak discharge is due to the large surface area of Kaskawulsh Glacier (2020 km^2) and the length of the proglacial drainage (20 km). The suspended sediment concentration (SSC) of the river also varies diurnally typically between 1 and 2 g l^{-1}, although the periodicity of the record is occasionally interrupted by anomalously high values. The density of the river water essentially mirrors the diurnal and longer-term changes in SSC; temperature and dissolved solids have only a minimal impact on the river water density. The mean particle size of the river dip samples typically ranges from 5 to 8 μm, but can reach upwards of 10 μm perhaps in response to local source variations such as bank slumps (Fig. 5.1). These values, however, are not representative of the average particles transported by Slims River since the water samples were obtained from the river surface. The fluvial suspended particle size is weakly correlated to SSC ($r^2 = 0.34$; $p=0.001$) and the relationship between particle size and discharge is insignificant.

The effects of mean daily temperature and total daily precipitation (Fig. 5.2) on Slims River discharge are not clearly evident in 2007. There is an insignificant correlation between discharge and mean daily temperature; while the mean daily temperature exhibits no significant linear trend over the month of July (mean 12.3°C), discharge increases by 30%. Similarly, with

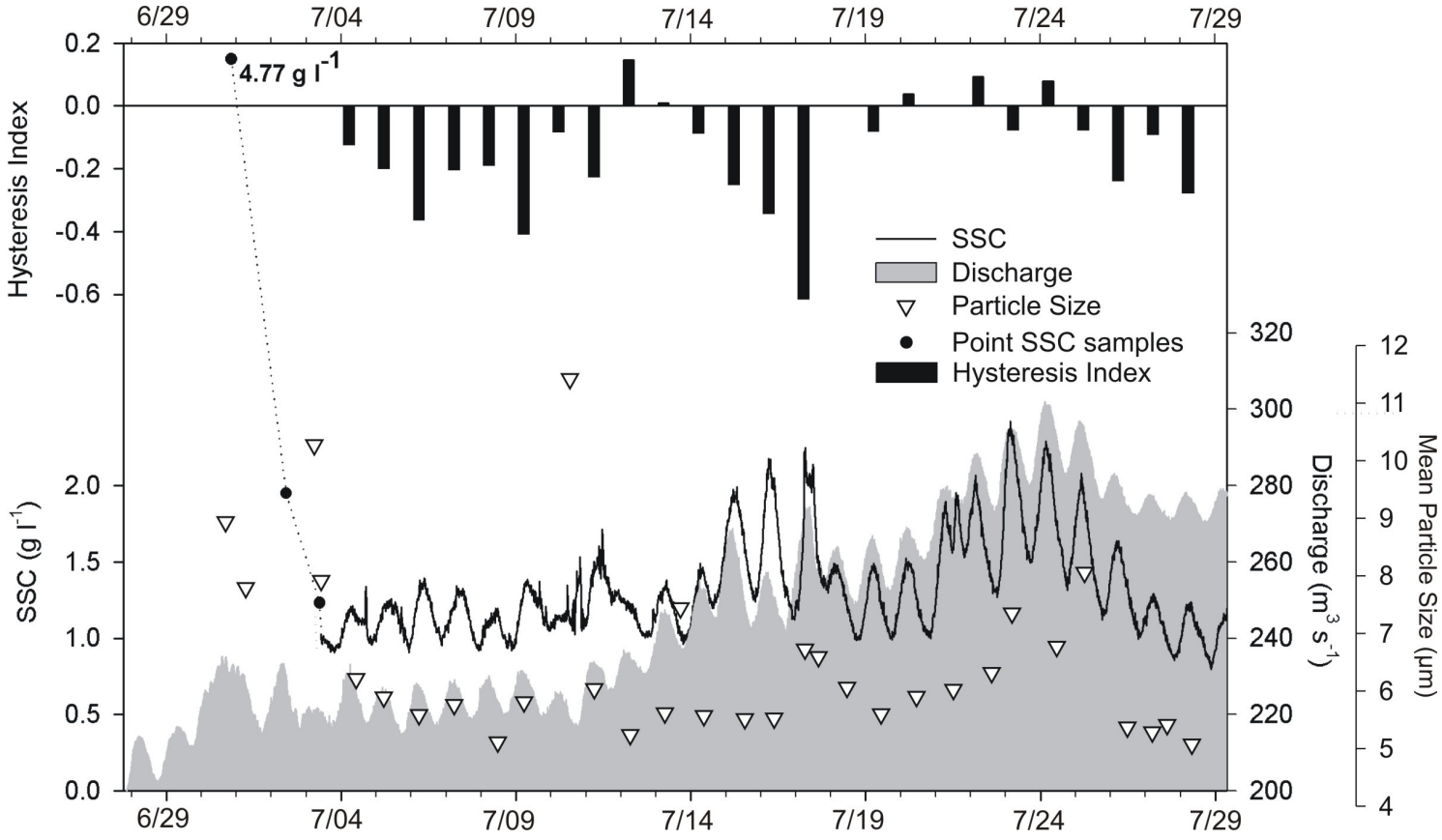

Figure 5.1 Slims River discharge, suspended sediment concentration (SSC), mean particle size, and hysteresis index (after Lawler et al., 2006) from June 27 to July 29, 2007. The turbidity meter was not installed prior to July 3; therefore the SSC record prior to that date is interpolated using point samples.

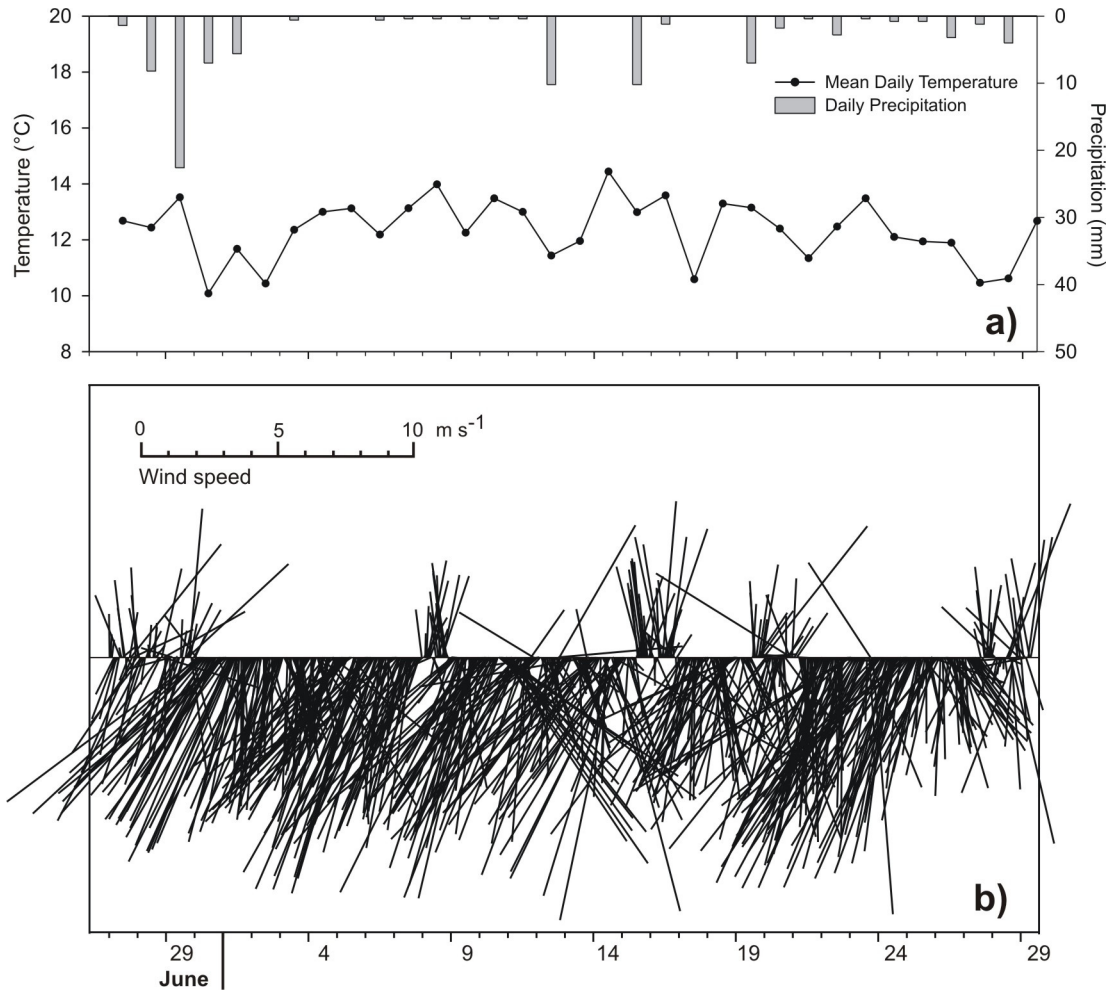

Figure 5.2 Meteorological characteristics at Kluane Lake for the 2007 field season from June 27 to July 29, including: a) mean daily air temperature and daily precipitation records from the Burwash MSC station, and b) the hourly average vector of wind speed and direction on the Slims River delta. See Figs. 5.1 and 5.2 for measurement locations.

the exception of the large rainstorm event of June 30 and July 1, precipitation events cannot be confidently associated with any changes in the discharge record. Because of the large watershed (5373 km^2) and highly regional precipitation patterns (Slocombe, 2001), the meteorological monitoring station at Burwash Landing is likely not representative of the entire Slims River basin; therefore, the data from the Burwash MSC station may contribute to the lack of relationship between river and meteorological records.

The flood that occurred from June 30 to July 1 can be distinguished in the discharge record likely because of the large magnitude and spatial extent of the rain event. The flood hydrograph extends over 48 hours and is relatively symmetrical in shape. This flood event is particularly notable because of its high suspended sediment load; the SSC (4.77 g l^{-1}) was over twice the maximum value observed for the rest of the monitoring season. Unfortunately, the turbidity monitor was not installed at this time; therefore, it was not possible to obtain a continuous record of SSC for this event.

The relationship between discharge and SSC in Slims River is complex and variable over time. Discharge explains only 33% of the variance of SSC during the monitoring period. This low correlation is partly due to a hysteresis relationship between SSC and discharge at multiple timescales. At a diurnal scale, the sediment transport regime is characterized by either a counterclockwise hysteresis relationship or a near-linear relationship between SSC and discharge, neither of which are commonly observed in glacial systems. The maximum daily SSC lags the peak daily discharge by an average of 2 hours. Examples of both types of diurnal hysteresis are shown in Fig. 5.3.

A hysteresis index (HI) developed by Lawler et al. (2006) is used to compare the magnitude of diurnal hysteresis relationships between suspended sediment concentration and discharge. A positive HI value indicates clockwise hysteresis, a negative HI value indicates

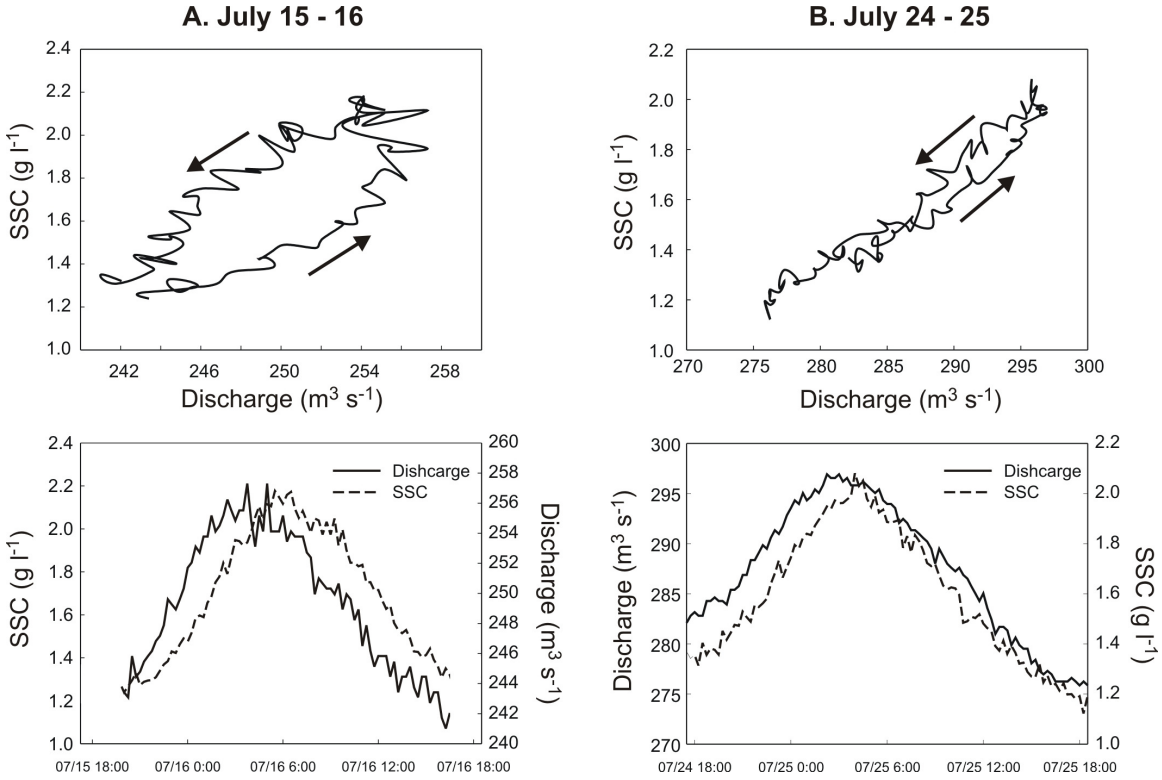

Figure 5.3 Typical relationships observed between suspended sediment concentration (SSC) and discharge in Slims River in 2007 during the study period. The upper panels show the diurnal hysteresis patterns over 21.5 hours on July 15-16 (A) and over 25 hours on July 24-25 (B), whereas the lower panels show the temporal variations of SSC and discharge for the equivalent time period. Arrows indicate the direction of the diurnal hysteresis. The time interval is 15 minutes for both discharge and SSC measurements.

counterclockwise hysteresis, and a zero HI value indicates no hysteresis. The index is calculated at the mid-value discharge (Q_{mid}), which is determined using:

$$Q_{mid} = k(Q_{\max} - Q_{\min}) + Q_{\min} \tag{5.1}$$

where k is the position at which the loop width is assessed relative to flow range, Q_{max} is the maximum discharge of the particular event, and Q_{min} is the discharge at the beginning of the event. A k value is chosen so that Q_{mid} represents the centre of the hysteresis curve, which is typically 0.5. Q_{mid} values were used to determine the suspended sediment concentration of the rising (rl) and falling limbs (fl) of the curve. For clockwise hysteresis, HI was calculated using:

$$HI = \frac{SSC_{rl}}{SSC_{fl}} - 1 \tag{5.2}$$

For counterclockwise hysteresis, HI was calculated using:

$$HI = \frac{-1}{SSC_{rl} \big/ SSC_{fl}} + 1 \tag{5.3}$$

A time series of the daily hysteresis index indicates that clockwise hysteresis occurs only rarely and often in association with anomalous SSC peaks on the falling limb of the hydrograph (Fig. 5.1). Because the hysteresis index has not previously been applied to the study of glacial rivers, a comparison with other glacial systems is not possible. When compared to values reported by others for an arctic catchment (McDonald, 2007) and an urban river system (Lawler, 2006), the Slims River hysteresis index values are relatively modest.

Hysteresis occurs not only diurnally in Slims River, but also over multiple-day periods. When the magnitude of the daily discharge volume is similar over the course of several days, the suspended sediment load is initially high, and then decreases significantly by 30 to 50%, which results in clockwise hysteresis at this time scale (Fig. 5.4). Variations in local sediment supply may also contribute to the low correlation between SSC and discharge. For example, several

incidents of anomalously high SSC events occur on July 4 and July 10 that are unrelated to a change in discharge (Fig. 5.1).

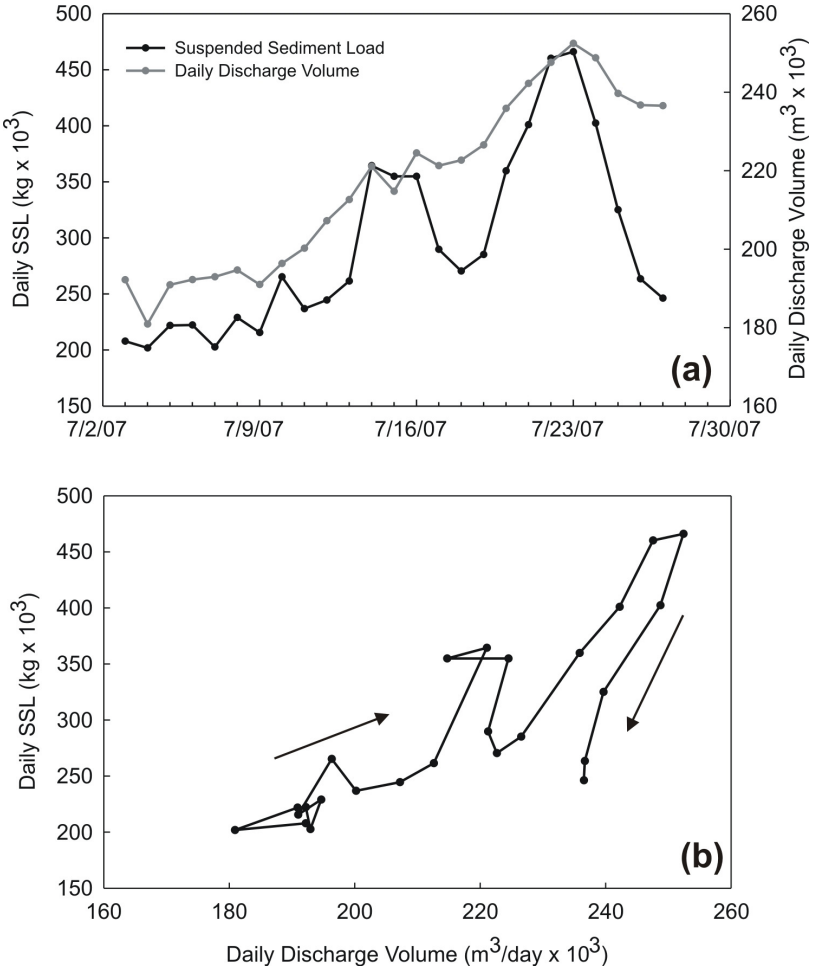

Figure 5.4 Sub-seasonal hysteresis pattern observed between daily suspended sediment load (SSL) and daily discharge volume in Slims River from July 3 to July 28 in 2007. Both the time series of discharge volume and suspended sediment load (a) and the sub-seasonal hysteresis patterns over 24 days (b) from July 3 to July 27, 2007. Arrows indicate the direction of the sub-seasonal hysteresis.

5.1.2 Lacustrine sedimentary processes

In 2006 and 2007, the Slims River outflow was oriented towards the island that is located in the prodelta region of Kluane Lake (Fig. 4.1). While part of the incoming water and sediment was directed to the east of the island, the majority was directed to the west. The inflowing sediment-laden water forms a visually distinct plunge line where its excess density causes it to sink to the lake bottom. Immediately lakeward of this plunge line, large billows of upwelling sediment were observed on numerous occasions, particularly during calm weather conditions (Appendix D). These billows measured between 0.5 and 1 m in width and were dynamic in nature, slowly changing their shape and size.

During peak melt season, the high suspended sediment load in the river generates turbid underflows that can be distinguished by CTD profiles (Fig. 5.5; Appendix E). While underflows are the primary mechanism of sediment distribution, the upper water column can become periodically charged with sediment. Classic interflows and overflows are not observed in Kluane Lake during the peak melt season, because the incoming river water is denser than the ambient lake water. Furthermore, the thermal stratification of the water column is inconsistent and weak and thus not conducive to interflow formation. However, CTD casts indicate that overflows occasionally form concurrently with underflows, particularly on days when strong underflows are observed (e.g. Fig. 5.6e). Minor interflows may also form along small deviations in the temperature profile (e.g. 5.6d). Satellite and aerial photographs also support the observation that an overflow plume may form at the same time as a plunging underflow (Appendix D).

The turbidity current water mass is distinctly different than the ambient water. The suspended sediment concentration (SSC) of the turbidity currents is much higher, up to 1.17 g l^{-1} greater, than the ambient water. Depending on the time of day, the temperature of the turbidity currents may be either cooler or warmer than the ambient water. Because the Slims River water

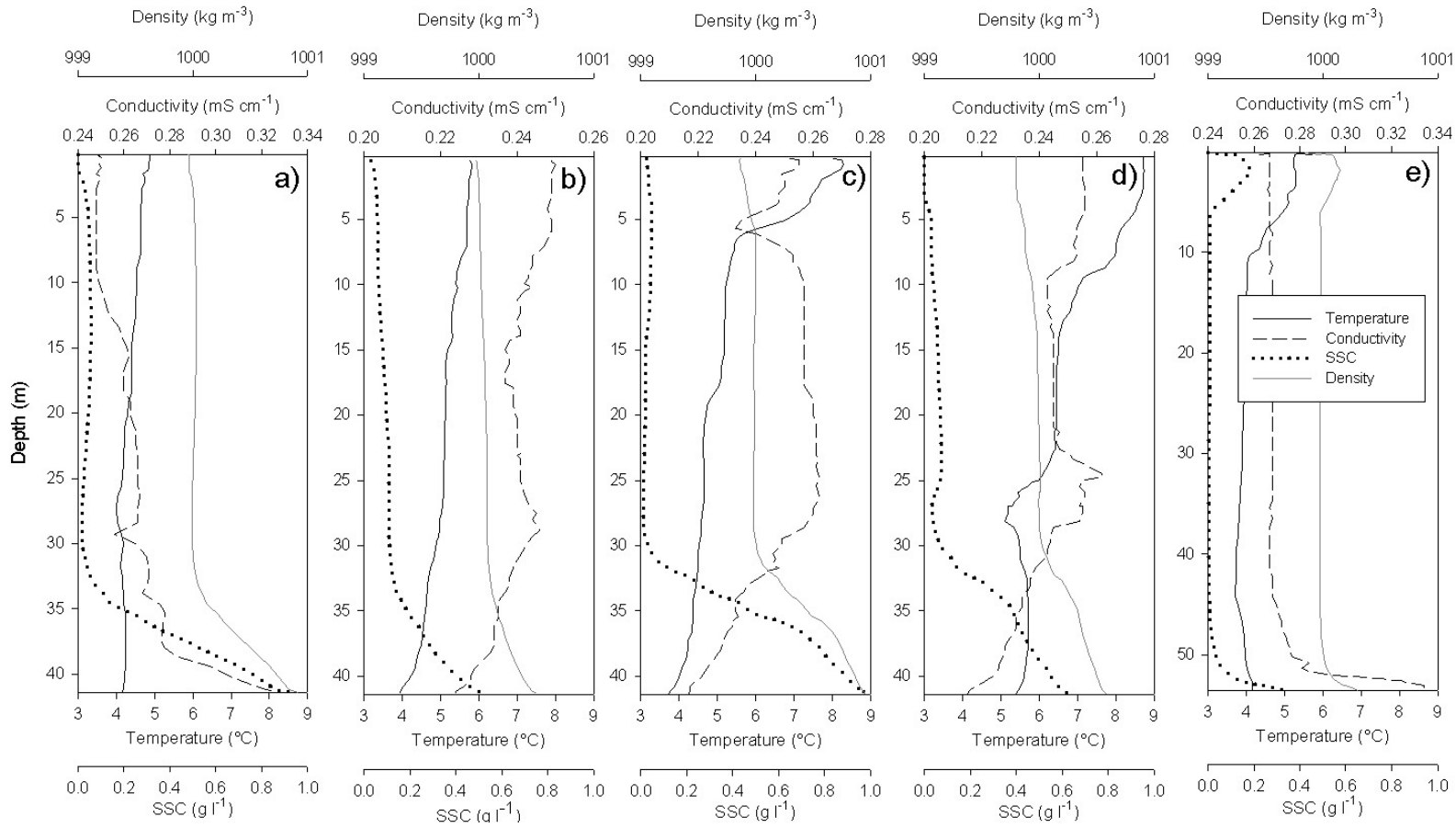

Figure 5.5 Several representative vertical profiles of temperature, conductivity, SSC, and density at Mooring D on a) June 30, b) July 10, c) July 24, and d) July 22 and at Mooring E on e) June 30. Note the difference in scale for the conductivity axes. Mooring locations are shown in Fig. 4.1.

is coolest (1.3 – 4°C; Appendix F) when the river water density is at a maximum, the largest volume of water being transported as a turbidity current in Kluane Lake is cooler than the ambient lake water temperature. The difference in density between the ambient lake water and the turbidity currents in Kluane Lake ranges from a maximum of 0.8 kg m^{-3} at delta-proximal locations to 0.02 kg m^{-3} at locations further lakeward.

The turbidity currents in Kluane Lake also have a distinctive conductivity signature (Fig. 5.5). The mean conductivity of Kluane Lake (240-270 μS cm^{-1}) is relatively high compared to other glacier-fed lakes (cf. Lillooet Lake 35-75 μS cm^{-1}, Hodder, 2007). The turbidity currents in Kluane Lake generally have a lower conductivity (~200 μS cm^{-1}) than the ambient water, except after the large rainstorm-induced flood on June 30, when the conductivity of the underflows was approximately 340 μS cm^{-1}. Conductivity variations at this scale only have a minimal effect on the formation of underflows; the density difference due to conductivity between the underflow water and the ambient lake water is typically on the order of 0.027 kg m^{-3}.

5.1.3 Turbidity current flow behaviour

5.1.3.1 Temporal and spatial flow patterns

The turbidity currents in Kluane Lake appear to be continuous at delta-proximal locations and fluctuate diurnally with peak velocities of over 0.6 m s^{-1} (Fig. 5.6). The minimum velocity measured by the EM current meter at mooring A is 0.035 m s^{-1}, although the velocity only rarely decreases below 0.2 m s^{-1} (Fig. 5.6). While the density of the ambient lake water was not monitored continuously, the maximum measured value (1000.17 kg m^3) is less than the minimum river density (1000.71 kg m^3), which supports the observation of continuous turbidity current activity in the prodelta area for the duration of the measurement period in 2007 (June 30 - July 29) and in 2006 (July 14 - 15). The velocity at mooring A lags the river density by 2 hours, as

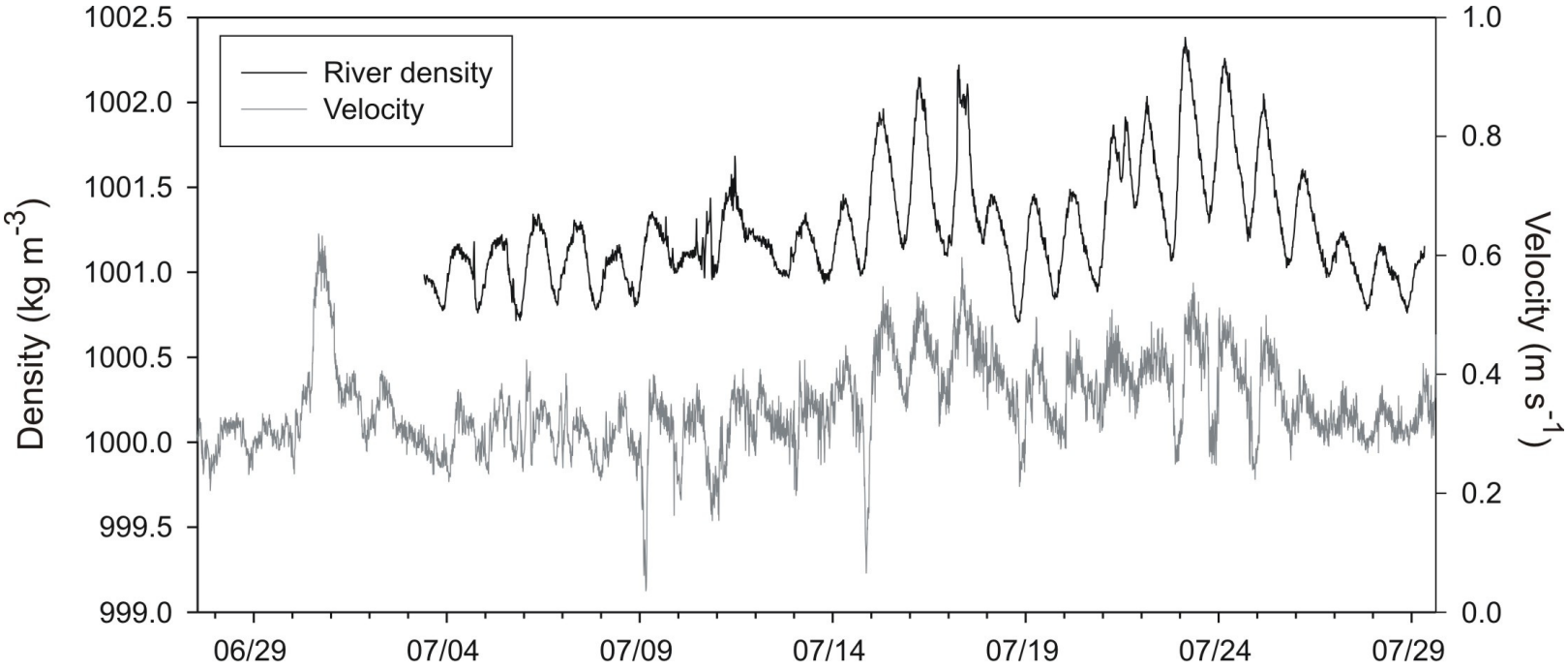

Figure 5.6 Comparison of 15-minute density of Slims River water at the river monitoring site with the turbidity current velocity record 1 m from the lake bottom at mooring A during the peak melt season of 2007. Density was calculated from temperature and SSC measurements (cf. Gilbert, 1975) and velocity was recorded by an EM velocity meter. See Fig. 4.1 for mooring locations.

determined by cross correlation analysis. At this lag, the river density record explains 57% of the variance in underflow velocity.

Variations in turbidity current velocity can be traced to a distance of at least 4.2 km from the delta at times of peak inflow (Fig. 5.7). Between mooring A and mooring G (a distance of 3.8 km), the maximum velocity decreases by 75% from 0.6 m s^{-1} to 0.15 m s^{-1}. While continuous turbidity currents are observed at a distance of 3 km from the delta (mooring F and L) from July 23 to 26, by 4.2 km from the delta (mooring G), turbidity current activity is detected only irregularly. It is more difficult to assess the duration of the currents at distal sites, because the lower limit of detection for the tilting current meters is approximately 0.07 m s^{-1}. At distal sites, however, low-velocity flow (< 0.07 m s^{-1}) is likely common and periodic or possibly continuous turbidity current may be occurring. The temperature record near the lake bottom at mooring G shows episodic increases in temperature that appear to be associated with peaks in velocity (Appendix F). This pattern suggests non-continuous flow at distal locations, although the indirect nature of this type of measurement prevents a definitive conclusion.

Because of the nature of glacial meltwater production, the turbidity current velocity fluctuates diurnally; however, unlike the river density record, the diurnal underflow velocity and SSC pattern is asymmetrical or sawtooth-shaped (Fig. 5.7). The velocity typically rises rapidly to

---

Figure 5.7 (next page) Variations in turbidity current velocity at various locations along longitudinal transects beginning west of the island (A) and east of the island (B) during the peak melt season. An EM current meter was installed at mooring A and B, whereas tilting current meters were installed at all other moorings. All velocity measurements were taken 0.5 m from the bottom. Gaps in the record indicate times when the current velocity decreased below the detection limit of the tilting current meters and a dashed line indicates when no data were available because of instrument malfunction. Distances from the delta front are indicated for each mooring. See Fig. 4.1 for mooring locations.

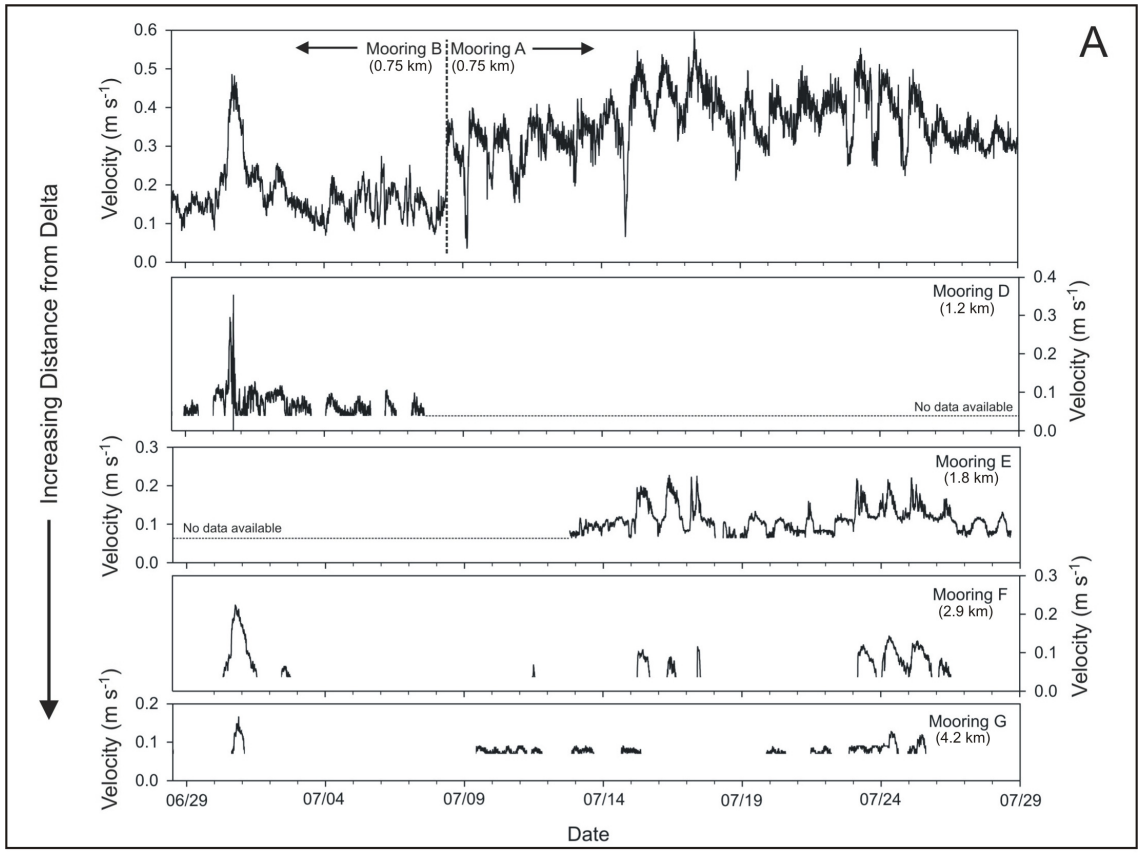
A
Mooring B
(0.75 km)
Mooring A
(0.75 km)
Mooring D
(1.2 km)
No data available
Mooring E
(1.8 km)
No data available
Mooring F
(2.9 km)
Mooring G
(4.2 km)
Velocity (m s-1)
Increasing Distance from Delta
06/29
07/04
07/09
07/14
07/19
07/24
07/29
Date

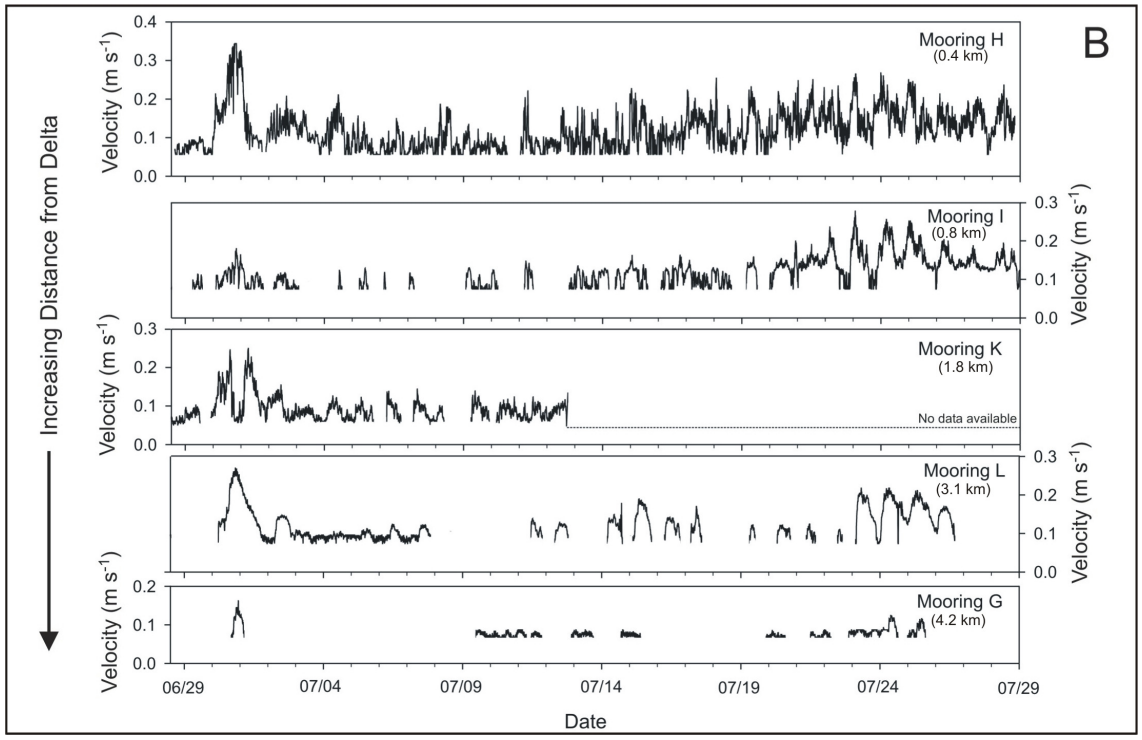
B
Mooring H
(0.4 km)
Mooring I
(0.8 km)
Mooring K
(1.8 km)
No data available
Mooring L
(3.1 km)
Mooring G
(4.2 km)
Velocity (m s-1)
Increasing Distance from Delta
06/29
07/04
07/09
07/14
07/19
07/24
07/29
Date

a maximum velocity between 2:00 and 7:00 a.m. (average 4:30 a.m.) then decreases more gradually to a minimum around midnight. When the turbidity current flow is particularly fast (e.g. June 23-25; Fig. 5.7), the velocity increases rapidly to its maximum, decreases very gradually over 16-20 hours, and then decreases rapidly by 0.2 m s^{-1} over a 1-hour period. The velocity remains at this level for approximately 5 hours, before rapidly increasing as the next diurnal cycle begins.

Sub-diurnal fluctuations in velocity are superimposed on the daily velocity pattern. Instantaneous downstream velocities may be up to 35% higher than the mean downstream velocity. High-frequency fluctuations (< 45 seconds) are more pronounced at higher velocities; the standard deviation of the current velocity over 45 seconds (5-second sampling interval) increases from 0.007 m s^{-1} at a mean velocity of 0.1 m s^{-1} to over 0.05 m s^{-1} at a mean velocity of 0.5 m s^{-1} (Fig. 5.8). Lower frequency variations can also be observed in the 10-minute averaged velocity record. Wavelet and spectral density analysis did not detect any dominant periodicity in the velocity fluctuations at any timescale less than 24 hours.

The average current direction for turbidity current flow at mooring A is 61° from true north, which is roughly perpendicular to the isobaths at that location (Fig. 5.8). When the velocity is averaged over 45 seconds (5-second sampling interval), the current direction varies between 50 and 90°. However, the current direction exhibits significant higher frequency fluctuations; raw current direction measurements (5-second, unaveraged measurements) range from 0 to 130°. This magnitude of variability is only observed at high velocities (> 0.2 m s^{-1}), and the standard deviation of the current direction increases as the mean velocity increases.

The rainstorm-induced flood that occurred from June 30 to July 1, while unexceptional in discharge magnitude, delivered a large amount of suspended sediment to Kluane Lake. The high SSC caused a large turbidity current event that extended well past the farthest mooring (4.2 km

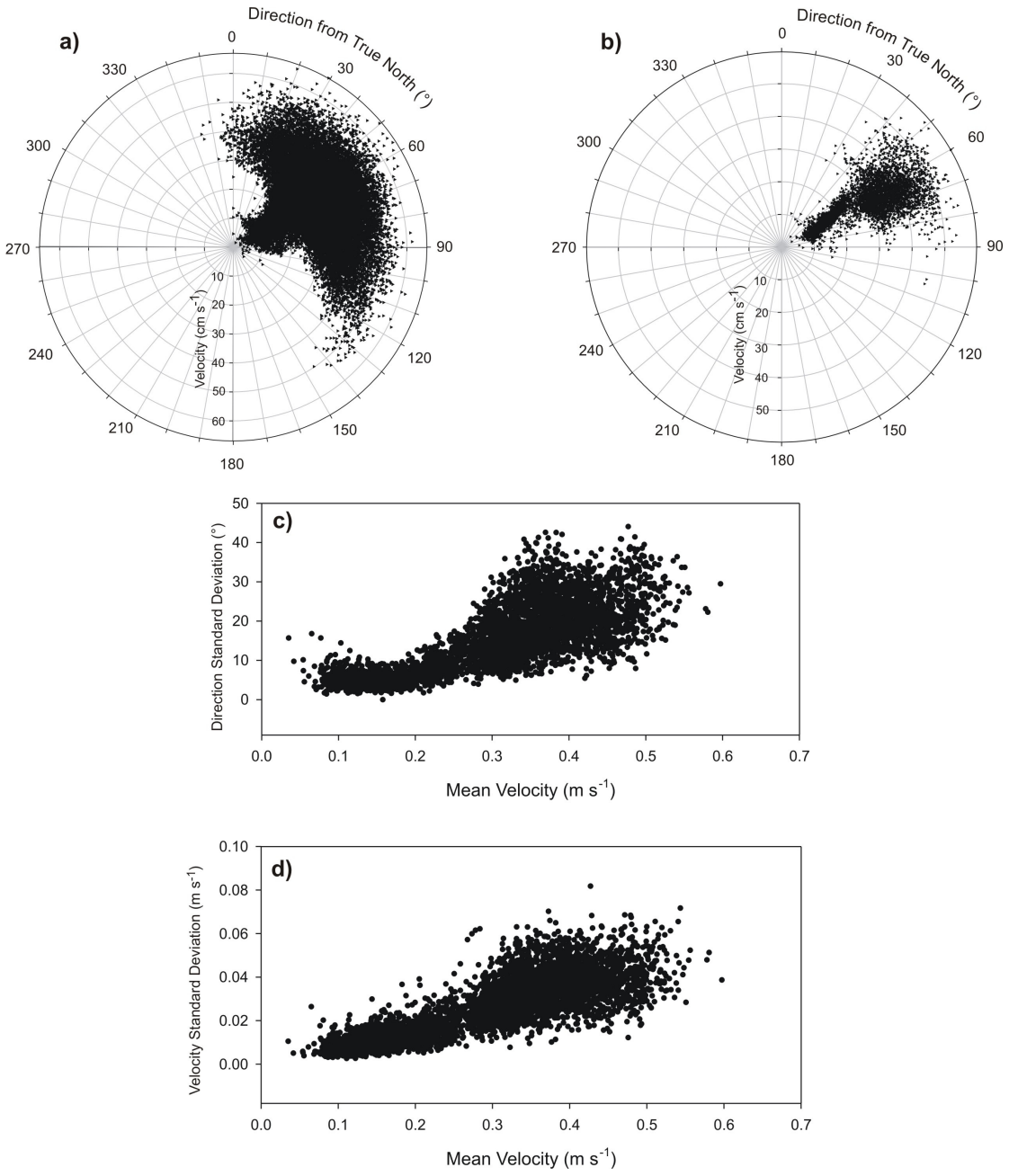

Figure 5.8 Range of turbidity current velocity and direction recorded at mooring A by an EM current meter from June 27 to July 29, 2007 in Kluane Lake, including: instantaneous velocity and current direction (a), velocity and current direction averaged over 45 seconds (5-second sampling interval) (b), average velocity over 45 seconds (5-second sampling interval) compared to the standard deviation of the instantaneous current direction (c) and instantaneous velocity (d) over the 45-second interval. See Fig. 4.1 for mooring location.

from the point of inflow). While the flood velocity was not particularly exceptional at delta-proximal moorings, the flood caused the highest recorded velocities of the measurement period at locations > 3 km from the delta (Fig. 5.7).

5.1.3.2 Velocity and concentration vertical profiles

At mooring D, three current meters were deployed 0.5, 1.0, and 1.5 m from the lake bottom over the course of three days. The velocity at 1.0 m is consistently higher than at the other two heights, while the minimum velocity occurs at 0.5 m (Fig. 5.9). The vertical velocity profile can be interpolated by applying the model developed by Kneller et al. (1999) (Fig. 5.10). The variance of the velocity record from the middle current meter is less than both the lower and upper meters.

The vertical suspended sediment concentration profiles of turbidity currents in Kluane Lake show distinctive changes in shape along a longitudinal gradient (Fig. 5.10). Closest to the delta (mooring A), the concentration profile increases roughly linearly to the maximum value. At mooring C and D (300 m and 450 m farther out, respectively), the current thickness increases dramatically and the maximum concentration near the lake bed decreases. At these locations, an inflection point can be more readily distinguished and the thickness of the profile can be easily measured. From 1.7 to 4.5 km from the delta (mooring E to G), the suspended sediment load decreases dramatically and the concentration profiles are approximately vertical, showing only a minimal gradational increase in concentration near the lake bottom.

5.1.3.3 Froude number calculations

Froude number (Fr) calculations are performed in order to define areas of supercritical (Fr > 1) and subcritical (Fr < 1) flow in Kluane Lake. The densiometric Froude number (Fr_d) is a

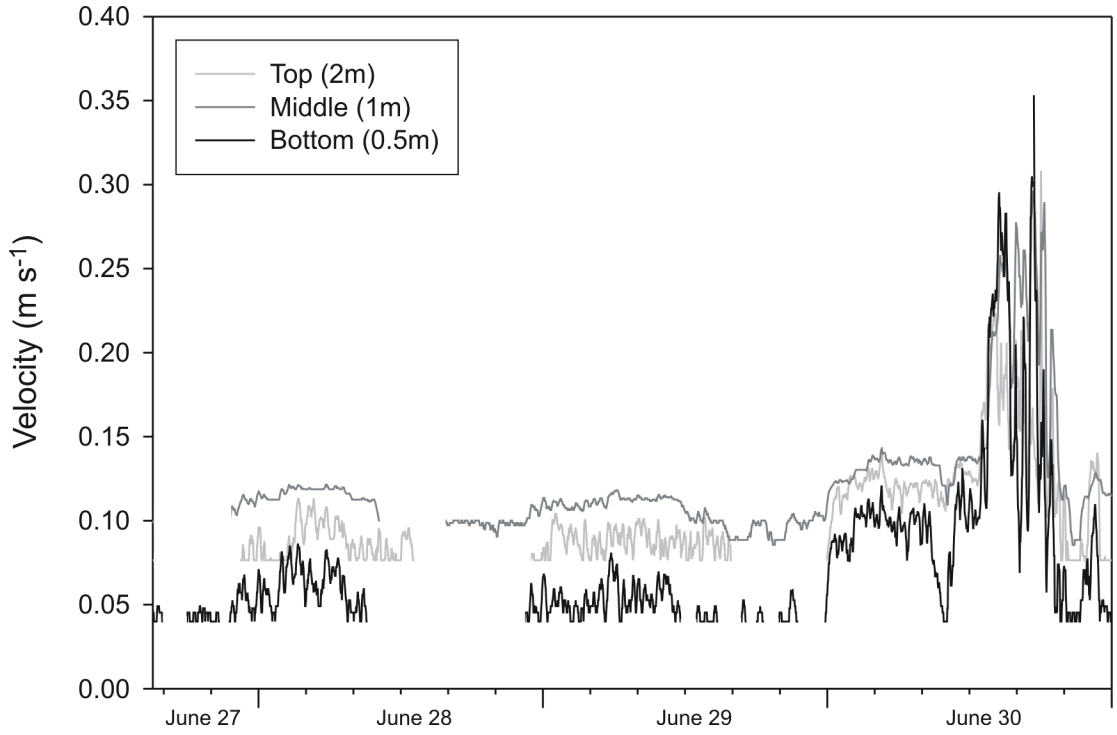

Figure 5.9 Velocity records from June 27 to June 30, 2007 for three tilting current meters at mooring D (see Fig. 4.1 for mooring location) located 0.5, 1, and 2 m from the lake bottom. Sampling interval was every 2 minutes, which was then averaged over 10 minutes. Gaps in the record indicate times when the current velocity decreased below the detection limit of the current meters. The lower limits of detection for the meters at 0.5, 1, and 2 m from the lake bottom are 0.04, 0.09, and 0.07 m s^{-1}, respectively.

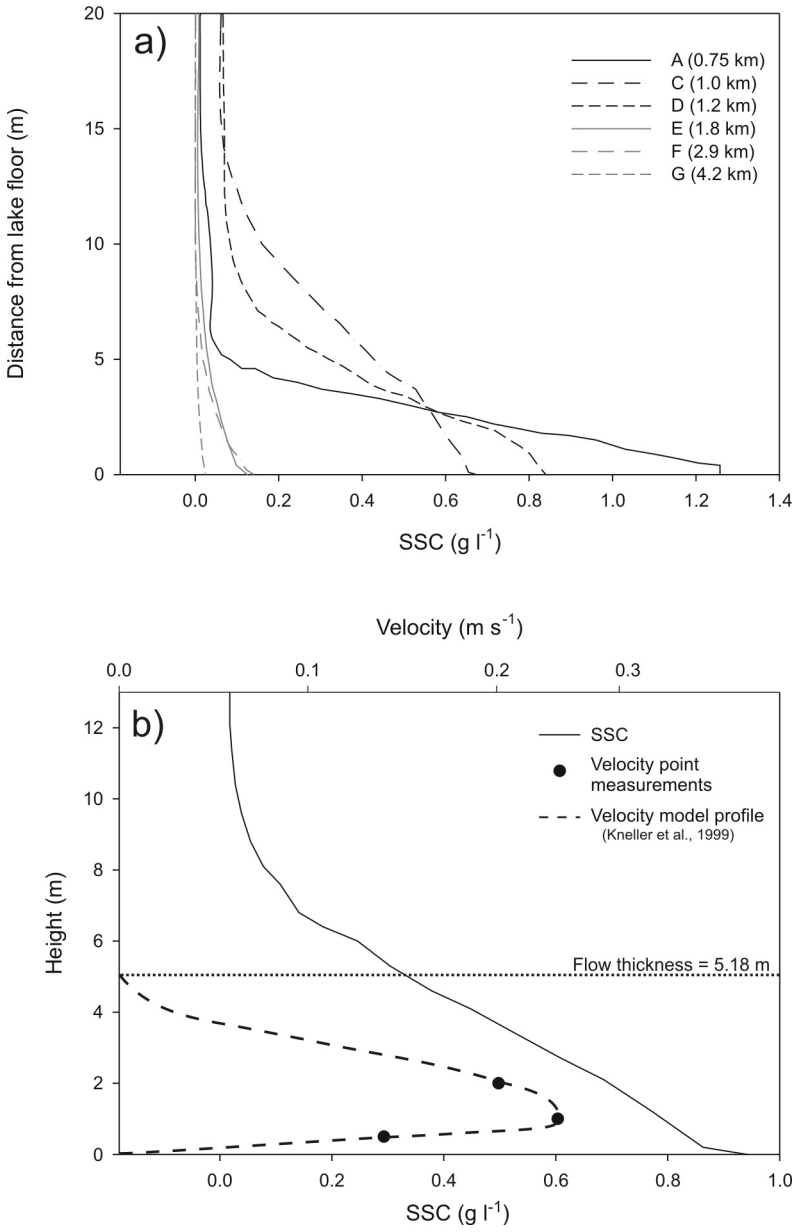

Figure 5.10 a) Representative suspended sediment concentration vertical profiles completed on July 15 along a longitudinal transect away from the delta, where mooring A is the closest profile to the delta and mooring G is the furthest. Distances from the delta are indicated for each mooring. b) Vertical SSC and velocity profile for mooring D at 16:30 on June 30, 2007. The velocity profile is based on three measurement points by tilting current meters and model results from Kneller et al. (1999). See Fig. 4.1 for mooring location.

dimensionless number proportional to the square root of the ratio of inertial to reduced gravity forces and is given by the expression:

$$Fr_d = \frac{U}{\sqrt{\left(\frac{\delta\rho}{\rho}\right)gD}} \tag{5.4}$$

where U is the average flow velocity, D is a typical flow dimension such as flow thickness, g is the acceleration because of gravity, δρ is the density difference between the ambient lake water and turbidity current water, and ρ is the density of the ambient water. These calculations were performed using CTD data (for density and thickness) and current meter data (for velocity). The current meters were all stationed 0.5 m above the lake floor and are assumed to represent the mean velocity.

The Froude numbers for the turbidity currents in Kluane Lake appear to be quite large with values of over 7 apparent at both proximal and distal locations; typical values range between 1 and 3 (Table 5.1). Subcritical flow conditions are only calculated to occur at mooring D. No longitudinal pattern in the Froude number is apparent; in fact, values at distal locations are often in excess of values at locations closer to the point of inflow. The velocity, density, and flow thickness values used to calculate the Froude numbers are given in Appendix G.

5.1.3.4 Sediment transport

By calculating the area under the curve of a suspended sediment profile, the suspended sediment load (SSL) contained within a volume of water with the dimensions 1 m^2 x depth may be determined at a given location and time by assuming a spatially consistent SSC value over an area of 1 m^2. Because velocity data are not available at all mooring sites for the whole monitoring period, the instantaneous SSL was not multiplied by the velocity of the current and, consequently, the SSL values reported have atypical units (kg m^{-2}). To compare the SSL in the

Table 5.1 Froude numbers for turbidity currents in Kluane Lake at various locations and times. Shaded cells indicate supercritical flow conditions. Blanks indicate times when no turbidity current activity was detected (i.e. velocity was below the resolution of the current meter) and "n/a" indicates times when no data are available. Data used to calculate these values are shown in Appendix G. Mooring locations are shown in Fig. 4.1

Mooring	Distance from Delta (km)	June 30 15:30	July 2 10:30	July 4 9:00	July 6 10:30	July 8 12:00	July 10 10:30	July 13 13:00	July 15 12:00	July 18 9:00	July 20 10:00	July 22 15:00	July 24 9:00	July 26 9:00
H	0.4	2.8	n/a	4.2	1.6	1.5	1.6	1	1.6	1.4	2	2	5.6	1.6
A	0.75	4.2	n/a	7.4	4.5	3.9	1.7	1.5	2.5	2.5	3.9	n/a	3.9	3.2
I	0.8	0.6	n/a	1.04	0.69	n/a	n/a	n/a	n/a	n/a	n/a	n/a	n/a	n/a
D	1.2	3.1	n/a	2.1	1.4	n/a	2.2	1.1	1.4	1.2	2.4	2.4	5.6	3.1
K	1.8	3.8	4	5.5	2.5	1.2	1.9	n/a	n/a	n/a	n/a	n/a	n/a	n/a
E	1.8	n/a	n/a	n/a	n/a	n/a	n/a	1.9	5.3	4.1	2.0	2.0	3	1.2
F	2.9	3.0	2.3			n/a			2.4				2.1	1.6
L	3.1	5.0	4.8	7.5	4.75	5.0		2.2	n/a				n/a	2.4
G	4.2								n/a				n/a	1.8

currents along a longitudinal transect, one must also assume that: a) variations in suspended sediment profiles are negligible over the one hour it takes to conduct the suspended sediment profiles; and b) the lateral spreading of turbidity currents is also negligible.

The mass of sediment in suspension within the underflows in Kluane Lake shows a consistent pattern distally (Fig. 5.11b). The instantaneous SSL of turbidity currents at mooring A is generally lower than at mooring C or D, which are located 250 and 450 m further lakeward respectively (see Fig. 4.1 for mooring locations). Mooring A not only is closer to the river inflow, but also experiences turbidity current velocities that are over twice as high. From mooring C lakeward, the SSL exponentially decreases from 5 kg m^{-2} to <1 kg m^{-2} by 4.2 km from the delta. On days when the turbidity currents have greater velocity, the suspended sediment load is higher at both proximal and distal locations; therefore, more material is being transported further into the lake (i.e. the runout distance is greater).

5.1.4 Sedimentation patterns

5.1.4.1 Bottom surface sediments

Four river bottom sediment samples were dredged from the bed of Slims River downstream of the river monitoring site. Mean particle size of these samples (17-31 μm) is significantly higher than the suspended particles collected through water dip samples from the

Figure 5.11 (next page) Longitudinal variations in a) slope (mooring locations indicated by red triangles); b) instantaneous turbidity current suspended sediment load (SSL) (grey lines) and mean SSL (black points) on 14 dates between June 30 and July 29; c) textural properties (geometric mean particle size and particle size distribution) of bottom sediments; d) water content of lake bottom sediments; and e) average diurnal mass accumulation rate (MAR) along the west transect (mooring A through mooring G), except where indicated, from June 27 to July 29, 2007. The east transect passes through moorings H, I, J, K, and G (see Fig. 4.1 for mooring locations).

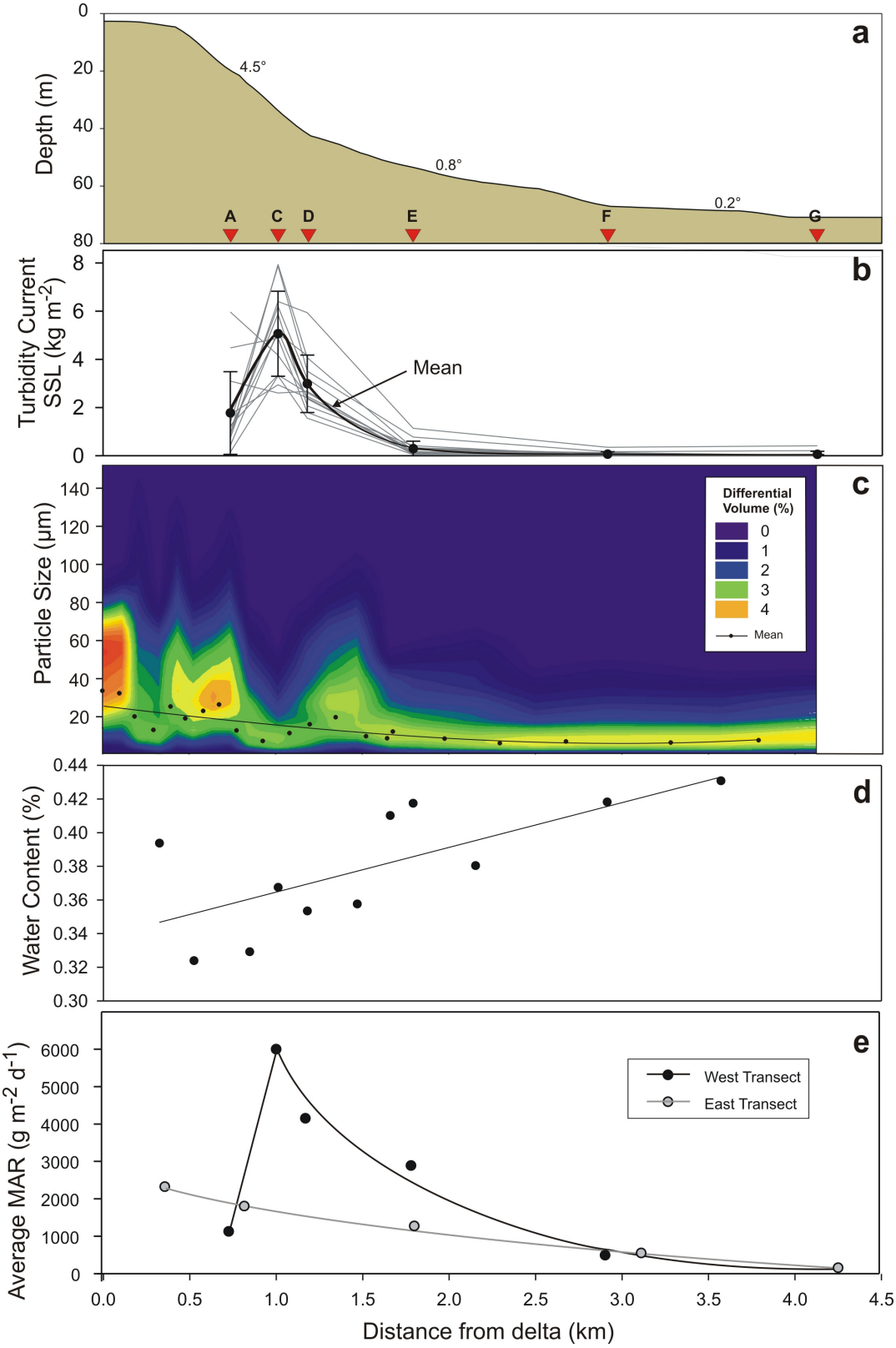
a
Depth (m)
0
20
40
60
80
4.5°
0.8°
0.2°
A
C
D
E
F
G
b
Turbidity Current SSL (kg m-2)
0
2
4
6
8
Mean
c
Particle Size (µm)
20
40
60
80
100
120
140
Differential Volume (%)
0
1
2
3
4
Mean
d
Water Content (%)
0.30
0.32
0.34
0.36
0.38
0.40
0.42
0.44
e
Average MAR (g m-2 d-1)
0
1000
2000
3000
4000
5000
6000
West Transect
East Transect
0.0
0.5
1.0
1.5
2.0
2.5
3.0
3.5
4.0
4.5
Distance from delta (km)

river surface (typically 5 to 8 μm); this difference in particle size is likely an artifact of the river sampling technique. In the lake, the mean particle size of the bottom sediment is highly variable, although there is a weak decreasing trend from 21 μm at delta-proximal locations to 5 to 7 μm by 1.5 km from the delta (Fig. 5.11c). Beyond 1.5 km, the mean particle size is remarkably consistent in both its distribution and mean. Mean particle size is correlated to distance from the delta ($r^2 = 0.65$; $p < 0.001$). The sand content of the lake bottom is less than 10% near the point of inflow and beyond 2.4 km from the delta is less than 1% with some samples containing no sand whatsoever (Gilbert and Crookshanks, in press). The sediment is composed of up to 50% clay size particles (< 4 μm), with the remaining and largest fraction composed of silt (50-80%). These results are consistent with the results of Bryan (1974c) who found that the mean grain size in Kluane Lake varied from 15 to 32 μm within 3 km of the delta, decreasing to 8 μm by 7 km from the delta.

The sediment in Kluane Lake is extremely unconsolidated; the water content of the surface sediments was calculated to be 30-50% of the weight of the sediment (Fig. 5.11d). This range of values is approximately twice as high as the water content in other glacilacustrine environments (e.g. Gilbert, 1975) and is consistent with the water content in sediment cores from the south end of Kluane Lake (Brahney, 2007). The water content is weakly correlated to both distance from the delta ($r^2 = 0.51$; $p = 0.01$) and mean particle size ($r^2 = 0.49$; $p = 0.02$).

5.1.4.2 Mass accumulation rate

The mass accumulation rate (MAR) along the lake bottom shows significant spatial variation during the measurement period in 2006 (July 14 to July 25; Fig. 5.12). The MAR averages approximately 4000 g m^{-2} d^{-1} at the delta-proximal locations, but decreases to approximately 180 g m^{-2} d^{-1} by 4 km from the delta. Along the far east side of the lake, settling

from the surface is more important relative to other sites in the prodelta region (Fig. 5.12); this difference is likely attributable to the influence of the Coriolis effect on surface plumes as well as the lack of turbidity current activity along the east shoreline.

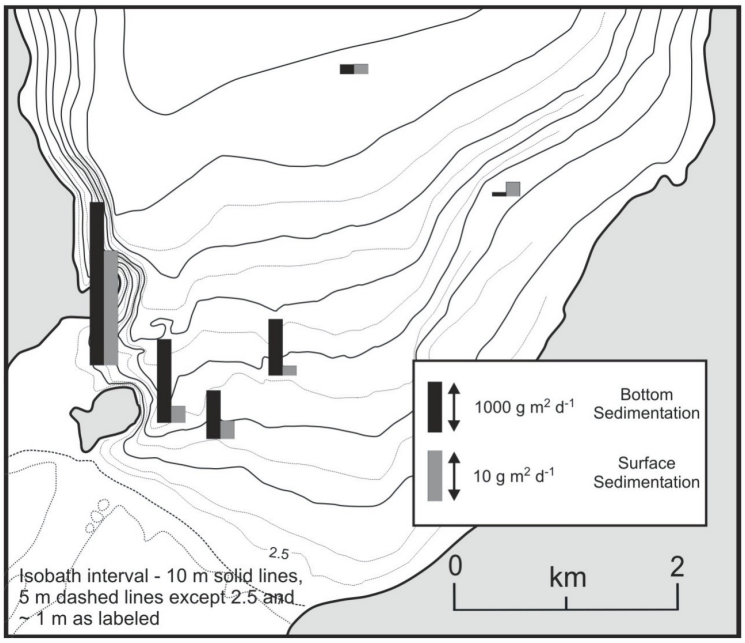

Figure 5.12 Bathymetric map of the prodelta region of Kluane Lake showing the average mass accumulation rate near the lake bottom (0.75 m from the lake floor) and at the lake surface (approximately 1m depth) from July 14 to July 25, 2006. Note that the lake bottom MAR scale is 100 times that of surface MAR.

Sedimentation in 2007 was much greater, accumulating at a rate of up to 6000 g m^{-2} d^{-1}. Increased sampling in 2007 allowed the spatial variations in MAR to be explored in more detail. The longitudinal pattern of MAR along the transect to the west of the island is similar to that of the turbidity current SSL; the maximum accumulation does not occur at the mooring closest to the delta, but instead at a mooring 1 km from the delta (Fig. 5.11e). Along the transect to the east of the island, the sedimentation rate was much lower at delta-proximal locations and, unlike the western transect, the maximum accumulation occurred closest to the delta.

The sedimentation rate is highly variable not only through space, but also over time. For example, in 2007 the MAR, at all but one mooring, increased by 30 to 200% during the second half of the monitoring season, a change that coincides with increased turbidity current activity. At mooring A, however, the MAR decreased substantially from over 2000 g m^{-2} d^{-1} for the period of June 27 to July 8 to under 200 g m^{-2} d^{-1} for the rest of July. This accumulation rate is exceptionally low; for example, the MAR at mooring G (4.2 km from the delta) is greater than at mooring A (750 m from the delta) for the period from July 8 to 29. CTD casts at mooring A indicate that the maximum suspended sediment concentration of the turbidity currents remained high (0.7 to 1.3 g l^{-1}) throughout July; therefore, sediment was being transported past this location, but was not being deposited. During the initial period of trap deployment (June 27 to July 8), 52 g of sediment were preserved at mooring A, including detailed internal sedimentary structures that show no effects of disturbance (Appendix H), whereas at mooring C, the next mooring downlake, the sedimentation rate was 4 times greater. These observations indicate that a) some change in either flow structure and/or depositional processes was occurring between these two locations, and b) that this difference was enhanced as the flow increased in strength during the latter half of July.

5.1.4.3 Sediment trap cores

Because of the extremely underconsolidated nature of the sediment in Kluane Lake, the sediment in the traps underwent significant dewatering during the process of core preservation, transportation to the laboratory, and core splitting. The sediment typically shrank by over 50% of its original volume, resulting in the loss of significant detail in the sedimentary record. Photographs of the clear plastic traps taken in the field soon after trap recovery show distinct laminations (Appendix H), yet these laminations were not as apparent after the sediment was dried.

The sediment trap core from mooring D retained distinct laminations that can be linked to the variations in velocity at that location (Fig. 5.13b). These laminations are likely a result of variations in textural characteristics generated by the diurnal velocity cycle. Because the laminations are so thin, particle size analysis could not be undertaken to verify differences in particle size. However, thin section microscopy analysis suggest that the darker laminations are finer and thus associated with diurnal velocity minima.

While the fine laminations in the sediment trap core from mooring D can related to the velocity record with reasonable confidence, the laminations present near the top of the sediment trap core from mooring C are not as obviously diurnal in nature (Fig. 5.13a). Above the flood deposit, there are 10 bundles of two or three pale laminations at regularly spaced intervals separated by thicker, relatively dark sediment layers. The sediment above the flood unit was deposited over approximately 11 days (July 2 to July 12); however, only 10 diurnal peaks in

---

Figure 5.13 (next page) Photographs and characteristics of the laminated sediment that accumulated in cylindrical traps deployed 0.5 m above the lake bottom at mooring C from June 27 to July 12 (a) and mooring D from June 27 to July 8 (b) in 2007. The laminations are associated with diurnal fluctuations in turbidity current velocity, which were measured at mooring B (a) and mooring D (b). The velocity at mooring D was recorded by a tilting current meter at 2-minute intervals and averaged over 10 minutes, whereas the velocity at mooring B was recorded by an EM current meter and averaged over 45 seconds (5-second sampling interval) every 10 minutes. The resulting variations in textural characteristics (geometric mean particle size and particle size distribution) are shown in the left-hand panels of (a) and (b) (after Beierle et al., 2002) as well as overlain on the photographs. Gaps in the velocity record indicate times when the velocity decreased below the detection limit of the current meter. A photograph of a thin section of the laminated sediment in the upper part of the core from mooring C is also shown (c). The location of this thin section in the context of the sediment trap is indicated by the black rectangle in (a). For mooring locations see Fig. 4.1.

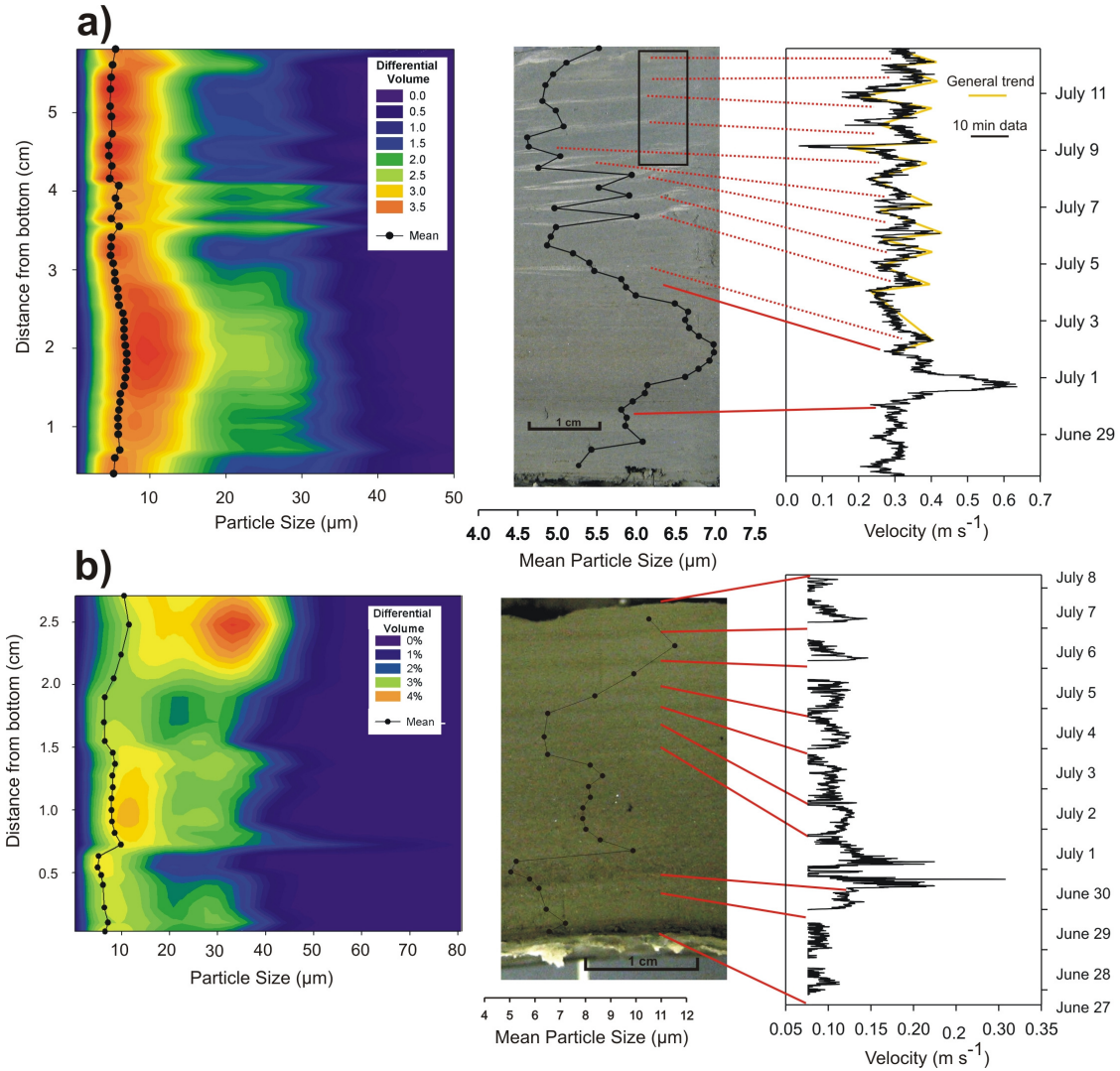
a)
Differential Volume
0.0
0.5
1.0
1.5
2.0
2.5
3.0
3.5
Mean
Distance from bottom (cm)
Particle Size (μm)
1 cm
General trend
10 min data
July 11
July 9
July 7
July 5
July 3
July 1
June 29
Mean Particle Size (μm)
Velocity (m s-1)
b)
Differential Volume
0%
1%
2%
3%
4%
Mean
Distance from bottom (cm)
Particle Size (μm)
1 cm
July 8
July 7
July 6
July 5
July 4
July 3
July 2
July 1
June 30
June 29
June 28
June 27
Mean Particle Size (μm)
Velocity (m s-1)


c)
crack
1 mm

velocity were measured, because no distinct velocity peak occurred on July 3. Therefore, the laminations can be tentatively associated with the velocity record, as shown in Fig. 5.13. Because of the small scale, sediment samples for particle size analysis could not be restricted to the laminations. However, bulk samples that included sediment from some of these laminations have a larger mean particle size (by approximately 1 μm) and contain coarser particles (from 15 to 53 μm) in greater quantity than the surrounding sediment. Closer examination of the sedimentology of these laminations using thin section analysis confirms that the laminations are composed of coarser sediment. Individual laminations vary in thickness from 0.3 mm to <0.01 mm (Fig. 5.13). It is unlikely that these laminations formed entirely as a function of the trap structure itself, because they are well preserved within the trap and can be associated with diurnal fluctuations in velocity at that location.

Diurnal laminations at moorings C and D do not form consistently over space or time. Diurnal laminations formed during a period of unexceptional velocity magnitude and range and did not form at the same locations later in the season, when both the mean velocity and diurnal velocity range were higher. At mooring D, the diurnal sediment accumulation is strongly correlated with daily mean particle size (Fig. 5.14). The daily current run (analogous to wind run) at mooring D is also inversely related to both mean daily particle size and diurnal lamination thickness (Fig. 5.14).

The particle size distribution (PSD) of the sediment deposited in the traps is generally consistent with the PSD of the surface sediment from the lake bottom. However, at locations near the delta, the PSD of lake bottom sediments often has a somewhat coarser tail than the sediment that is found in the traps. This observation suggests the traps, moored 0.7 m off the lake bottom, are not capturing the coarsest sediment, which is typically concentrated towards the lower part of the flow (Kneller and Buckee, 2000).

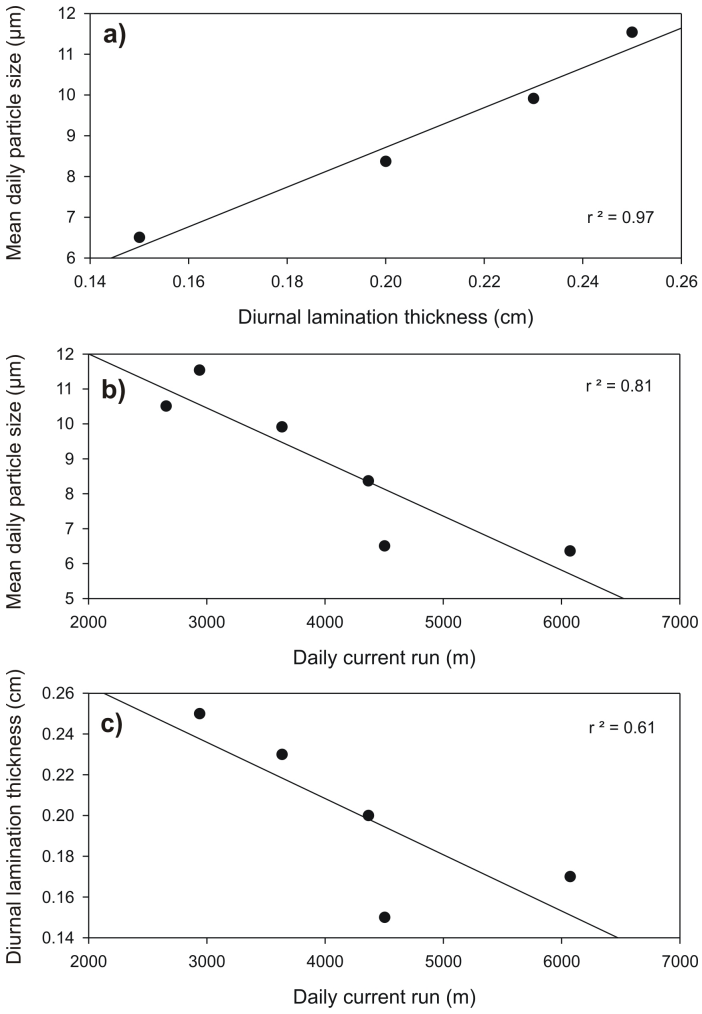

Figure 5.14 A comparison between the turbidity current flow characteristics and the sediment that accumulated in a trap deployed 0.7 m off the lake bottom at mooring D from June 27 to July 8, 2007. Linear correlations are shown for a) mean daily particle size and diurnal lamination thickness; b) mean daily particle size and daily current run (analogous to wind run); and c) diurnal lamination thickness and daily current run . Daily current run was calculated as the total distance that the water has traveled past a measuring point during a 24-hour period. Because current meter has a lower detection limit of 0.07 m s^{-1}, the current run calculations do not take into account fluctuations below that velocity and are, therefore, conservative values. For mooring location see Fig. 4.1.

The large flood of June 30 to July 1 resulted in the deposition of a large amount of sediment that can be visually distinguished in the sedimentary record. Approximately 2.5 times more sediment was deposited over the course of the two-day flood relative to the average sedimentation rate. At mooring C, the flood deposit is composed of an inversely-graded unit capped by a normally graded unit. Similarly, the maximum mean particle size of the flood deposit at mooring D does not occur at the base of the flood sequence, but instead in the middle of the sequence. Despite the ease with which the flood deposit can be visually distinguished in the sedimentary sequences at moorings C and D, the mean particle size in the flood deposit is at most 3 μm larger than the surrounding sediment and contains only minimal amounts of very fine sand (<2%). Similar deviations in mean particle size are observed in the flood deposits at other locations, although no sand is found in any of the other deposits. The organic matter of the flood deposit at moorings C and D is enhanced by 0.3 to 0.4% relative to the surrounding sediment (Appendix I).

5.2 Discussion

5.2.1 River discharge and suspended sediment dynamics

The occurrence of minor diurnal counterclockwise hysteresis between SSC and discharge in Slims River is highly unusual for a glacierized basin. Diurnal and seasonal clockwise hysteresis is widely reported in proglacial systems and generally attributed to sediment exhaustion (Østrem, 1975; Collins, 1979; Bogen, 1980; Hammer and Smith, 1984; Gurnell, 1987; Willis et al., 1996; Hodgkins, 1999). Only several cases of counterclockwise hysteresis have been observed in proglacial rivers. Hodgkins (1996) documents counterclockwise hysteresis in a river that drains a small arctic glacier on Svalbard where an ice-marginal drainage system structure was dominant. Sawada and Johnson (2000) also report diurnal counterclockwise

hysteresis in Slims River, but this relationship was observed only on several occasions in late June and early July and was attributed to the initiation of the subglacial drainage system. This explanation is unlikely in 2007, because counterclockwise hysteresis was observed in Slims River throughout July and the Kaskawulsh subglacial drainage system would have been fully functional during this time.

In non-glacierized basins, counterclockwise hysteresis has been most often attributed to a distal sediment source area. For example, in a classic study of the Bighorn basin in Wyoming, Heidel (1956) found a progressive lag in the arrival time of suspended sediment concentration as a flood traveled downstream, a finding that indicates that the sediment wave generally travels slower than the discharge wave. Hudson (2003) suggests that that this study area is unusual in that the dominant source of sediment is from a distal part of the basin.

In smaller basins, counterclockwise hysteresis has also been observed during intense flood events when the sediment source area is not the channel area, but rather the upper part of the slopes (Walling et al., 1979; Klein, 1984; Kurashige, 1994). In these situations, the distance from the centre of gravity of the sediment source area to the basin outlet is greater than the distance from the centre of gravity of water contributing area to the basin outlet; this distance causes a lag between the flood and sediment concentration maxima. Similarly, a study of an arctic catchment on Svalbard suggests that as the melt season progressed, the dominant sediment source migrated up-glacier and the overall area of meltwater generation expanded, resulting in a seasonal decrease in the lead of SSC over discharge (Gurnell et al., 1994). In the case of Kaskawulsh Glacier, the dominant sediment source probably migrates up-glacier as the melt season progresses. Because the ablation zone extends over 46 km during the melt season (Ewing, 1972), the primary sediment source area potentially could be located a significant distance from the ice margin. If the centre of gravity of the dominant sediment source was located up-glacier

from the centre of gravity of glacial meltwater production, a counterclockwise hysteresis relationship may be apparent in Slims River.

Another possible explanation for the counterclockwise hysteresis observed in Slims River involves riverbank slumping during the falling limb of the discharge cycle. This effect has been observed at Glacier Bay, Alaska where unstable bank sediment remained saturated and non-cohesive following a period of rapidly decreasing discharge, causing bank failure to occur in response to a steepened water table (Smith, N., pers. comm. 2008). Bank slumping is most common in fine, muddy sand, which is the dominant particle size of the Slims River sandur beyond 5 km downstream from the glacier (Fahnestock, 1969). However, for counterclockwise hysteresis to occur consistently for over a month, slumping would have to take place nearly every day and along a significant length of the river.

Finally, counterclockwise hysteresis may occur in Slims River if supraglacial meltwater is contributing relatively more to the rising limb of the diurnal hydrograph and subglacial meltwater is contributing relatively more to the falling limb. Glacial surface meltwater typically transports little sediment (<1 mg L^{-1}), except where surficial moraines or aeolian activity is significant (Tranter, 2005). Aerial and satellite photographs of Kaskawulsh Glacier indicate the presence of significant medial moraines; however, their contribution to supraglacial meltwater is relatively small (Ewing, 1972). While supraglacial meltwater channels frequently terminate in moulins, some supraglacial streams on Kaskawulsh Glacier discharge at ice-marginal sites or at the glacier terminus (Ewing, 1972). The relatively low SSC in supraglacial meltwater on Kaskawulsh Glacier, therefore, may form a significant contribution to the rising limb of the hydrograph and contribute to counterclockwise hysteresis between SSC and discharge in Slims River.

The lack of clockwise hysteresis suggests that relative sediment exhaustion is not a factor at a diurnal scale in Slims River; however, the availability of sediment for fluvial transport appears to decrease over the melt season. A mechanism within the subglacial or proglacial system, such as those discussed here, may offset this factor such that minor counterclockwise hysteresis or no hysteresis whatsoever is observed at a diurnal scale. The hysteresis relationship between suspended sediment concentration and discharge likely changes seasonally and interannually, depending on the hydrometeorological conditions (McDonald, 2007).

5.2.2 Lacustrine sedimentary processes

Turbidity currents dominate the sedimentary environment in Kluane Lake; settling from suspension accounts for less than 2% of total sedimentation in the prodelta region during the peak melt season in both 2006 and 2007. SSC profiles confirm that the largest mass of suspended sediment in the water column is consistently found near the lake bottom and velocity records indicate that this sediment is transported at speeds of up to 0.6 m s^{-1}. The maximum velocity of turbidity currents in Kluane Lake is comparable to those measured in other high-energy lacustrine environments (Table 2.1). Water temperature records show diurnal variations consistent with the fluctuations in velocity (Appendix F); this correspondence indicates that the turbidity currents were fluvially generated, as delta slumping cannot produce a cyclical change in water temperature.

Continuous lacustrine turbidity current activity, which is observed in Kluane Lake for an entire month during the peak melt season of 2007, has been occasionally documented in other glacial lakes, but generally only lasts for several days (cf. 50 hours Gilbert, 1975; 33 hours Lewis et al., 2002). Most turbidity currents in glacier-fed lakes are periodic in nature, wherein the diurnal melt cycle generates turbidity current activity for several hours every day at approximately the same time (Gilbert, 1975; Weirich, 1986a; Schiefer and Gilbert, in press). This

observation has led to the development of a duration-exceedance curve for turbidity current events that last from 0.2 to 50 hours (Schiefer and Gilbert, in press). In non-glacial environments, continuous turbidity current flow has been observed in Lake Superior associated with anthropogenic mine tailing discharge (Normark and Dickson, 1976) and over 9 days during spring thaw at Katsurazawa Reservoir in Japan (Chikita and Okumara, 1990).

The concurrent formation of overflows or interflows with underflows in Kluane Lake may be in part due to the billows that form off the plunge line (Appendix D). These billows are likely similar to what Pharo and Carmack (1984) have previously described as small-scale gyres (0 to 1 m), which shed off larger (0 to 100 m) cusps that form along the plunge line in Kluane Lake. The gyres display even smaller rope and/or drapery-like features (0 to 0.1 m) that appear to actively entrain ambient lake water and promote mixing within the sinking gyres. Mixing also probably occurs in response to strong winds, which reached velocities of up to 40 km h^{-1} on the Slims River delta during the measurement period in 2007 (Fig. 5.2). These mixing processes along the plunge line result in the water column becoming charged with sediment and likely contribute to the formation of overflows and interflows. Even if an overflow is slightly denser than the underlying ambient water, it may not not plunge to the lake bottom and form an underflow; underflows tend to form when the difference in density is greater than 0.19 kg m^{-3} (Weirich, 1986a). Strong katabatic wind conditions that blow along the Slims River valley may also assist in moving the overflow material downlake (Weirich, 1986a).

The high conductivity of the water in Kluane Lake is likely due to solute-enriched groundwater (150 to 3000 mg l^{-1}) that enters the lake from the south and the west (Harris, 1990). Because turbidity currents in Kluane Lake are formed typically by relatively fresh glacial meltwater, they can normally be identified by their lower conductivity. A spring rainstorm-induced flood event, however, resulted in the formation of high-conductivity turbidity currents.

The large solute load in the underflows during the flood is derived likely from the rapid flushing of solute-enriched groundwater. The soils on the Slims River delta are known to contribute a significant volume of high-salinity water to the river particularly during large rainstorms (Harris, 1990). Throughout the spring snowmelt, the frozen ground in the delta prevents the downward percolation of water and salts that drain from the adjacent mountains. By the end of June, the frozen layer becomes intermittent, allowing downward leaching into the groundwater and subsequently into the river and lake. The large rainstorm on June 30 and July 1 likely accelerated this leaching process, flushing the saline, muddy water from the delta surface into the river and from there into Kluane Lake where the water, solutes, and sediment were distributed as turbidity currents. This process may also occur during a summer rainstorm evaporated from the sandur surface, leaving the solutes to accumulate in the sediment. A large rainstorm may then flush the accumulated solutes into the Slims River system. The dissolved solute concentration of underflows in Kluane Lake, therefore, may be a useful signal of water source and routing during the melt season.

5.2.3 Turbidity current flow behaviour

5.2.3.1 Temporal variations

Previous studies have suggested a variety of mechanisms for unsteady flow conditions in density underflows. The pronounced sub-diurnal fluctuations in the velocity record of turbidity currents in Kluane Lake may be associated with variations in inflow characteristics related to changes in local sediment supply within the proglacial river (Hammer and Smith, 1983). While this process may account for some of the fluctuations, variations in inflow cannot be wholly responsible, because the fluvial SSC record does not show an equal range of variance. A shifting plunge line has also been invoked to describe velocity fluctuations in lacustrine turbidity currents

(Best et al., 2005); however, in Kluane Lake the plunge line is relatively constrained between the prodelta island and the shore, and thus is prevented from dynamic movement. Lambert et al. (1976) documented pulsating flow with a periodicity of 15 to 20 minutes in Walensee, Switzerland and ascribe this behavior to supercritical flow conditions. Normark (1989) similarly suggest that fluctuating flow velocities may reflect supercritical flow. While supercritical flow conditions may exist in Kluane Lake (see discussion below), the lack of a well-defined periodicity in the velocity record suggests that the fluctuations may simply relate to turbulent structures within the current. All turbulent flows, regardless of their Froude number, are inherently unsteady over short time scales because of the presence of large eddies and internal waves (Kneller et al., 1997, 1999). Instantaneous downstream velocities in experimental turbidity currents may be up to 40% higher than the maximum mean downstream velocity (Kneller et al., 1997; Buckee et al., 2001); this variance is comparable to the range measured in Kluane Lake (up to 35% higher than the mean downstream velocity). The larger variance of velocity and direction at high current velocities has also been observed in experimental currents. Kneller et al. (1997) found that the Reynolds stress, which is a measure of the turbulent energy within the current and equivalent to shear stress, is highest when the downstream velocity reaches a maximum. This finding has important implications for sedimentary processes, since the instantaneous downstream current velocity may be a better predictor of potential sediment entrainment than the mean downstream current velocity (Kneller and Buckee, 2000).

5.2.3.2 Vertical flow structure

The height of the maximum velocity in a turbidity current is a function of the ratio of the drag forces at the upper and lower boundaries (Middleton, 1966b; Kneller et al., 1997). In experimental flows, the maximum velocity is generally located 0.2d above the lower flow boundary for currents that flow over a smooth bed, where d is the flow thickness (Altinaker et al.,

1996; Kneller et al., 1997, 1999; Best et al., 2001). The flow thickness and velocity measurements from Kluane Lake are consistent with this experimentally derived relationship. For example, a CTD cast at mooring D on June 30 indicates that the thickness of the current is approximately 5.18 m (Fig. 5.10). The height of the maximum velocity from the bed at mooring D (approximately 1 m) is comparable to the theoretical value (1.04 m). The lower variance in the velocity record at the mid-current height may reflect lower turbulence at that location; turbulence is often generated near the upper and lower boundaries because of shear with either the bed or the ambient fluid (Felix et al., 2005).

The vertical concentration profiles of distal turbidity currents in Kluane Lake are generally consistent with the field measurements performed in other lakes (Normark, 1989; Chikita, 1989; Best et al., 2005); the sediment concentration gradually increases to the bed, following a gradational profile. These profiles are similar to those that laboratory experiments have observed in weakly depositional currents; the concentration profiles are generally smooth, where the concentration gradient is greatest near the bottom and decreases rapidly near the velocity maximum (Altinaker et al., 1996; Garcia, 1994). At mooring A, closest to the delta, the concentration profile typically shows very little evidence of mixing along its upper boundary, likely because it is located within 400 m of the plunge line. This particular profile is not similar to any experimental models described in the literature. The thick, stepped vertical concentration profiles observed at moorings C and D represent the transitional profile between proximal and distal sites. Because the velocity maximum is located below the inflection point, this type of profile is more similar to the stepped profile that has been observed in subcritical flows rather than erosional currents or currents with a high entrainment (Simpson and Britter, 1979; Garcia, 1993; Middleton, 1993). These comparisons point to the difficulty in applying experimental and theoretical models to the natural environment. While there appears to be a general

correspondence between theory and observation, the concentration profiles observed in Kluane Lake cannot easily be associated with known theoretical or experimental vertical concentration models. Various factors in the natural environment, including variations in inflow characteristics, slope, bed roughness, and ambient lake currents, may contribute to deviations from experimental models.

5.2.3.3 Froude number

The Froude number calculations for turbidity currents in Kluane Lake suggest that supercritical flow conditions dominate the prodelta region. The high Froude number values (up to 7) are particularly surprising at distal locations where subcritical flow conditions would be expected. While the velocity of the currents are relatively small at distal locations (0.1 to 0.2 m s^{-1}), the small flow thickness raises the Froude number values substantially. In experimental currents, Froude number calculations for supercritical flows are generally less than 5 and more typically between 1 and 3 (Hand, 1974; Mulder et al., 1997; Garcia, 1993). In natural lacustrine or marine environments, the calculation of the Froude number for turbidity currents has often been limited to several point measurements and relied on indirect inferences for one or more parameters (Menard, 1964; Gustavson, 1975; Lambert et al., 1976; Normark and Dickson, 1976; Weirich, 1984; Chikita and Okumara, 1990; Zeng et al., 1991; Best et al., 2005). Froude numbers that have been calculated for lacustrine systems have been both subcritical (Gustavson, 1975; Normark and Dickson, 1976; Chikita, 1989) and supercritical, ranging from 1.5 to over 10 (Lambert et al., 1976; Weirich, 1984; Chikita and Okumara, 1990; Best et al., 2005).

Of the variables used to calculate the Froude number of the turbidity currents in Kluane Lake, the flow thickness and mean current velocity values are most difficult to constrain. Convention suggests that the thickness should be measured at the inflection point of the vertical concentration profile (Middleton, 1993). However, inflection points do not typically occur in the

concentration profiles of the turbidity currents in Kluane Lake. As such, it is difficult to delineate a boundary between the current itself and the upper, mixed portion of the current. Mean velocity is equally difficult to constrain with only one or several point measurements in the water column; a vertical velocity profile determined either through multiple current meters on a single mooring or an acoustic Doppler current profiler would greatly facilitate the calculation of mean current velocity. Because Froude numbers can vary substantially based on the choice in flow thickness and mean velocity, conclusions about flow characteristics are difficult to form with confidence. In a study of supercritical flow in density currents, Hand (1974) also cautions that the Froude number calculation is highly sensitive to the flow thickness value, yet there is no general agreement about how thickness should be measured. These results suggest that Froude number calculations in natural environments can be approximations at best until further research is able to develop a method of more precisely defining underflow thickness based on the vertical concentration profile.

5.2.4 Implications for sedimentation

5.2.4.1 Bulk sedimentation

The largest mass of sediment is deposited in Kluane Lake at a small break of slope approximately 1 km from the delta, beyond which the accumulation rate and turbidity current SSL decrease rapidly (Fig. 5.11). By comparing the acoustic survey completed in 2006 with the acoustic survey by Bryan (1974b), accumulation in the prodelta area of Kluane Lake has averaged 0.4 m a^{-1} between 1970 and 2006 (Gilbert and Crookshanks, in press). This range is consistent with the approximate accumulation rate in the sediment traps deployed in 2006 and 2007 near the Slims River delta (0.3 – 0.5 m a^{-1}). The daily mass accumulation rate in Kluane Lake (up to 6000 g m^{-2} d^{-1}) is much higher than values reported from other glacial lakes (cf.

Lewis et al., 2002; Gilbert and Butler, 2004). The longitudinal variations in the textural characteristics and water content of the lake bottom sediment are consistent with both previous studies of Kluane Lake (Bryan et al., 1974b) as well as other glacial lakes (Gilbert, 1972; Pickrill and Irwin, 1983; Desloges and Gilbert, 1998).

The increase in turbidity current thickness, suspended sediment load (SSL), and mass accumulation rate (MAR) concurrent with a change in the vertical concentration profile between mooring A and mooring C indicate that a) the current is gaining more sediment, and b) the flow structure is changing over the distance of 300 m between the moorings. One possible explanation is that the turbidity currents are being funneled by the bathymetry into a smaller cross-sectional area, thereby increasing the apparent suspended sediment load. Close examination of the bathymetry to the west of the island does not indicate any obvious morphological control that would contribute to significant underflow funneling. Alternatively, the turbidity currents may be eroding sediment along the delta slope when the currents reach very high velocities. The peak flow velocities measured at mooring A are certainly competent enough to erode bottom sediment in the range of silt to fine sand, particularly since the lake bottom sediments are unconsolidated (Postma, 1967). Recent work, however, suggests that flow capacity, which is the maximum sediment mass flux per unit discharge, may be more important in determining erosion and deposition in particulate flows (Hiscott, 1994; Kneller and McCaffrey, 2003). Suspension of sediment is largely dependent on the upward component of fluid turbulence, which can be quantified by the turbulent kinetic energy. Because the turbulent kinetic energy is a finite value, the amount of sediment that can be maintained in suspension in a given flow must also be finite. Quantifying this sediment capacity is highly problematic given the current state of knowledge (Kneller and McCaffrey, 2003). While the concentration of sediment is dependent on turbulence, the presence of sediment itself modifies the turbulence (Sato et al., 1996). Because the potential

energy of turbidity currents is solely due to their excess density, they are generally thought to be at or near full capacity when they are depositing material. Only at a hydraulic jump or during the initial surging phase, are turbidity currents thought to be below capacity and capable of significant erosion (Normark and Piper, 1991).

.While densiometric Froude number calculations are inconclusive, other factors indicate that supercritical flow conditions may contribute to the variations in flow structure and depositional patterns present on the delta slope. Immediately beyond mooring C, the longitudinal bed profile shows a distinct break in slope, which is where hydraulic jumps typically occur in experimental models and in observations from the marine and lacustrine environment (Komar, 1971; Hand, 1974; Normark and Dickson, 1976; Garcia and Parker, 1989; Garcia, 1993). At this site, the flow thickness suddenly increases and the largest mass of sediment is deposited here; both of these observations are characteristic of a transition from supercritical to subcritical flow conditions (Hand, 1974). The vertical concentration profiles observed at mooring A, C, and D are also similar with the profiles observed by Garcia (1993) in laboratory experiments of sediment-laden turbidity currents undergoing a hydraulic jump along a slope transition. While these observations are consistent with a regime change from supercritical to subcritical flow, it is uncertain at this time if a hydraulic jump is occurring at this location or the flow is simply responding to the change in slope.

The longitudinal pattern in turbidity current flow characteristics is important for determining the spatial pattern of sediment distribution within Kluane Lake and other dynamic systems. In experimental currents, the flow structure of a current is fundamental in determining the nature of the sedimentary deposit (Kneller and Branney, 1995; Alexander and Mulder, 2002; Kneller and McCaffrey, 2003). For example, temporal or spatial variations in the flow capacity or flow competence are important factors in the development of the vertical sequence within

turbidites along a longitudinal transect (Kneller and McCaffrey, 2003). Where a turbidity current is below capacity and competent to entrain the bottom sediment, erosion may occur during times of peak flow. This type of erosion has important implications for depositional patterns, delta morphology, and the continuity of the sedimentary record. Erosion by turbidity currents that form in response to high-density river inflow has also been inferred in several other high-energy glacial lake environments (Brodie and Irwin, 1970; Weirich, 1986b; Gilbert and Desloges, 2005).

5.2.4.2 Sedimentary record

Because quasi-continuous turbidity currents are uncommon in both lacustrine and marine environments, the implications of this type of flow for the sedimentary record have not been widely documented. In lower-energy sedimentary environments, turbidity currents are rare, episodic events induced by slumping on the delta-front (e.g. Lamoureux, 1999) or large flood events, that can last up to several days (e.g. Gilbert and Shaw, 1981). These events can be distinguished in the sedimentary record by anomalously coarse deposits that range in thickness from a sub-millimetre to multi-centimetre scale depending on the event magnitude (Schiefer et al., 2006; Gilbert et al., 2006). In higher-energy proglacial lakes that experience periodic turbidity current activity, the sediment in deeper portions of the basin is often deposited as varves; a homogenous layer of coarse material is capped by a fine layer of clay, which may be interrupted by subannual deposits from events such as floods and slumps (Smith and Ashley, 1985). In the case of quasi-continuous flow, the sediment trap results from this study allow inferences to be made regarding the nature of the sedimentary record for this type of flow.

The diurnal nature of glacial meltwater production generates a distinct record of waxing and waning turbidity current flow in Kluane Lake. This flow pattern is manifested in the sedimentary record at delta-proximal sites as variations in textural characteristics, which in certain cases may be visually distinguished as diurnal laminations. To distinguish laminations in

a clastic sedimentary record, the mass accumulation rate must be high enough to resolve textural variations and the range in particle size must also be large enough so the textural variations may be distinguished as a change in color. In Kluane Lake, the particle size distribution is so narrow that laminations can be difficult to distinguish, particularly after compaction and dewatering of the sediment; therefore, it is uncertain if the laminations would be preserved within the longer sedimentary record. In high-sedimentation marine environments, diurnal laminations have been observed to form in response to tidal fluctuations (e.g. Gilbert et al., 2002). Diurnal laminations in the lacustrine environment are much rarer, particularly in minerogenic sediment, partially because of the high sediment load that is necessary for such textural variations to be detected. One example of diurnal lacustrine laminations was found in a sedimentary record from a lake in southern Finland, where the laminations were associated with diurnal variations in wind strength (Simola and Tolonen, 1981). Daily rhythmites have also been inferred from ice-dammed lakes where a large volume of sediment is delivered by a strongly diurnal hydrological regime (Johnson, 1997).

Because the diurnal laminations in the sediment traps from Kluane Lake are not observed continuously over time or space, highly specific conditions are likely necessary for their formation. The formation and characteristics of the laminations at mooring D cannot easily be explained by various turbidity current flow parameters or river inflow characteristics. The strong direct linear relationship between mean daily particle size and diurnal sediment accumulation from the sediment trap suggests, at first glance, that more energetic turbidity currents are responsible for increased deposition of coarser material. However, current run is inversely related to both lamination thickness and particle size; this relationship implies that weaker currents are depositing coarser sediment in greater quantities. Because the tilting current meter at mooring D has a detection limit of approximately 0.07 m s^{-1}, the current run values are

approximations; therefore, it is possible that current run does not relate to sedimentation in any meaningful way. The laminations were also deposited after the rainstorm-induced flood of June 30 and July 1, and consequently the inverse relationship is perhaps a response to hysteresis effects in the proglacial system. Nevertheless, assuming that the correlation is valid, the inverse relationship between current run and sedimentary properties may reflect a similar process as the one governing the lack of sediment deposition observed at mooring A. At mooring A, virtually no deposition was observed later in the melt season when strong flow conditions prevailed, whereas earlier in the season, when flow conditions were relatively weaker, the sedimentation rate was over 10 times greater. The inverse relationship between sediment accumulation and current velocity at mooring A and D suggests that the turbidity currents were perhaps operating below their flow capacity on the proximal delta slope, resulting in erosion and/or reduced deposition during higher flow velocities. The processes governing sediment deposition and erosion by turbidity currents are highly complex and cannot be easily understood by measuring simple flow characteristics at individual mooring sites throughout the delta.

The lack of significant deposition at mooring A, despite vigorous turbidity current flow conditions, has important implications for the distribution of sediment within lake basins. These results suggest that in high-energy lacustrine environments the amount of sediment deposition is not necessarily directly related to the energy-state of the water column, as is generally assumed. When flow conditions are energetic enough to prevent the deposition of either all or a portion of the material in suspension, the sedimentary record may not reflect the change in flow conditions. Therefore, spatial and temporal variability in hydrologically-controlled depositional processes may introduce a considerable bias to sedimentary record interpretation if they are not properly identified.

The rainstorm-induced flood that occurred from June 30 to July 1 formed a deposit in Kluane Lake that can be distinguished in the sedimentary record by its large magnitude, coarser particle size, and visual appearance. Mulder and Alexander (2001) hypothesize that the shape of hyperpycnal turbidites deposited by quasi-steady marine turbidity currents can take a variety of forms, depending on the shape of the flood hydrograph. When a distinct waxing phase is observed, the sedimentary sequence may contain inversely-graded units overlain by a normally-graded sequence; however, depending on the magnitude of the flood, the flow may become non-depositional at delta-proximal locations producing an erosion surface at the top of the inversely-graded unit or, in extreme cases, producing no record of any original inversely-graded layer. Because the Slims River hydrograph of the flood that occurred from June 30 to July 1 is symmetrical, the waxing and waning flow of the flood may be responsible for the variations in particle size in the flood deposits at delta-proximal locations such as at mooring C, where an inversely-graded unit is capped by a normally-graded unit. Similar sequences have been observed in the marine environment, including the Saguenay turbidite (Mulder et al., 2003) and Var turbidity system (Mulder et al., 1998). The small thickness of inversely-graded units produced by waxing flow relative to the waning flow deposits has been previously attributed to the reduced particle deceleration, and thus smaller sediment fallout rate, during the rising limb of the flood (Kneller and Branney, 1995).

Because a change in particle size cannot be responsible for the sudden, sharp, distinct flood deposit base, the change in color may instead be associated with a change in sediment source area. A spatially extensive and high-magnitude precipitation event, such as this rainstorm, would erode a significant amount of catchment material that is, at least in part, non-glacial in origin and transport this sediment into the lake. In the sedimentary record of Summit Lake at White Pass in British Columbia, Cockburn and Lamoureux (2007) similarly found enhanced

macro-organic content in late-summer, rainfall-induced subannual sedimentary laminae. The flood deposit in Kluane Lake, therefore, may be distinct within the sedimentary record because of its enhanced organic material and possibly a different minerogenic composition relative to the glacial material that dominates the bulk of the sedimentary record.

Chapter 6
Conclusions and Future Research

Kluane Lake is an ideal site at which to study high-energy sedimentary processes, because it is not only an intermediate-scale environment that is logistically-manageable, but also a dynamic sedimentary system. Previous process studies of glacial lakes have generally focused on low- or mid-energy sedimentary environments where periodic or episodic turbidity currents are the norm. Furthermore, these studies typically have relied on several isolated measurement locations. The only study with a spatial distribution of instrumentation comparable to this study examined a small glacilacustrine system with periodic turbidity current activity (Weirich, 1986a).

The results from this research are significant in terms of our general understanding of both modern and historical glacilacustrine environments and deposits. Spatially and temporally variable sedimentary processes have a substantial impact on the distribution of sediment throughout Kluane Lake as well as the vertical sequence of sediment accumulation. Four major conclusions can be drawn from this research on high-energy sedimentary processes at Kluane Lake:

1. The dynamics of suspended sediment transport in a large proglacial fluvial system deserves further consideration. The general consensus in the literature is that proglacial environments exhibit a clockwise hysteresis relationship between suspended sediment and discharge because of diurnal and seasonal sediment exhaustion effects. However, results from Slims River during the peak melt season of 2007 suggest that counterclockwise hysteresis may predominate in some rivers in response to variations in sediment availability and/or hydrological routing through the glacial or fluvial system.

2. Turbidity current activity in Kluane Lake exhibits significant temporal and spatial variability. Continuous, diurnally fluctuating currents are observed at delta-proximal locations (750 m from the delta), with velocities ranging from 0.2 to 0.6 m s^{-1}. At more distal locations (up to 4.2 km), the duration of the currents is more difficult to assess because of the lower detection limit of the current meters; however, interpolation of the velocity records suggests that turbidity current flow may be periodic or perhaps continuous at these sites. At a finer temporal resolution, high-frequency fluctuations (< 45 seconds) in both current velocity and direction become increasingly important at higher current velocities, possibly because of turbulent structures within the flow.
3. The flow structure of turbidity currents in Kluane Lake is spatially and temporally variable and thus difficult to quantify using simple relationships. Vertical concentration profiles and sediment accumulation patterns indicate that a distinct change in flow structure occurs approximately 1 km from the point of inflow at a minor break in slope: (i) the flow thickness increases dramatically; (ii) the vertical concentration profile changes in shape; (iii) the suspended sediment load within the currents is greater than upflow; and (iv) the sediment accumulation rate increases substantially. Beyond this location, the flow thickness, suspended sediment load, and accumulation rate rapidly decline in magnitude. At delta-proximal locations, the amount of sediment deposited on the lake bed is not directly related to the energy-state of the water column. Instead, the turbidity currents appear to be dynamic enough to cause reduced deposition and/or erosion.
4. Understanding the sedimentary processes in Kluane Lake is important to determine the spatial pattern of sediment distribution and vertical sequence of sedimentation within the lake. Because turbidity currents are so dominant in this environment, a significant

amount of relatively coarse material is transported to the deepest portions of the basin. Sediment traps document the presence of diurnal laminations at delta-proximal locations. These laminations do not occur consistently over space or time, which suggests that highly specific flow conditions are necessary for their formation. Furthermore, their properties are not related to turbidity current flow in a straightforward manner; the lamination thickness and mean particle size appear to be inversely related to current velocity.

Studying turbidity currents in the natural environment is considerably more complex than experimental or theoretical analysis; not only are logistics more challenging because of the larger scale, but natural variability within the system also complicates the interpretation of results. While experimental and theoretical models are widely recognized to be useful tools in isolating relationships between flow variables, models can only accurately describe that which is observed in simple, controlled environments. The results presented in the preceding chapters suggest that continuous, long-term measurement records from natural lacustrine environments provide valuable additional insights regarding the multiple scales of environmental variability.

Further research is needed to better understand the spatial component of turbidity current flow in lacustrine environments. Individual monitoring sites spaced throughout the delta are useful in providing a temporal record of site specific flow characteristics; however, the vertical and spatial dimensions of flow variability remain unsatisfactorily constrained. Without the deployment of a prohibitive number of moorings, it is difficult to interpolate both longitudinal and lateral variability in large lake systems. This spatial consideration is particularly important at delta-proximal sites where flow conditions change rapidly over a short distance. Technologies such as acoustic Doppler current profiling (Best et al., 2005) and improved remote acoustic

sensing (Hay et al., 1982) may be particularly useful in future research to quantify the three-dimensional flow variability within turbidity currents at multiple timescales.

The interaction between turbidity current flow properties and sediment dynamics also warrants further examination. While concepts such as flow competence and flow capacity are relatively simple to grasp, their relationship to sediment transport, erosion, and deposition in turbidity currents is highly complex and not well understood. Turbulence within turbidity currents is, by definition, what maintains the sediment in suspension; however, the very presence of sediment also modifies the turbulence. These interactions are even more difficult to quantify if the characteristics of the inflowing sediment-laden water are changing over time. For example, both sediment supply and hysteresis effects between sediment and discharge are commonly temporally variable in proglacial fluvial systems. While general patterns of turbidity currents are relatively well understood, more research is required to understand the relationship between flow conditions and sedimentation patterns by turbidity currents, particularly in dynamic environments.

References

Akiyama, J., and Fukushima, Y. 1985. Entrainment of noncohesive bed sediment into suspension. Third International Symposium on River Sedimentation, University of Mississippi, pp. 804-813.

Alexander, J., and Mulder, T. 2002. Experimental quasi-steady density currents. Marine Geology 186: 195-210.

Altinakar, M.S., Graf, W.H., and Hopfinger, E.J. 1996. Flow structure in turbidity currents. Journal of Hydraulic Research 34: 713-718.

Bagnold, R.A. 1962. Auto-suspension of transported sediment; turbidity currents. Processes of the Royal Society of London 265A: 315-319.

Bale, A.J. 1998. Sediment trap performance in tidal waters: comparison of cylindrical and conical collectors. Continental Shelf Research 18: 1401-1418.

Ballantyne, C.K., and McCann, S.B. 1980. Short-lived damming of a high-Arctic ice-marginal stream, Ellesmere Island, N.W.T., Canada. Journal of Glaciology 25: 487-491.

Barnett, A.P. 1974. Hydrological studies of the Slims River, Yukon, June-August 1970, in Icefields Ranges Research Project, Scientific Results Vol. 4, V.C. Bushnell and M.G., Marcus eds. American Geographical Society, New York and Arctic Institute of North America, Montreal, Quebec, pp. 143-150.

Beecroft, I. 1983. Sediment transport during an outburst from Glacier de Tsidjoire Nouve, Switzerland, 16-19 June 1981. Journal of Glaciology 29: 185-190.

Beierle, B., Lamoureux. S.F., Cockburn, J.M.H., and Spooner, I. 2002. A new method for visualizing sediment particle size distributions. Journal of Paleolimnology 27: 279-283.

Best, J., Peakall, J., and Kirkbride, A. 2001. Mean flow and turbulence structure of sediment-laden gravity currents: new insights using ultrasonic Doppler velocity profiling. In: Kneller, B.C., McCaffrey, W.D., Peakall, J. and Druitt, T. (eds.), "Sediment Transport and Deposition by Particulate Gravity Currents." Special Publication of the International Association of Sedimentologists 31, pp. 159-172.

Best, J.L., Kostachuk, R.A., Peakall, J., Villard, P.V., and Franklin, M. 2005. Whole flow field dynamics and velocity pulsing within natural sediment-laden underflows. Geology 33: 765-768.

Bogen, J. 1980. The hysteresis effect of sediment transport systems. Norsk Geografisk Tidsskrift 34: 45-54.

Bogen, J., and Bonsnes, T.E. 2003. Erosion and sediment transport in High Arctic rivers, Svalbard. Polar Research 22: 175-189.

Boothroyd, J.C. and Ashley, G.M. 1975. Processes, bar morphology and sedimentary structures on braided outwash fans, northeastern Gulf of Alaska. In: Jopling, A.V., and McDonald, B.C. (eds.), "Glaciofluvial and Glaciolacustrine Sedimentation." Society of Economic Petrologists and Mineralogists Special Publication 23: 193-222.

Bostock, H.S. 1952. Geology of northwest Shakwak Valley, Yukon Territory. Geological Survey of Canada, Memoir 267, 54 pp.

Bostock, H.S. 1969. Kluane Lake, Yukon Territory, its drainage and allied problems. Geological Survey of Canada. Paper 36–65.

Bradley, R.S., Retelle, M.J., Ludlam, S.D., Hardy, D.R., Zolitschka, B., and Lamoureux, S. 1996. The Taconite Inlet Lakes Project: a systems approach to paleoclimatic reconstruction. Journal of Paleolimnology 16: 97-110.

Brahney, J. 2007. Paleolimnology of Kluane Lake. M.Sc. thesis, Simon Fraser University, Burnaby, BC.

Brahney, J., Clague, J.J., Menounos, B., and Edwards, T.W.D. *in press*. Geochemical reconstruction of late Holocene drainage and mixing in Kluane Lake, Yukon Territory. Journal of Paleolimnology.

Brasington, J., and Richards, K. 2000. Turbidity and suspended sediment dynamics in small catchments in the Nepal Middle Hills. Hydrological Processes 14: 2559-2573.

Brodie, J.W., and Irwin, J. 1970. Morphology and sedimentation in Lake Wakatipu, New Zealand. New Zealand Journal of Marine and Freshwater Resources 4: 479-496.

Bryan, M.L. 1974a. Sedimentation in Kluane Lake. In: Icefields Ranges Research Project, Scientific Results Vol. 4, V.C. Bushnell and M.G., Marcus eds. American Geographical Society, New York and Arctic Institute of North America, Montreal, Quebec, pp. 143-150.

Bryan, M.L. 1974b. Sublacustrine morphology and deposition, Kluane Lake, Yukon Territory. In: Icefields Ranges Research Project, Scientific Results Vol. 4, V.C. Bushnell and M.G., Marcus eds. American Geographical Society, New York and Arctic Institute of North America, Montreal, Quebec, pp. 143-150.

Bryan, M.L. 1974c. Variations in quality and quantity of Slims River water, Yukon Territory. In: Icefields Ranges Research Project, Scientific Results Vol. 4, V.C. Bushnell and M.G., Marcus eds. American Geographical Society, New York and Arctic Institute of North America, Montreal, Quebec, pp. 143-150.

Bryan, M.L. 1974d. Water masses in Southern Kluane Lake. In: Icefields Ranges Research Project, Scientific Results Vol. 4, V.C. Bushnell and M.G., Marcus eds. American Geographical Society, New York and Arctic Institute of North America, Montreal, Quebec, pp. 143-150.

Buckee, C.M., Kneller, B.C., and Peakall, J. 2001. Turbulence structure in steady, solute-driven gravity currents. In: Kneller, B.C., McCaffrey, W.D., Peakall, J., and Druitt, T. (eds.), "Sediment Transport and Deposition by Particulate Gravity Currents." Special Publication International Association of Sedimentologists 31: 173-187.

Chikita, K. 1989. A field study on turbidity currents initiated from spring runoffs. Water Resources Research 25: 257-271.

Chikita, K., and Okumura, Y. 1990. Dynamics of turbidity currents measured in Katsurazawa Reservoir, Hokkaido, Japan. Journal of Hydrology 117: 323-338.

Church, M. 1972. Baffin Island sandurs: a study of Arctic fluvial processes. Geological Survey of Canada Bulletin 216.

Church, M., and Gilbert, R. 1975. Proglacial fluvial and lacustrine environments. In: Jopling, A.V. and McDonald, B.C. (eds.), "Glaciofluvial and Glaciolacustrine Sedimentation." Society of Economic Petrologists and Mineralogists Special Publication 23: 22-100.

Clague, J.J. 1981. Landslides at the south end of Kluane Lake, Yukon Territory. Canadian Journal of Earth Sciences 18: 959-971.

Clague, J.J., Luckman, B.H., Van Dorp, R.D., Gilbert, R., Froese, D., Jensen, B.J.L, and Reyes, A.V. 2006. Rapid changes in the level of Kluane Lake in Yukon Territory over the last millennium. Quaternary Research 66: 342-355.

Clifford, N.J., Richards, K.S., Brown, R.A., and Lane, S.N. 1995. Scales of variation of suspended sediment concentration and turbidity in a glacial meltwater stream. Geografiska Annaler 77A: 45-65.

Cockburn, J.M.H., and Lamoureux, S.F. 2007a. Century-scale variability in late-summer rainfall events recorded over seven centuries in subannually laminated lacustrine sediments, White Pass, British Columbia. Quaternary Research 67: 193-203.

Cockburn, J.M.H., and Lamoureux, S.F. 2007b. Inflow and lake controls on short-term mass accumulation and particle size: implications for interpreting varved lacustrine sedimentary records. Geological Society of America Northeastern Section – 42nd Annual Meeting (12-14 March 2007): Paper No. 47-3.

Collins, D.N. 1979. Sediment concentration in melt waters as an indicator of erosion processes beneath an alpine glacier. Journal of Glaciology 223: 247-257.

Csanady, G.T. 1978. Water circulation and dispersal mechanisms. In: Lerman, A. (ed.), "Lakes: chemistry, geology, physics." New York: Springer-Verlag, pp. 21-64.

Dade, W.B., Lister, J.R., and Huppert, H.E. 1994. Fine-sediment deposition from gravity surges on uniform slopes. Journal of Sedimentary Research A64: 423-432.

de Geer, G. 1912. A geochronology of the last 12,000 years. 11th International Geological Congress (1910), Stockholm: 1241-1253.

Desloges, J.R. 1994. Varve deposition and the sediment yield record at three small lakes of the southern Canadian Cordillera. Arctic and Alpine Research 26: 130-140.

Desloges, J.R., and Gilbert, R. 1994. Sediment source and hydroclimatic inferences from glacial lake sediments: the proglacial sedimentary record of Lillooet Lake British Columbia. Journal of Hydrology 159: 375-393.

Desloges, J.R., and Gilbert, R. 1998. Sedimentation in Chilko Lake: a record of the geomorphic environment of the eastern Coast Mountains of British Columbia, Canada. Geomorphology 25: 75-91.

Ellison, T.H., and Turner, J.S. 1959. Turbulent entrainment in stratified flows. Journal of Fluid Mechanics 6: 423-448.

Ewing, K.J. 1972. Supraglacial streams of the Kaskawulsh Glacier. In: Bushnell, V.C., and Ragle, R.H. (eds.), Icefield Ranges Research Project scientific results. American Geographical Society, NY, and Arctic Institute of North America, Montreal, PQ, Volume 3, pp 153-162.

Fahnestock, R.K. 1963. Morphology and hydrology of a glacial stream – White River, Mount Ranier, Washington. U.S.G.S. Professional Paper 422A: 1-70.

Fahnestock, R.K. 1969. Morphology of the Slims River. In: Bushnell, V.C., and Ragle, R.H. (eds.), Icefield Ranges Research Project scientific results. American Geographical Society, NY, and Arctic Institute of North America, Montreal, PQ, Volume 1, pp 161-172.

Felix, M., Sturton, S., and Peakall, J. 2005. Combined measurements of velocity and concentration in experimental turbidity currents. Sedimentary Geology 179: 31-47.

Fenn, C.R., Gurnell, A.M., and Beecroft, I.R. 1985. An evaluation of the use of suspended sediment rating curves for the prediction of suspended sediment concentration in a proglacial stream. Geografiska Annaler 67A: 71-82.

Flood, R.D. 1988. A lee wave model for deep-sea mudwave activity. Deep-Sea Research 35: 973-983.

Francus, P., Bradley, R.S., Abbott, M.B., Patridge, W., and Keimig, F. 2002. Paleoclimate studies of minerogenic sediments using annually resolved textural parameters. Geophysical Research Letters 29: 1998-2002.

Garcia, M. 1993. Hydraulic jumps in sediment-driven bottom currents. Journal of Hydraulic Engineering 119: 1094-1116.

Garcia, M. 1994. Depositional turbidity currents laden with poorly sorted sediment. Journal of Hydraulic Engineering 120: 1094-1117.

Garcia, M., and Parker, G. 1989. Experiments on hydraulic jumps in turbidity currents near a canyon-fan transition. Science 245: 393-396.

Garcia, M., and Parker, G. 1993. Experiments on the entrainment of sediment into suspension by a dense bottom current. Journal of Geophysical Research 98: 4793-4807.

Gardner, W.D. 1980. Sediment trap dynamics and calibration: a laboratory evaluation. Journal of Marine Research 38: 17-39.

Gilbert, R. 1972. Observations on sedimentation at Lillooet Delta, British Columbia. In: Slaymaker, H.O., MacPherson, H. (eds.) Mountain Geomorphology. Tanatalus Press, Vancouver, pp. 187-194.

Gilbert, R. 1975. Sedimentation in Lillooet Lake, British Columbia. Canadian Journal of Earth Sciences 12: 1697-1711.

Gilbert, R.G. and Shaw, J. 1981. Sedimentation in proglacial Sunwapta Lake, Alberta. Canadian Journal of Earth Sciences 18: 81-93.

Gilbert, R., and Desloges, J.R. 1987. Sediments of ice-dammed, self-draining Ape Lake, British Columbia. Canadian Journal of Earth Sciences 24: 1735-1747.

Gilbert, R., and Butler, R.D. 2004. The physical limnology and sedimentology of Meziadin Lake, Northern British Columbia, Canada. Arctic, Antarctic, and Alpine Research 36: 33-41.

Gilbert, R., and Desloges, J.R. 2005. The record of Glacial Lake Champagne in Kusawa Lake, southwestern Yukon Territory. Canadian Journal of Earth Sciences 42: 2127-2140.

Gilbert, R., and Crookshanks, S. *in press*. Sediment waves in a modern high-energy glacilacustrine environment. Sedimentology.

Gilbert, R., Desloges, J.R., and Clague, J.J. 1997a. The glacilacustrine sedimentary environment of Bowser Lake in the northern Coast Mountains of British Columbia, Canada. Journal of Paleolimnology 17: 331-346.

Gilbert, R., Desloges, J.R., and Lemmen, D.S. 1997b. Paleoenvironmental assessment from the physical properties of lacustrine and marine sediments; a Canadian contribution to IGCP 374. Journal of Paleolimnology 17: 295-296.

Gilbert, R., Nielsen, N., Moller, H., Desloges, J.R., and Rasch, M. 2002. Glacimarine sedimentation in Kangerdluk (Disko Fjord), West Greenland, in response to a surging glacier. Marine Geology 191: 1-18.

Gilbert, R., Crookshanks, S., Hodder, K.R., Spagnol, J., and Stull, R.B. 2006. The record of an extreme flood in the sediments of montane Lillooet Lake, British Columbia: implications for paleoenvironmental assessment. Journal of Paleolimnology 35: 737-745.

Graf, W.H. 1998. "Fluvial Hydraulics: Flow and Transport Processes in Channels of Simple Geometry." John Wiley & Sons, Chichester, 681 pp.

Gurnell, A.L. 1987. Suspended Sediment. In: Gurnell, A.M. and Clark, M.J. (eds.), "Glacio-fluvial Sediment Transfer: an Alpine Perspective." John Wiley & Sons Ltd, Chichester, pp. 305-354.

Gurnell, A.M. and Warburton, J. 1990. The significance of suspended sediment pulses for estimating suspended sediment load and identifying suspended sediment sources in Alpine glacier basins. International Association of Hydrological Sciences Publication 193: 463-470.

Gurnell, A.M., Hodson, A., Clark, M.J., Bogen, J., Hagen, J.O., and Tranter, M. 1994. Water and sediment discharge from glacier basins: an arctic and alpine comparison. In: Variability in Stream Erosion and Sediment Transport (Symposium at Canberra 1994), International Association of Hydrological Sciences Publication 224, pp. 235-334.

Gustavson, T.C. 1975. Sedimentation and physical limnology in proglacial Malaspina Lake, Southeastern Alaska. In: Jopling, A.V. and McDonald, B.C. (eds.), "Glaciofluvial and Glaciolacustrine Sedimentation." Society of Economic Petrologists and Mineralogists Special Publication 23: 249-263.

Gustavson, T.C., and Boothroyd, J.C. 1987. A depositional model for outwash, sediment sources, and hydrological characteristics, Malaspina Glacier, Alaska: A modern analog of the southeastern margin of the Laurentide ice sheet. Geological Society of America Bulletin 99, pp. 187–200.

Guy, H.P., and Norman, V.W. 1970. Field methods for measurement of fluvial sediment. In: "Techniques of Water-Resources Investigations of the United States Geological Survey." United States Government Printing Office, Washington: 1970, 59 pp.

Hamblin, P.F., and Carmack, E.C. 1978. River-induced currents in a fjord lake. Journal of Geophysical Research 83: 885-899.

Hammer, K.M. and Smith, N.D. 1983. Sediment production and transport in a proglacial stream: Hilda glacier, Alberta, Canada. Boreas 12: 91-106.

Hand, B.M. 1974. Supercritical flow in density currents. Journal of Sedimentary Petrology 44: 637-648.

Hand, B.M., Middleton, G.V., and Skipper, K. 1972. Antidune cross-stratification in a turbidite sequence, Cloridorme Formation, Gaspe, Quebec – Discussion. Sedimentology 18: 135-138.

Hardy, D.R., Bradley, R.S., and Zolitschka, B. 1996. The climatic signal in varved sediments from Lake C2, northern Ellesmere Island, Canada. Journal of Paleolimnology 16: 227-238.

Harris, S.A., 1990. Dynamics and Origin of Saline Soils on the Slims River Delta, Kluane National Park, Yukon Territory. Arctic 43: 159-175.

Hay, A.E., Burling, R.W., and Murray, J.W. 1982. Remote acoustic detection of a turbidity current surge. Science 217: 833-835.

Heidel, S.G. 1956. The Progressive Lag of Sediment Concentration with Flood Waves. Transactions, American Geophysical Union 37: 56-66.

Heiri, O., Lotter, A.F., and Lemcke, G. 2001. Loss on ignition as a method for estimating organic and carbonate content in sediments: reproducibility and comparability of results. Journal of Paleolimnology 25: 101-110.

Henderson, F.M. 1966. "Open Channel Flow." Macmillan Co., New York. 522 p.

Hendricks, T.J. 1985. Use of inclinometer current meters in weak currents. Ocean Engineering and the Environment. Oceans 85: 742-748.

Hicks, D.M., McSaveney, M.J., and Chinn, T.J.N. 1990. Sedimentation in proglacial Ivory Lake, Southern Alps, New Zealand. Arctic and Alpine Research 2: 1-7.

Hiscott, R.N. 1994. Loss of capacity, not competence, as the fundamental process governing deposition from turbidity currents. Journal of Sedimentary Research A54: 209-214.

Hodder, K.H. 2007. The process-network of alpine, glacier-fed lakes with particular reference to flocculation. Ph.D. thesis, Department of Geography, Queen's University, Kingston, ON.

Hodder, K.R., Gilbert, R., and Desloges, J. 2007. Glaciolacustrine varved sediment as an alpine hydroclimatic proxy. Journal of Paleolimnology 38: 365-394

Hodgkins, R. 1996. Seasonal trend in suspended transport from an arctic glacier and implications for drainage-system structure. Annals of Glaciology 22: 147-151.

Hodgkins, R. 1999. Controls on suspended-sediment transfer at a High-Arctic glacier, determined from statistical modeling. Earth Surface Processes and Landforms 24: 1-21.

Hodgkins, R., Cooper, R., Wadham, J., and Tranter, M. 2003. Suspended sediment fluxes in a high-Arctic glacierised catchment: implications for fluvial sediment storage. Sedimentary Geology 162: 105-117.

Hudson, P.F. 2003. Event sequence and sediment exhaustion in the lower Panuco Basin, Mexico. Catena 52: 57-76.

Johnson, P.G. 1991. Discharge regimes of a glacierized basin, Slims River Yukon. In: Prowse, T.D., and Ommanney, C.S.L. (eds.), "Northern Hydrology Selected Perspectives." NHRI Symposium 6: 151-164.

Johnson, P.G. 1997. Spatial and temporal variability of ice-dammed lake sediments in alpine environments. Quaternary Science Reviews 16: 635-647.

Johnson, R.C. 1992. Towards the design of a strategy for sampling suspended sediments in small headwater catchments. In: Bogen, J., Walling, D.E., and Day, T.J. (eds.), "Erosion and Sediment Transport Monitoring Programmes in River Basin." International Association of Hydrological Sciences Publication No. 210: 225-232.

Klein, M. 1984. Anti-clockwise hysteresis in suspended sediment concentration during individual storms: Holbeck Catchment: Yorkshire, England. Catena 11: 251-257.

Kneller, B.C., and Branney, M.J. 1995. Sustained high-density turbidity currents and the deposition of thick massive sands. Sedimentology 42: 607-616.

Kneller, B.C., and Buckee, C. 2000. The structure and fluid mechanics of turbidity currents: a review of some recent studies and their geological implications. Sedimentology 27: 62-94.

Kneller, B.C., and McCaffrey, W.D. 2003. The interpretation of vertical sequences in turbidite beds: the influence of longitudinal flow structure. Journal of Sedimentary Research 73: 706-713.

Kneller, B.C., Bennet, S.J., and McCaffrey, W.D. 1997. Velocity and turbulence structure of gravity currents and internal solitary waves: potential sediment transport and the formation of wave ripples in deep water. Sedimentary Geology 112: 235-250.

Kneller, B.C., Bennet, S.J., and McCaffrey, W.D. 1999. Velocity structure, turbulence and fluid stresses in experimental gravity currents. Journal of Geophysical Research, Oceans 104: 5281-5291.

Komar, P.D. 1971. Hydraulic jumps in turbidity currents. Geological Society of America Bulletin 82: 1477-1487.

Komar, P.D. 1973. Continuity of turbidity current flow and systematic variations in deep-sea channel morphology. Geological Society of America Bulletin 84: 3329- 3338.

Kurashige, Y. 1994. Mechanisms of suspended sediment supply to headwater rivers. Proceedings of IAHS Workshop on concepts and methods in hydrogeomorphology, 16 July, Yokohama, Japan. Transactions, Japanese Geomorphological Union 15A: 109-130.

Lambert, A. 1982. Trübeströme des Rheins am Grund des Bodensees (Turbidity currents from the Rhine River on the bottom of Lake Constance). Wasserwirschaft 72:1-4.

Lambert, A. and Hsü, K.J. 1979. Non-annual cycles of varve-like sedimentation in Walensee, Switzerland. Sedimentology 26: 453-461.

Lambert, A. and Giovanoli, F. 1988. Records of riverborne turbidity currents and indications of slope failures in the Rhone delta of Lake Geneva. Limnology and Oceanography 33: 458-468.

Lambert, A.M., Kelts, K.R., and Marshall, N.F. 1976. Measurements of density underflows from Walensee, Switzerland. Sedimentology 23: 87-105.

Lamoureux, S.F. 1999. Spatial and interannual variations in sedimentation patterns recorded in nonglacial varved sediments from the Canadian High Arctic. Journal of Paleolimnology 21: 73-84.

Lamoureux, S.F. 2000. Five centuries of interannual sediment yield and rainfall-induced erosion in the Canadian High Arctic recorded in lacustrine varves. Water Resources Research 36: 309-318.

Lamoureux, S.F. 2001. Varve chronology techniques. In: Last, W.M., and Smol, J.P. (eds.), "Tracking Environmental Change Using Lake Sediments: Basin Analysis, Coring and Chronological Techniques." Kluwer Academic Publishers, Dordrecht, The Netherlands, pp. 247-260.

Lamoureux, S.F., and Gilbert, R. 2004. Long term variability in autumn snowfall and temperature variability and winter storminess recorded in the varved sediments of Bear Lake, Devon Island, Arctic Canada. Quaternary Research 61: 134-147.

Lawler, D.M., Petts, G.E., Foster, I.D.L., and Harper, S. 2006. Turbidity dynamics during spring storm events in an urban headwater river system: The Upper Tame, West Midlands, UK. Science of the Total Environment 360: 109-126.

Lee, H.J., Syvitski, J.P.M., Parker, G., Orange, D., Locat, J., Hutton, E.W.H., and Imrain, J. 2002. Distinguishing sediment waves from slope failure deposits: field examples, including the 'Humboldt Slide' and modelling results. Marine Geology 192: 79-104.

Leemann, A., and Niessen, F. 1994. Varve formation and the climatic record in an alpine proglacial lake: calibrating annually-laminated sediments against hydrological and meteorological data. The Holocene 4: 1-8.

Lewis, T., Gilbert, R., and Lamoureux, S.F. 2002. Spatial and Temporal Changes in Sedimentary Processes at Proglacial Bear Lake, Devon Island, Nunavut, Canada. Arctic, Antarctic, and Alpine Research 34: 119-129.

Liu, K.F., and Mei, C.C. 1990. Approximate equations for the slow spreading of a thin sheet of Bingham plastic fluid. Physics of Fluids A2: 30-36.

Lliboutry, L., Arnao, B.M., Pautre, A., and Schneider, B. 1977. Glaciological problems set by the control of dangerous lakes in Cordillera Blanca, Peru. 1. Historical failures of morainic dams, their causes and prevention. Journal of Glaciology 18: 239-254.

Maizels, J.K. 1979. Proglacial aggradation and changes in braided channel patterns during a period of glacier advance: an alpine example. Geografiska Annaler 61A: 87-101.

McDonald, D.M. 2007. Hydroclimatic influences on suspended sediment delivery in a small, High Arctic catchment. M.Sc. thesis, Queen's University, Kingston, ON.

Menard, H.W. 1964. Marine geology of the Pacific. McGraw-Hill Book Co., New York, 271 pp.

Menounos, B., Clague, J.J., Gilbert, R., and Slaymaker, O. 2005. Environmental reconstruction from a varve network in the southern Coast Mountains, British Columbia, Canada. The Holocene 15: 1163-1171.

Middleton, G.V. 1966a. Experiments on density and turbidity currents: I. Motion of the Head. Canadian Journal of Earth Sciences 3: 523-546.

Middleton, G.V. 1966b. Experiments on density and turbidity currents II. Uniform flow of density currents. Canadian Journal of Earth Sciences 3: 627-637.

Middleton, G.V. 1969. Turbidity currents. In: Stanley, D.J. (ed.), "The New Concepts of Continental Margin Sedimentation: Application to the Geological Record." American Geological Institute short course, Lecture 10.

Middleton, G.V. 1993. Sediment Deposition from Turbidity Currents. Annual Reviews of Earth and Planetary Science 21: 89-114.

Mulder, T. and Alexander, J. 2001. The physical character of subaqueous sedimentary density flows and their deposits. Sedimentology 48: 269-299.

Mulder, T., Savoye, B., and Syvitski, J.P.M. 1997. Numerical modelling of a mid-sized gravity flow: the 1979 Nice turbidity current (dynamics, processes, sediment budget and seafloor impact). Sedimentology 44: 305-326.

Mulder, T., Savoye, B. Piper, D.J.W., and Syvitski, J.P.M. 1998. The Var submarine sedimentary system: understanding Holocene sediment delivery processes and their importance to the geological record. In: Stocker, M.S., Evans, D., and Cramp, A. (eds.), "Geological processes on continental margins: sedimentation, mass-wasting and stability." Geological Society of London, Special Publication 129: 145-166.

Mulder, T., Syvitski, J.P.M., Migeon, S., Fraugères, J.C., and Savoye, B. 2003. Marine hyperpycnal flows: Initiation, behavior and related deposits: A Review. Marine and Petroleum Geology 20: 861-881.

Nakajima, T., Satoh, M., and Okumara, Y. 1998. Channel-levee complexes, terminal deep-sea fan and sediment wave fields associated with the Toyama deep-sea channel system in the Japan Sea. Marine Geology 147: 25-42.

Nanson, G.C. 1974. Bedload and suspended-load transport in a small, steep, mountain stream. American Journal of Science 274: 471-486.

Nickling, W. G. 1978. Eolian sediment transport during dust storms: Slims River Valley, Yukon Territory. Canadian Journal of Earth Sciences 15: 1069-1084.

Normark, W.R. 1989. Observed parameters for turbidity-current flow in channels, Reserve Fan, Lake Superior. Journal of Sedimentary Petrology 59: 423-431.

Normark, W.R. and Dickson, F.H. 1976. Man-made turbidity currents in Lake Superior. Sedimentology 23: 815-831.

Normark, W.R. and Piper, D.J.W. 1991. Initiation processes and flow evolution of turbidity currents: implications for the depositional record. In: Osborne, R.H. (ed.) "From Shoreline to Abyss." Society of Economic Petrology and Mineral Special Publication 46: 207-230.

Normark, W.R., Hess, G.R., Stow, D.A.V., and Bowen, A.J. 1980. Sediment waves on the Monterey Fan levee: a preliminary physical interpretation. Marine Geology 37: 1-18.

O'Sullivan, P.E. 1983. Annually-laminated lake sediments and the study of Quaternary environmental changes – a review. Quaternary Science Reviews 1: 245-313.

Orwin, J.F., and Smart, C.C. 2004. Short-term spatial and temporal patterns of suspended sediment transfer in proglacial channels, Small River Glacier, Canada. Hydrological Processes 18: 1521-1542.

Østrem, G. 1975. Sediment transport in glacial meltwater streams. In: Jopling, A.V. and McDonald, B.C. (eds.), "Glaciofluvial and Glaciolacustrine Sedimentation." Society of Economic Petrologists and Mineralogists Special Publication 23: 193-222.

Parker, G., Fukushima, Y., and Yu, Q. 1987. Experiments on turbidity currents over an erodible bed. Journal of Hydraulic Research 25: 123-147.

Peakall, J., McCaffrey, B., and Kneller, B. 2000. A process model for the evolution, morphology, and architecture of sinuous submarine channels. Journal of Sedimentary Research 70: 434-448.

Pharo, C.H. and Carmack, E.C. 1979. Sedimentation processes in a short residence-time intermontane lake, Kamloops, British Columbia. Sedimentology 26: 523-541.

Pharo, C.H., and Carmack, E.C. 1984. Observations of turbulent structures associated with the formation of sediment-gravity currents in a glacially fed lake. Transactions – American Geophysical Union 65: 898.

Pickrill, R.A., and Irwin, J. 1983. Sedimentation in a deep glacier-fed lake – Lake Tekapo, New Zealand. Sedimentology 30: 63-75.

Piper, D.J.W., and Savoye, B. 1993. Processes of late Quaternary turbidity current flow and deposition on the Var deep-sea fan, north-west Mediterranean Sea. Sedimentology 40: 557-582.

Postma, H. 1967. Sediment transport and sedimentation in the estuarine environment. In: Lauff, G.H. (ed.), "Estuaries." American Association for the Advancement of Science, Washington, pp. 158-169.

Prior, D.B., and Coleman, J.M. 1978. Disintegrating retrogressive landslides on very low-angle subaqueous slopes, Mississippi Delta. Marine Geotechnology **3**: 37-60.

Renberg, I. 1981. Formation, structure, and visual appearance of iron-rich, varved lake sediments. Boreas 10: 255-258.

Richards, K.S. 1984. Some observations on suspended sediment dynamics in Storbregrova, Jotunheimen. Earth Surface Processes and Landforms 9: 101-112.

Röthlisberger, H. and Lang, H. 1987. Glacial hydrology. In: Gurnell, A.M. and Clark, M.J. (eds.), "Glaciofluvial Sediment Transfer: An Alpine Perspective." John Wiley & Sons Ltd, Chichester, pp. 207-284.

Russell, A.J., Van Tatenhove, F.G.M., Van de Wal, R.S.W. 1995. Effects of ice-front collapse and flood generation on a proglacial river channel near Kangerlussuaq (Sondre Stromfjord), west Greenland. Hydrological Processes 9: 213-226.

Sato, Y., Hishida, K., and Meeda, M. 1996. Effect of dispersed phase on modification of turbulent flow. Journal of Fluids Engineering 118: 307-315.

Sawada, M.C. 1996. Seasonal and short-term periodic suspended sediment concentration and bulk hydrochemical variations, Slims River 1993 and 1994, Yukon Territory, Canada. Unpublished M.Sc. thesis, Department of Geography, University of Ottawa, Ottawa, ON.

Sawada, M., and Johnson, P.G. 2000. Hydrometeorology, suspended sediment and conductivity in a large glacierized basin, Slims River, Yukon Territory, Canada. Arctic 53: 101-117.

Schiefer, E., and Gilbert, R. *in press*. Proglacial sediment trapping in recently formed Silt Lake, upper Lillooet Valley, Coast Mountains, British Columbia. Earth Surface Processes and Landforms.

Schiefer, E., Menounos, B., and Slaymaker, O. 2006. Extreme sediment delivery events recorded in the contemporary sediment record of a montane lake, southern Coast Mountains, British Columbia. Canadian Journal of Earth Sciences 43: 1777-1790.

Shanmugam, G., and Moiola, R.J. 1985. Submarine fan models: Problems and solutions. In: Bouma, A.H., Normark, W.D., and Barnes, N.E. (eds.), "Submarine fans and related turbidite systems." New York, Springer-Verlag, pp.29-34.

Simola, H. and Tolonen, K. 1981. Diurnal laminations in the varved sediment of Lake Lovojärvi, south Finland. Boreas 10: 19-26.

Simpson, J.E. and Britter, R.E. 1979. The dynamics of the head of a gravity current. Journal of Fluid Mechanics 94: 477-495.

Slocombe, D.S. 2001. Climate and other sources of change in the St. Elias region. In: Visconti, G. (ed.), "Global Change and Protected Areas." Kluwer Academic Publishers, Dordrecht, pp. 61-69.

Smith, N.D. 1978. Sedimentation processes and patterns in a glacier-fed lake with low sediment input. Canadian Journal of Earth Sciences 15: 741-756.

Smith, N.D. 1985. Proglacial Fluvial Environment. In: Ashley, G.M., Shaw, J., and Smith, N.D. (eds.), "Glacial Sedimentary Environments." Society of Economic Paleontologists and Mineralogists Short Course 16: 85-134.

Smith, N.D., and Ashley, G.M. 1985. Proglacial Lacustrine Environment: Physical Processes. In: Ashley, G.M., Shaw, J., and Smith, N.D. (eds.), "Glacial Sedimentary Environments." Society of Economic Paleontologists and Mineralogists Short Course 16: 135-215.

Stacey, M.W. and Bowen, A.J. 1988. The vertical structure of density and turbidity currents: theory and observations. Journal of Geophysical Research 93: 3528-3542.

Stacey, M.W. and Bowen, A.J. 1990. A comparison of an autosuspension criterion to field observations of five turbidity currents. Sedimentology 37: 1-5.

Stihler, S., Stone, D., and Beget, J. 1992. Varve counting vs. tephrachronology and ^{137}Cs and ^{210}Pb dating: a comparative test at Skilak Lake, Alaska. Geology 20: 1019- 1022.

Stott, T.A., and Grove, J.R. 2001. Short-term discharge and suspended sediment fluctuation in the proglacial Skeldal River, north-east Greenland. Hydrological Processes 15: 407-423.

Stow, D.A.V., and Bowen, A.J. 1980. A physical model for the transport and sorting of fine-grained sediments by turbidity currents. Sedimentology 27: 31-46.

Sturm, M. 1979. Origin and composition of clastic varves. In: Schlüchter, C. (ed.), "INQUA symposium on genesis and lithology of Quaternary deposits; Moraines and varves; origin, genesis, classification." Zurich, Switzerland, pp. 281-285.

Sturm, M. and Matter, A. 1978. Turbidites and varves in Lake Brienz (Switzerland): deposition of clastic detritus by density currents. In: Matter, A., and Tucker, M.E. (eds.), "Modern and Ancient Lake Sediments." International Association of Sedimentologists Special Publication 2: 147-168.

Sundborg, A., and Calles, B. 2001. Water discharges determined from sediment distributions: a paleohydrological method. Geographiska Annaler 83A: 39-54.

Swift, D.A., Nienow, P.W., and Hoey, T.B. 2005. Basal sediment evacuation by subglacial meltwater: suspended sediment transport from Haut Glacier d'Arolla, Switzerland. Earth Surface Processes and Landforms 30: 867-883.

Terrain Analysis and Mapping Services. 1978. Geology and Limnology of Kluane Lake, Yukon Territory: Preliminary Assessment. Terrain Sciences Division, Geological Survey of Canada. Open File 527, 50 pp.

Thayyen, R.J., and Gergan, J.T., and Dobhal, D.P. 1999. Particle size characteristics of India. Hydrological Sciences Journal 33: 47-61.

Tomkins, J.D., and Lamoureux, S.F. 2005. Multiple hydroclimatic controls over recent sedimentation in proglacial Mirror Lake, southern Selwyn Mountains, Northwest Territories. Canadian Journal of Earth Sciences 42: 1589-1599.

Tranter, M. 2005. Sediment and solute transport in glacial meltwater streams. In: Anderson, M.G. (ed.), "Encyclopedia of Hydrological Sciences." John Wiley & Sons, pp. 1-31.

Turner, J.S. 1973. "Buoyancy Effects in Fluids." Cambridge, 368 pp.

Vendl, M.A. 1978. "Sedimentation in glacier-fed Peyto Lake, Alberta." M.S. thesis. University of Chicago at Chicago Circle, Chicago, IL.

Walling, D.E., Peart, M.R., Oldfield, F., and Thompson, R. 1979. Suspended sediment sources identified by magnetic measurements. Nature 281: 110-113.

Warburton, J. 1990. An alpine proglacial fluvial sediment budget. Geografiska Annaler 70A: 261-272.

Warburton, J., and Fenn, C.R. 1994. Unusual flood events from an Alpine glacier: observations and deductions on generating mechanisms. Journal of Glaciology 40: 176-186.

Weirich, F.H. 1984. Turbidity Currents: Monitoring their Occurrence and Movement with a Three-Dimensional Sensory Network. Science 224: 384-387.

Weirich, F.H. 1985. Sediment budget for a high energy glacial lake. Geografiska Annaler 67A: 83-99.

Weirich, F.H. 1986a. The record of density-induced underflows in a glacial lake. Sedimentology 33: 261-277.

Weirich, F.H. 1986b. A study of the nature and incidence of density currents in a shallow glacial lake. Annals of the Association of American Geographers 76: 396-413.

Weirich, F.H. 1989. The generation of turbidity currents by subaerial debris flows, California. GSA Bulletin 101: 278-291.

Williams, G.P. 1989. Sediment concentration versus water discharge during single hydrologic events in rivers. Journal of Hydrology 111: 89-106.

Willis, I. 2005. Hydrology of Glacierized Basins. In: Anderson, M.G. (ed.), "Encyclopedia of Hydrological Sciences." John Wiley & Sons, pp. 1-31.

Willis, I.C., Richards, K.S., and Sharp, M.J. 1996. Links between proglacial stream suspended sediment dynamics, glacier hydrology, and glacier motion at Midtdalsbreen, Norway. Hydrological Processes 10: 629-648.

Wright, L.D., Wiseman, W.J., Bornhold, B.D., Prior, D.B., Syhayda, J.N., Keller, G.H., Yang, Z.S., and Fan, Y.B. 1988. Marine dispersal and deposition of Yellow River silts by gravity-driven underflows. Nature 332: 629-632.

Wynn, R.B., and Stow, D.A.V. 2002. Classification and characterization of deep-water sediment waves. Marine Geology 12: 7-22.

Wynn, R.B., Masson, D.G., Stow, D.A.V., and Weaver, P.P.E. 2000a. Turbidity current sediment waves on the submarine slopes of the western Canary Islands. Marine Geology 163: 185-198.

Wynn, R.B., Masson, D.G., Stow, D.A.V., and Weaver, P.P.E. 2000b. The Northwest African slope apron: a modern analogue for deep-water systems with complex seafloor topography. Marine and Petroleum Geology 17: 253-265.

Wynn, R.B., Weaver, P.P.E., Ercilla, G., Stow, D.A.V., and Masson, D.G. 2000c. Sedimentary processes in the Selvage sediment-wave field, NE Atlantic: New insights into the formation of sediment waves by turbidity currents. Sedimentology 47: 1181-1197.

Zeng, J., and Lowe, D.R. 1997. Numerical simulation of turbidity current flow and sedimentation: I. Theory. Sedimentology 44: 67-84.

Zeng, J., Lowe, D.R., Prior, D.B., Wiseman, W.J., and Bornhold, B.D. 1991. Flow properties of turbidity currents in Bute Inlet, British Columbia. Sedimentology 38: 975-996.

Appendix A

Temperature records for the Kluane Lake region

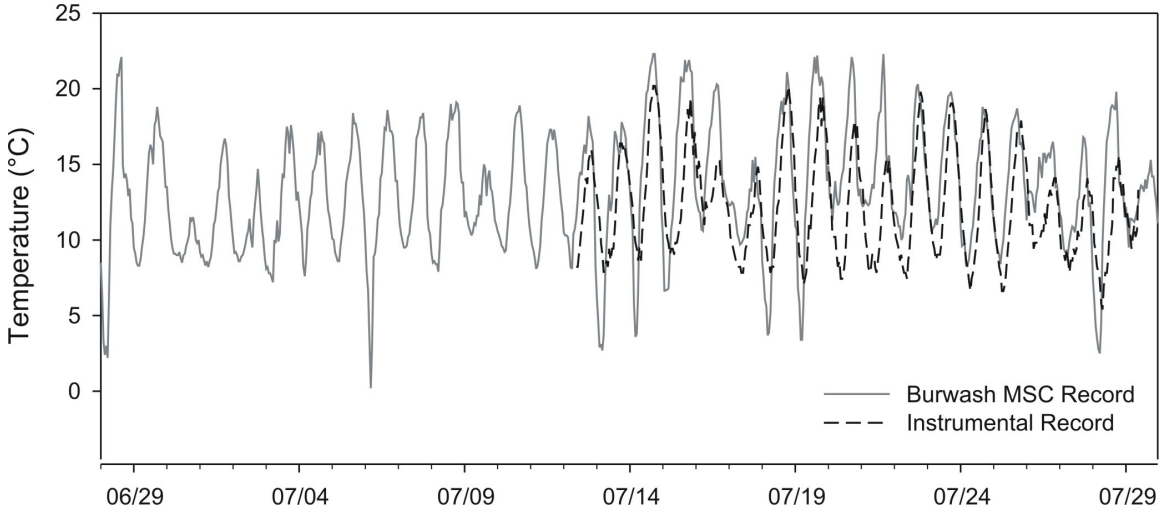

Figure A.1 Overlapping temperature records for the Burwash MSC station and the instrumental record as measured by a Hobo temperature logger at the river monitoring station in 2007 (see Figs. 3.1 and 4.1 for measurement locations).

Appendix B

Slims River bottom surveys

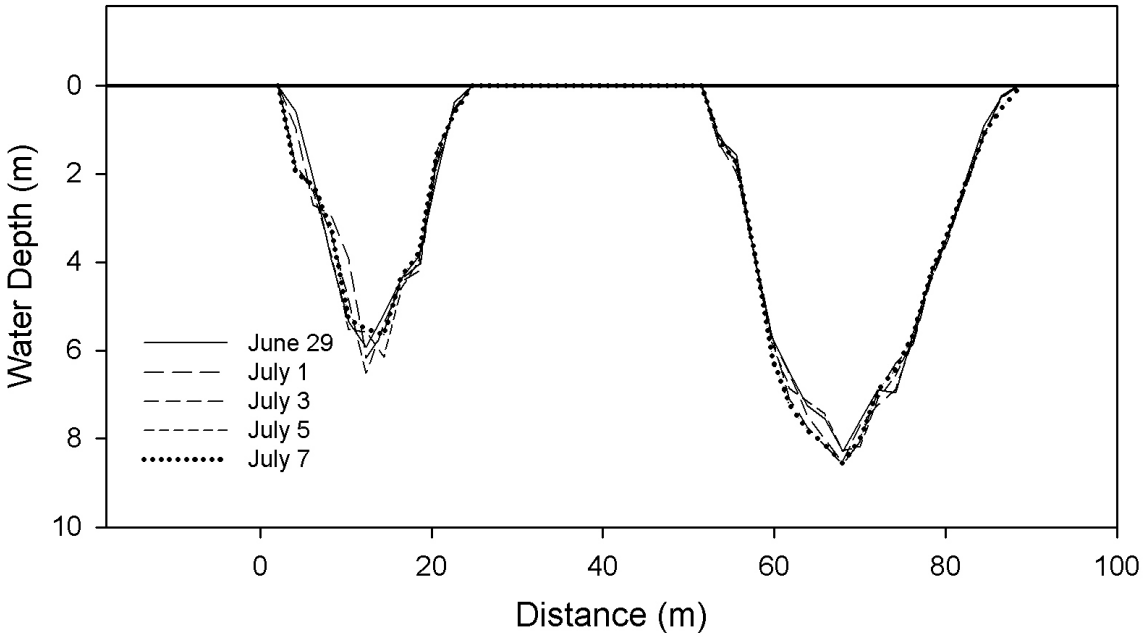

Figure B.1 Depth profiles for a cross-section of the Slims River measured on various dates in 2007 at the river monitoring station normalized to a standard water surface (see Fig. 4.1 for location).

Appendix C

Tilting current meter construction and calibration

Tilting current meters were constructed after Hendricks (1985), but with significant modifications. These tilting meters are potentially useful to measure low to mid velocities (10 to 30 cm s^{-1}). The following report outlines the process of construction and calibration.

C.1 Construction

A Hobo Pendant G logger (accuracy 0.735 m s^{-2}) was secured within a waterproof case using foam pipe insulation. Steel washers were placed inside the waterproof case (4 at the bottom, 1 at the top) to provide neutral buoyancy and to control the current velocity at which the waterproof case begins to tilt. Brass rods were fasted to the waterproof case with a stainless steel hose clamp. Two eye bolts were attached to the top and bottom of a rectangular aluminum frame. Two holes were drilled on either side of the frame, through which the brass rods were fed and loosely secured with nuts. The case was thus able to freely tilt within the rectangular metal frame. Two fins were glued to the waterproof case at an appropriate dihedral angle such that the meter could orient itself into the flow. This apparatus was then fastened to a mooring line in the water column with swivels above and below the frame. The tilt meter in operation in a flume is shown in Fig. C.1.

C.2 Parts list

1. Hobo Pendant G logger (Onset Computer)
2. Hobo Submersible Case, Clear (Onset Computer)
3. 1/8” white ABS plastic
4. Lepage 5 minute epoxy
5. West System 404 high density filler
6. **2** 2” long 3/16” diameter brass rods for pivots threaded with 12NC24 dye except for outer ½”
7. **8** 3/16” stainless steel nuts
    - 24 threads per inch

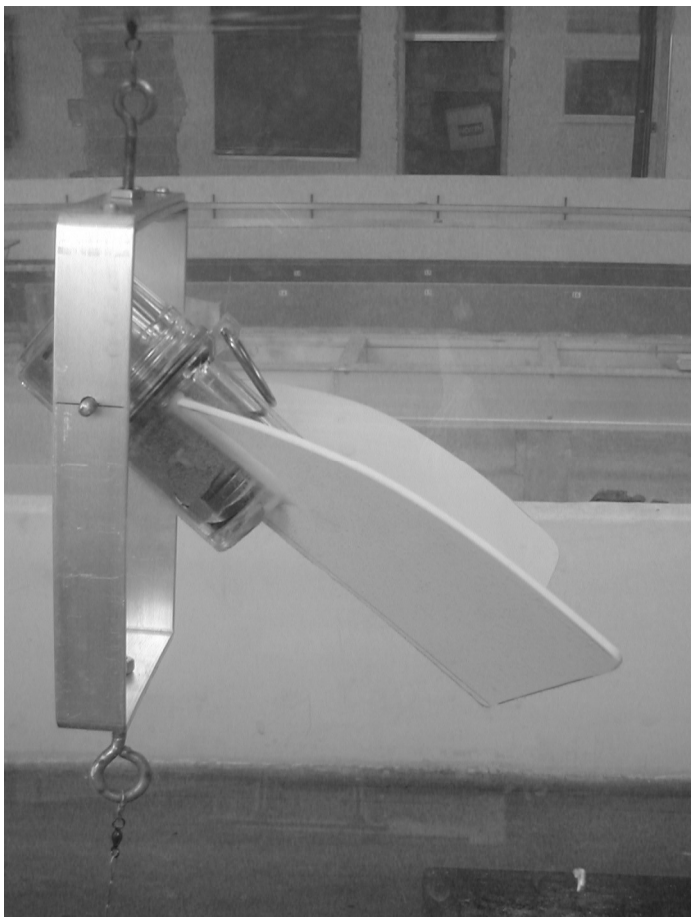

Figure C.1 A tilting current meter in a flume at a flow velocity of approximately 0.15 m s^{-1} (Photograph: R. Gilbert)

8. Stainless Steel hose clamp (61-81 mm diameter)
9. 1 x 1/8 x 30" aluminum for frame
10. **2** stainless steel eye bolts 3/16" diameter
    - 3/8 to ½" diameter eye
    - bolt at least 1" long
11. **4** nuts for eye bolts (3/16" diameter)
12. **5** 5/8" steel washers
    - Outside diameter 1 ¾"
    - Thickness 1/8"
13. 2" long ¾" pipe insulation foam tubing
14. **2** Spro solid ring swivels (ball-bearing)
    - Size 6

C.3 Calibration

The current meters were individually calibrated in a flume to allow the conversion between tilt and velocity. The current meters began to tilt between 0.04 and 0.09 m s^{-1}, reached their maximum tilt (90 to 100°) between 0.35 and 0.4 m s^{-1}, and are most sensitive to variations in velocity (i.e. smallest rate of change of velocity with respect to tilt) between 0.1 and 0.15 m s^{-1}. Using the method of least squares, third degree polynomial regression models were derived for the relationship between tilt and velocity for all current meters (s_{est} =1.90 – 2.45; r^2 = 0.905 – 0.948, $p<0.001$). A third degree polynomial relationship between tilt and velocity is consistent with the theoretical equation derived by Hendricks (1985), as the meter is most sensitive to variations in velocity when it is tilted 45° from vertical.

The calibration curves are generally consistent with each other except for two notable exceptions (Fig. C.2). Differences between calibration curves are not surprising, considering that each current meter was constructed individually by hand. Because of slight difference between calibration curves, individual calibration curves were used to convert tilt values into velocity. A representative calibration curve with 95% confidence intervals is shown in Fig. 4.3.

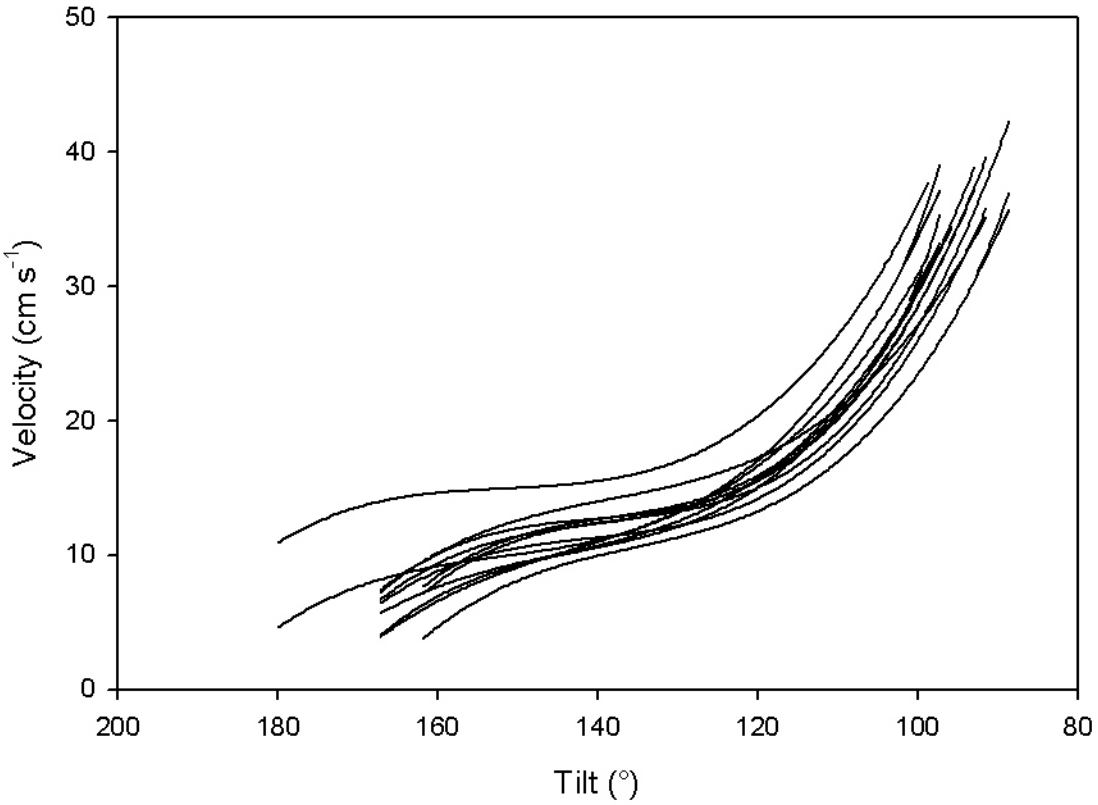

Figure C.2 The calibration curves used to convert tilt values to velocity values for individual tilting current meters.

Appendix D

Plunge line photographs

Figure D.1 Plunge line at Kluane Lake on July 13, 2006 (Photograph: R. Gilbert)

Figure D.2 Plunge line at Kluane Lake on July 13, 2006 (Photograph: R. Gilbert).

Figure D.3 Plunge line at Kluane Lake on July 13, 2006 (Photograph: R. Gilbert).

Figure D.4 Plunge line at Kluane Lake on July 13, 2006 (Photograph: R. Gilbert).

Figure D.5 Ikonos satellite image showing the Slims River delta and the southern end of Kluane Lake on June 27, 2000.

Appendix E

CTD profile results

a) June 30, 2007

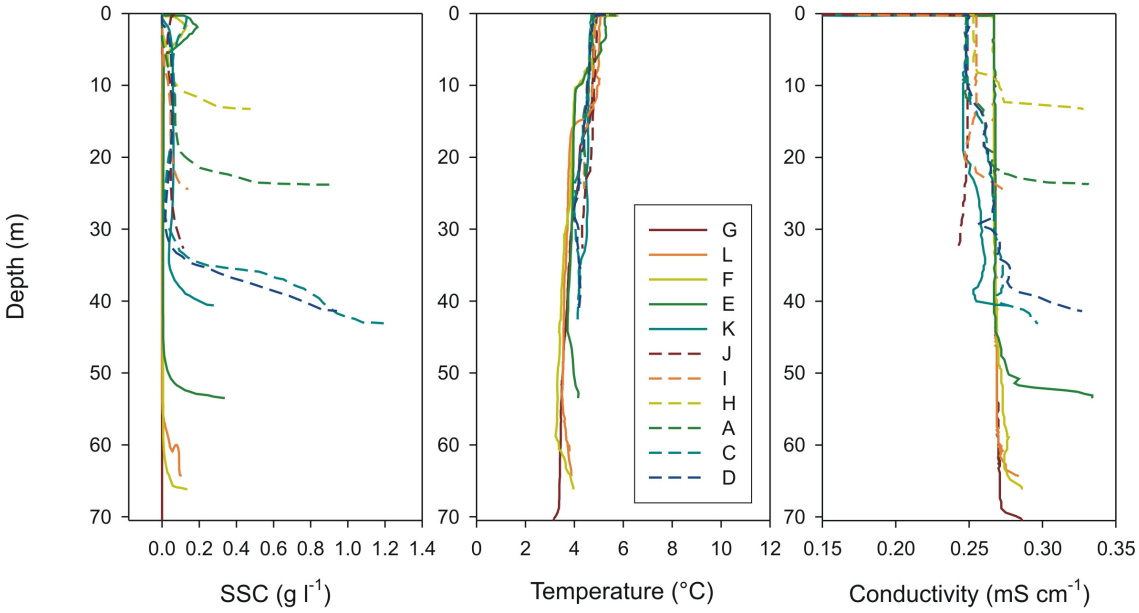

(Figure E.1 continues next page)

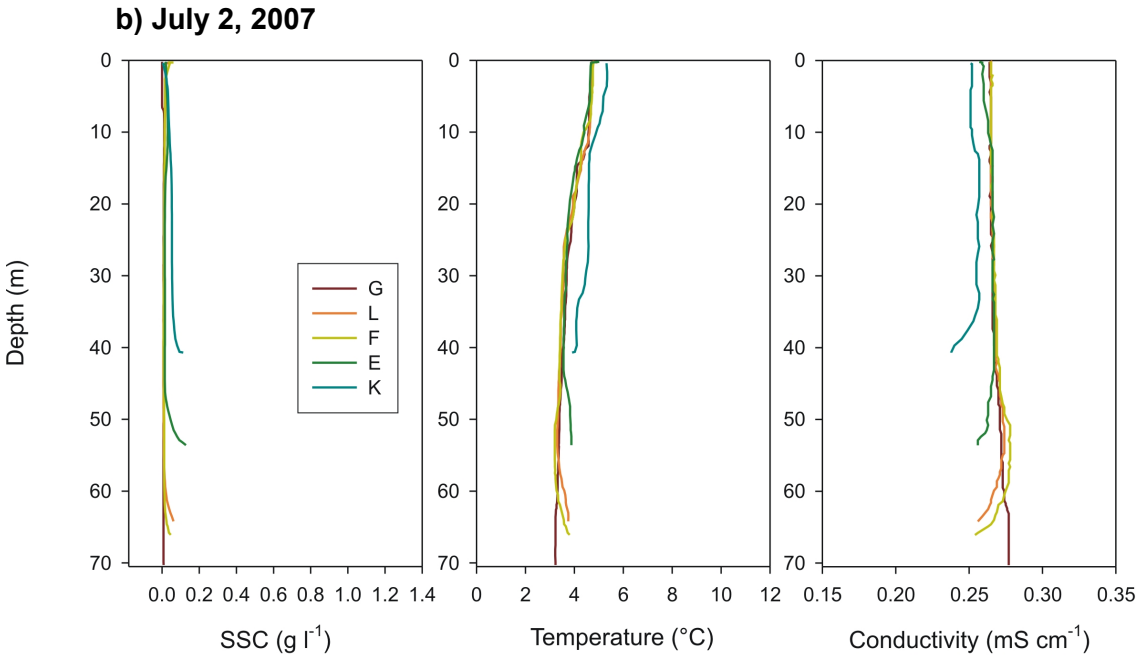

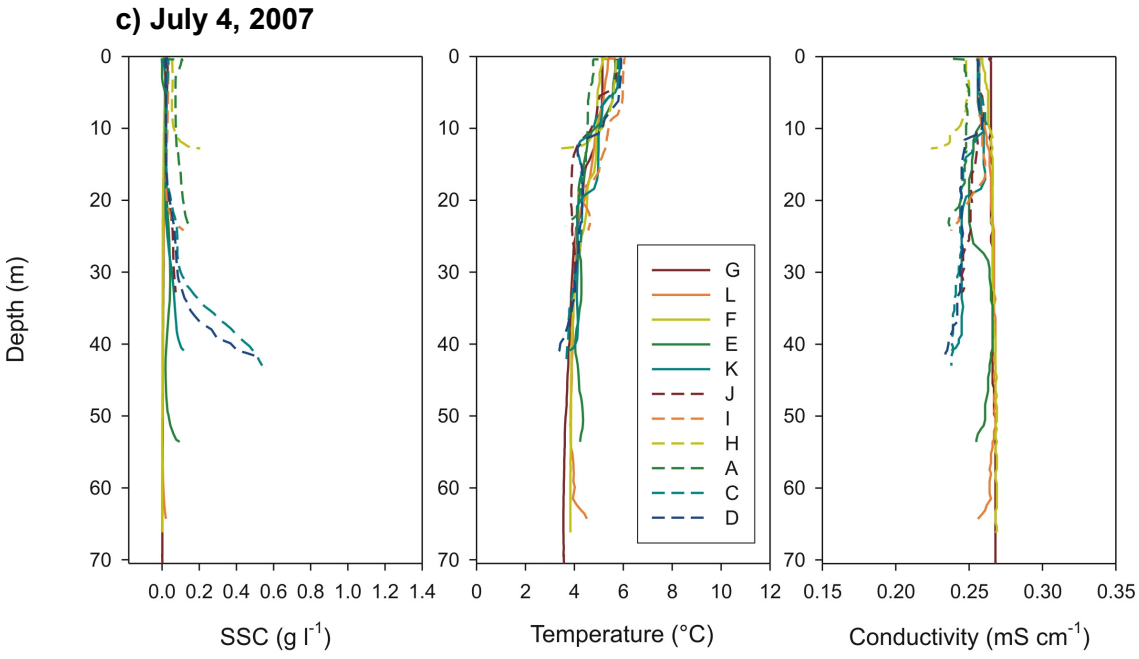

(Figure E.1 continues next page)

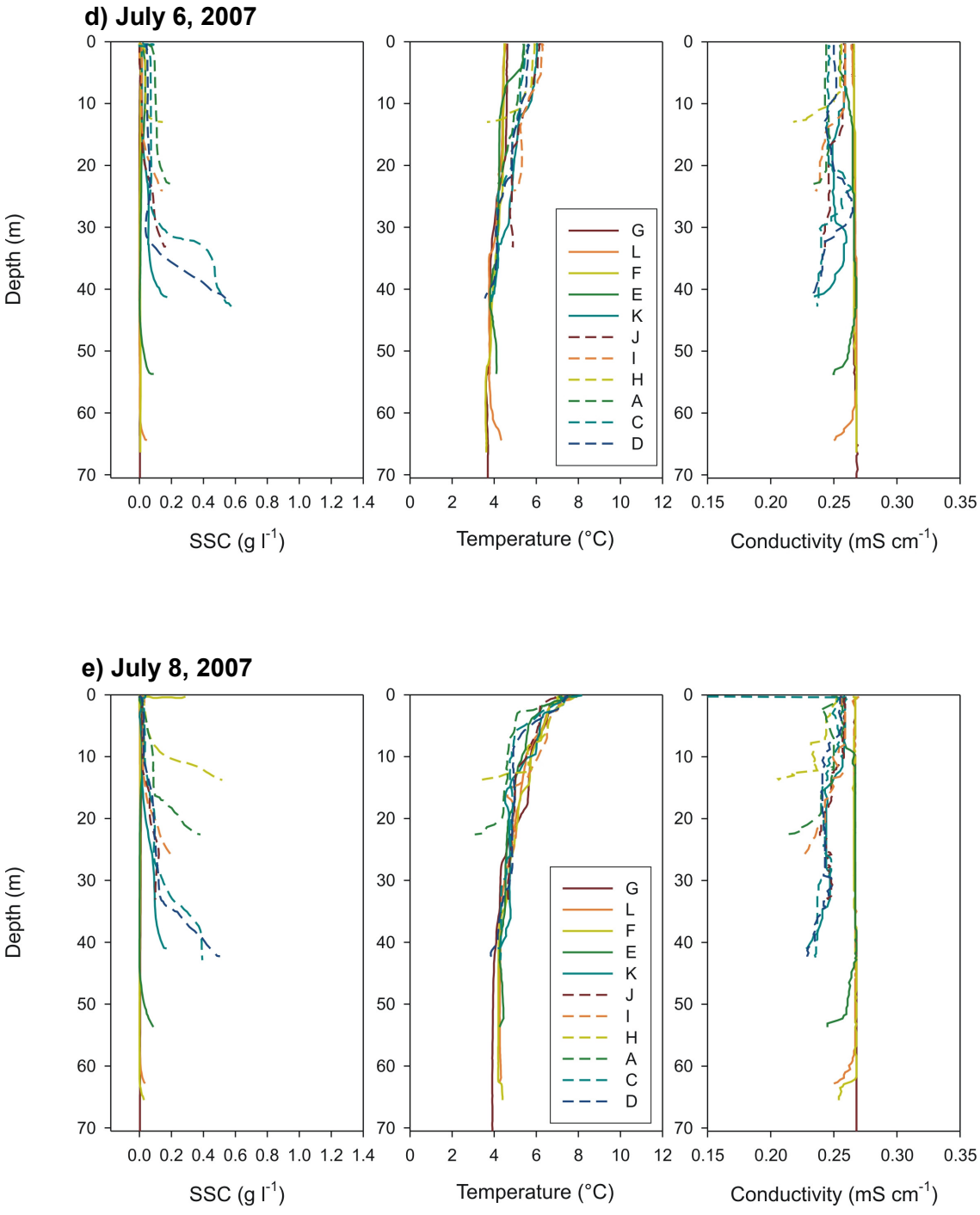

(Figure E.1 continues next page)

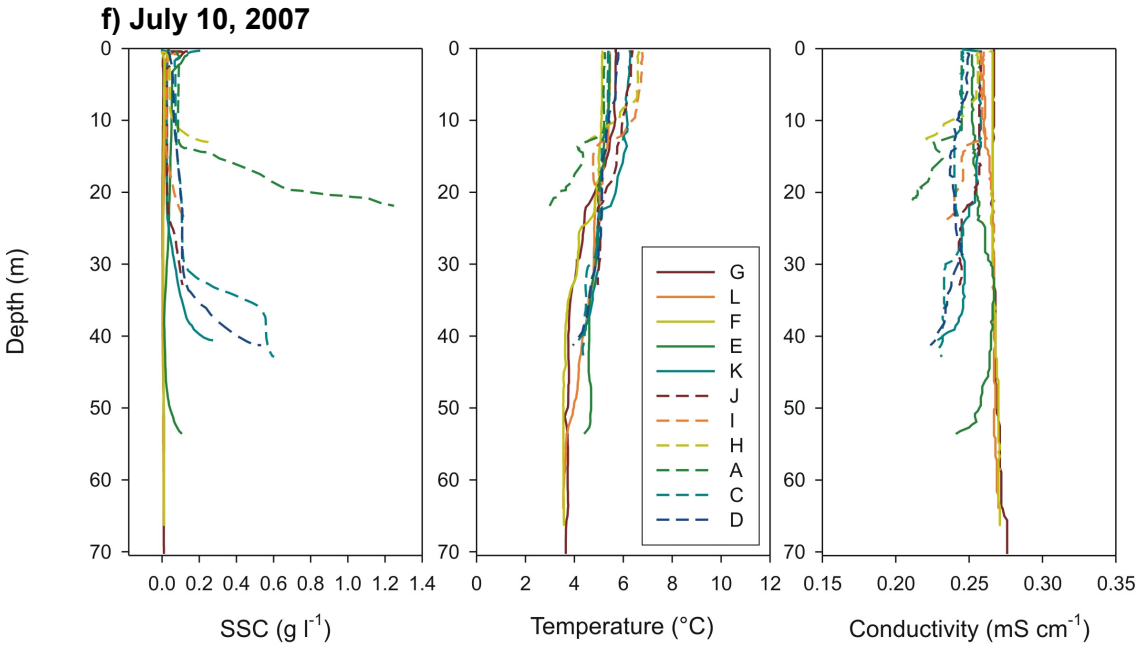

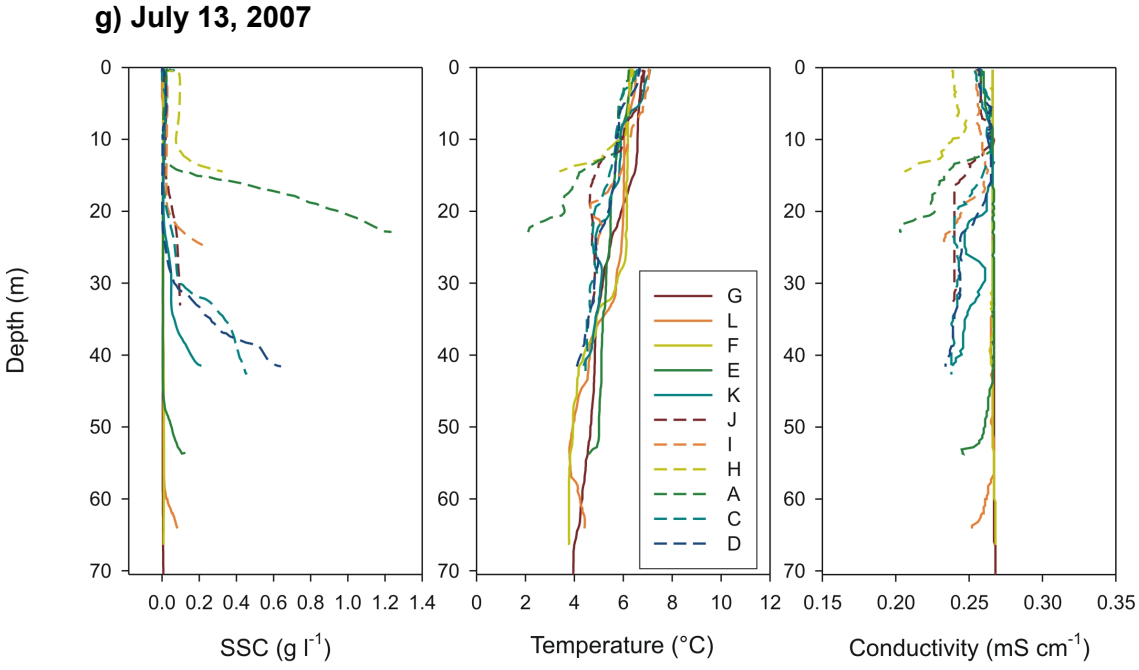

(Figure E.1 continues next page)

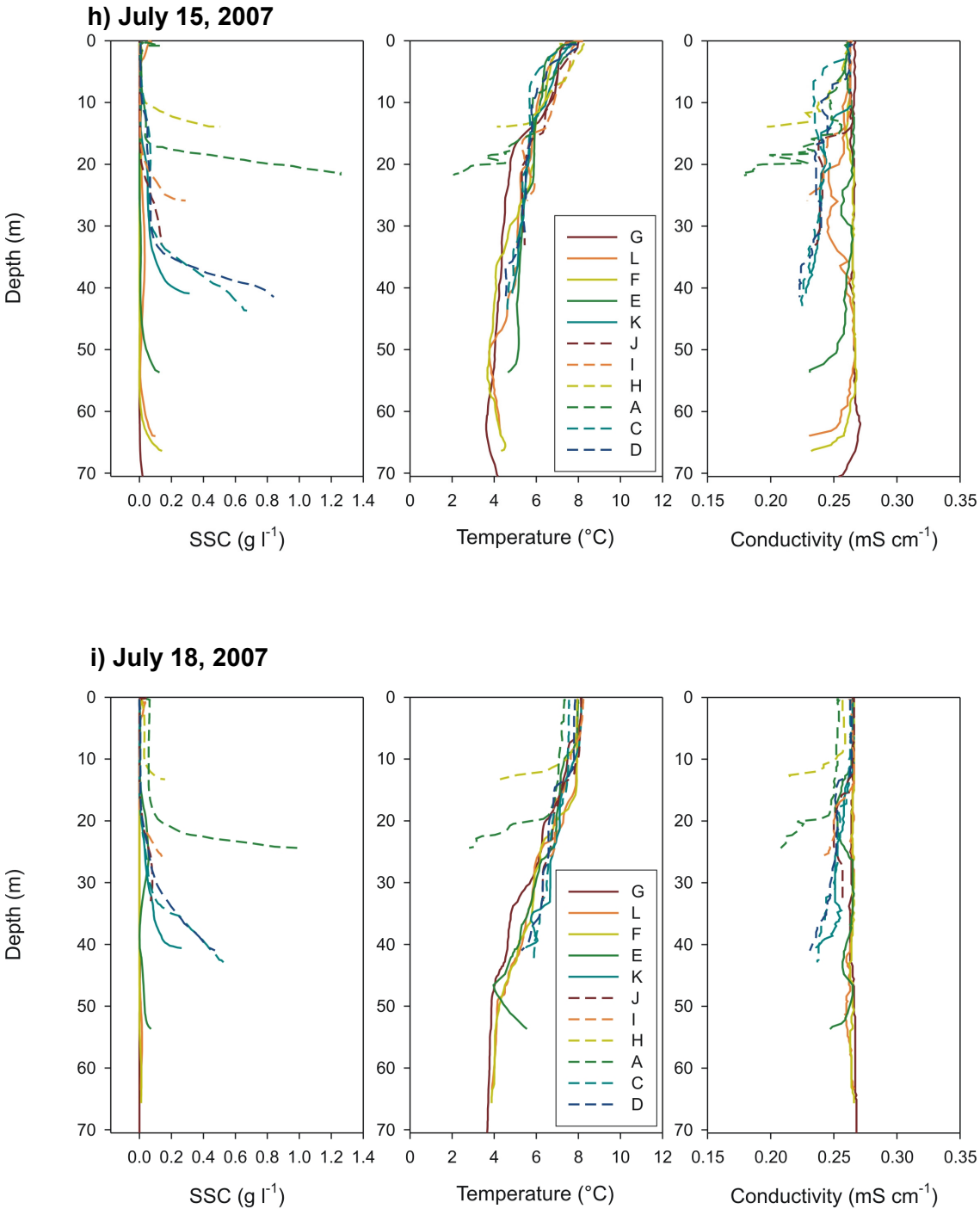

(Figure E.1 continues next page)

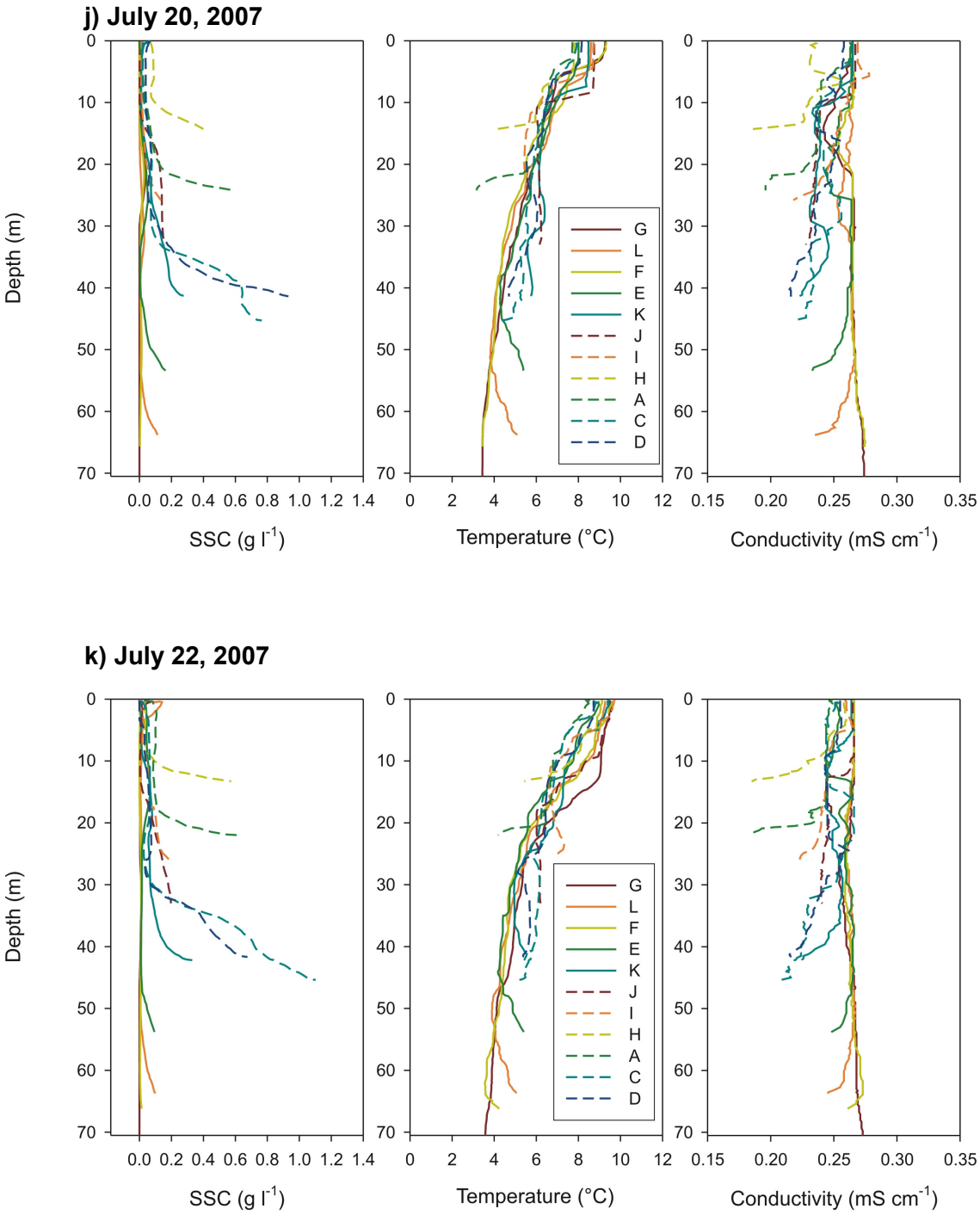

(Figure E.1 continues next page)

l) July 24, 2007

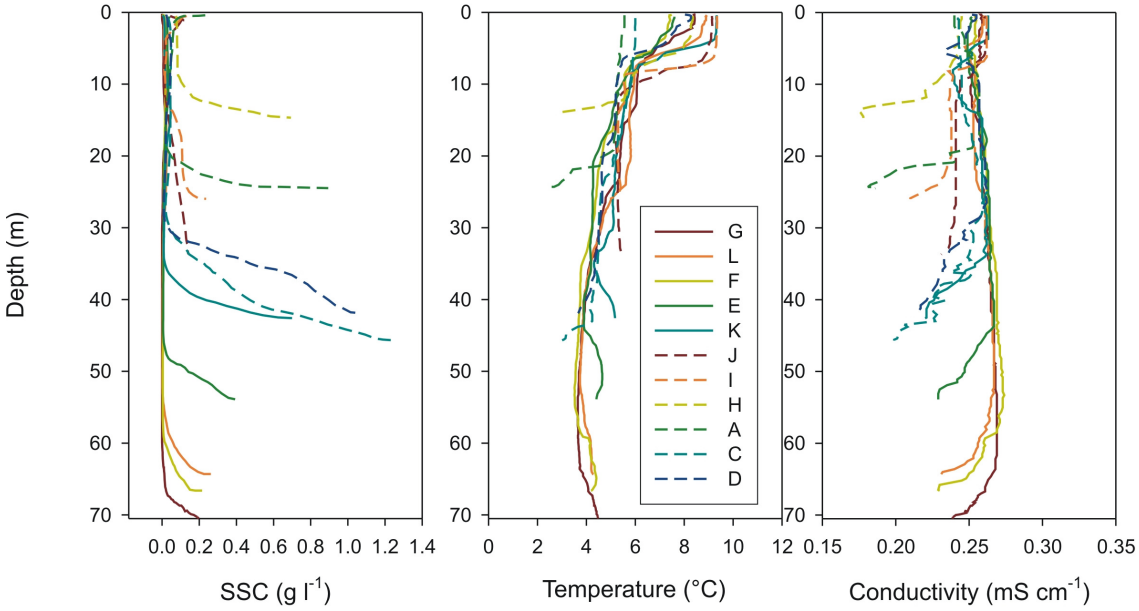

m) July 26, 2007

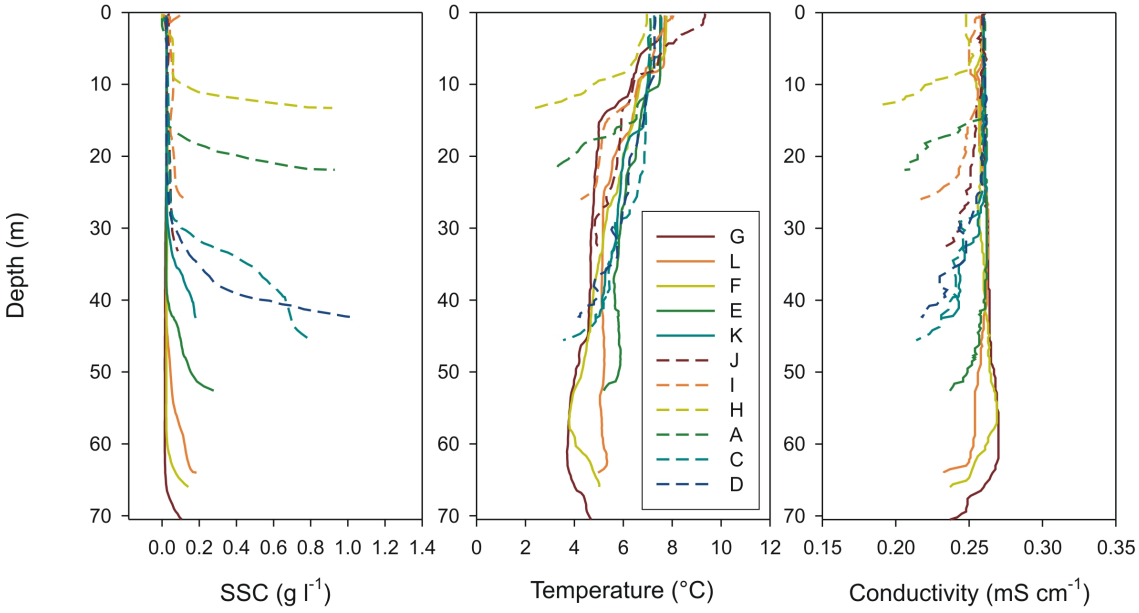

(Figure E.1 continues next page)

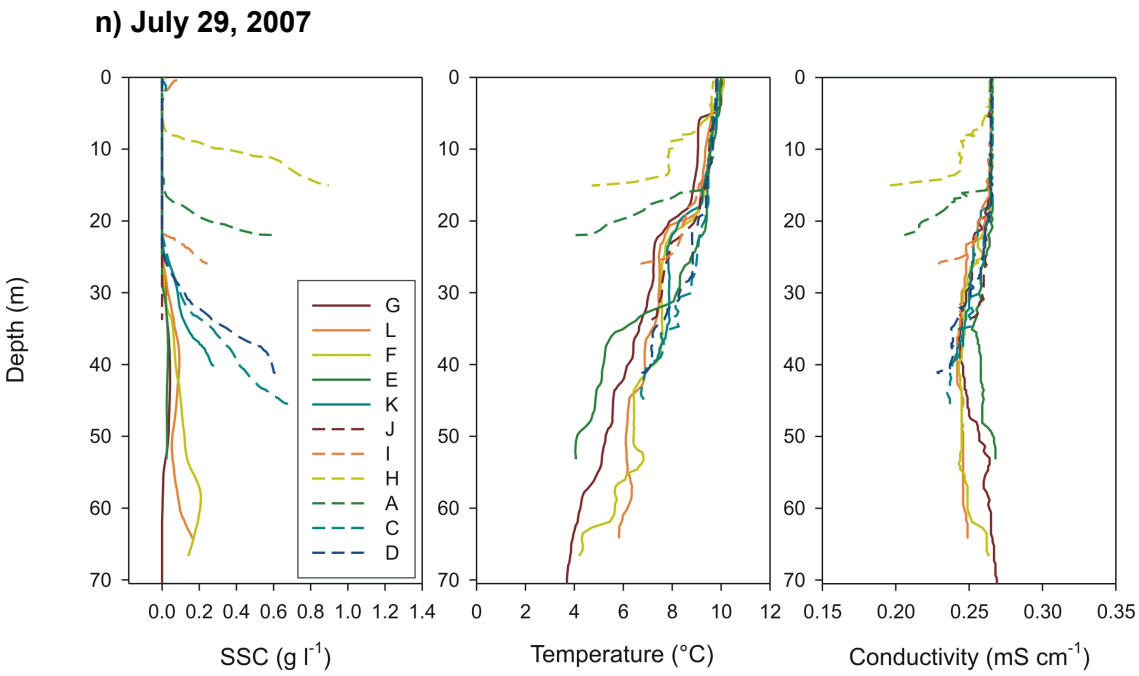

Figure E.1 Vertical profiles of suspended sediment concentration (SSC), temperature, and conductivity on various dates from June 30, 2007 to July 27, 2007 at various moorings (A to G). Mooring locations are shown in Fig. 4.1.

Appendix F

Air and water temperature records

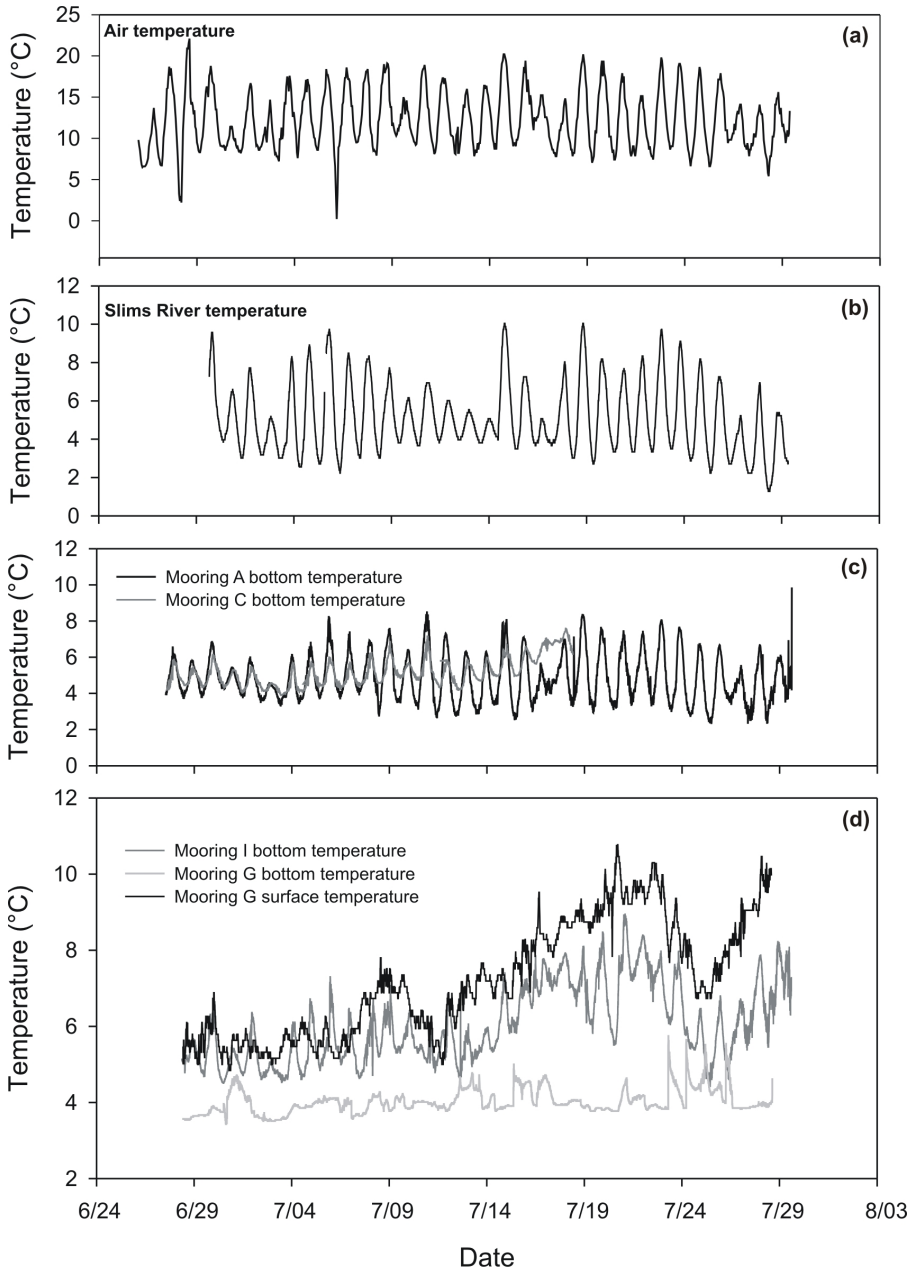

Figure F.1 Air temperature record from the Burwash MSC station (a) and water temperature records for Slims River (b) and various locations in Kluane Lake (c,d) from June 29 to July 29, 2007. For measurement locations see Figs. 3.1 and 4.1.

Appendix G

Froude number calculations

Table G.1 Flow thickness values (in metres) for turbidity currents in Kluane Lake at various locations and times. Zeros indicate times when to turbidity current activity was detected (i.e. no change in vertical suspended sediment concentration profile) and "n/a" indicates times when no data are available. Mooring locations are shown in Fig. 4.1

Mooring	Distance from Delta (km)	June 30 15:30	July 2 10:30	July 4 9:00	July 6 10:30	July 8 12:00	July 10 10:30	July 13 13:00	July 15 12:00	July 18 9:00	July 20 10:00	July 22 15:00	July 24 9:00	July 26 9:00
H	0.4	2.5	n/a	1.5	0.8	3	1.8	1.5	2.2	2.5	2.8	2.8	2.5	2.2
A	0.75	2.2	n/a	1	2.7	4.7	6.5	7	3.8	4	2.8	2.5	1.9	2.5
I	0.8	1.6	n/a	1.7	3.5	5	1.2	3.2	3.9	4.3	3.6	1.1	1	0.5
D	1.2	5.18	n/a	4.8	7	7.2	5.2	5	4	7.7	9.8	10.5	11	13.5
K	1.8	1.8	2	0.5	1.5	2.5	2.2	3.5	1.2	1.7	3.6	4.7	4.8	4.4
E	1.8	1.2	5.5	0.5	1	2.8	1.8	3.5	1.2	1.7	3.6	4.7	4.8	4.4
F	2.9	2.2	3	0	0	1.25	0	0	1.2	0	0	0	3.2	1.5
L	3.1	3.1	2	3	1	1	1.3	0	3.5	1.2 0	0	0	3.2	2
G	4.2	0.8	0	0	3.5	0	0	0	n/a	0	0	0	n/a	0.7

Table G.2 Density values ($\delta\rho/\rho \times 10^{-3}$, where $\delta\rho$ is the density difference between the lake and the turbidity current, and ρ is the density of the ambient water) for turbidity currents in Kluane Lake at various locations and times. Zeros indicate times when no turbidity current activity was detected (i.e. no change in vertical suspended sediment concentration profile) and "n/a" indicates times when no data are available. Mooring locations are shown in Fig. 4.1

Mooring	Distance from Delta (km)	June 30 15:30	July 2 10:30	July 4 9:00	July 6 10:30	July 8 12:00	July 10 10:30	July 13 13:00	July 15 12:00	July 18 9:00	July 20 10:00	July 22 15:00	July 24 9:00	July 26 9:00
H	0.4	0.299	n/a	0.112	0.192	0.345	0.193	0.183	0.410	0.207	0.264	0.417	0.496	0.564
A	0.75	0.470	n/a	0.054	0.067	0.181	0.726	0.758	0.816	0.655	0.398	0.362	0.525	0.480
I	0.8	0.072	n/a	0.082	0.085	0.214	0.110	0.146	0.174	0.132	0.118	0.120	0.149	0.148
D	1.2	0.557	n/a	0.300	0.309	0.290	0.301	0.420	0.497	0.183	0.473	0.408	0.649	0
K	1.8	0.145	0.047	0.068	0.122	0.131	0.189	0.143	0.175	0.230	0.177	0.144	0.425	0
E	1.8	0.21	0.065	0.079	0.056	0.06	0.083	0.106	0.038	0.093	0.084	0.080	0.241	4.4
F	2.9	0.084	0.022	0	0	0.021	0	0	0.112	0	0	0	0.132	0.070
L	3.1	2.4	0.028	0.016	0.028	0.027	0	0.049	0.065	0	0.056	0.063	0.16	0.104
G	4.2	0	0	0	0	0	0	0	0.16	0	0	0	0.131	0.076

Appendix H

Sediment trap photographs

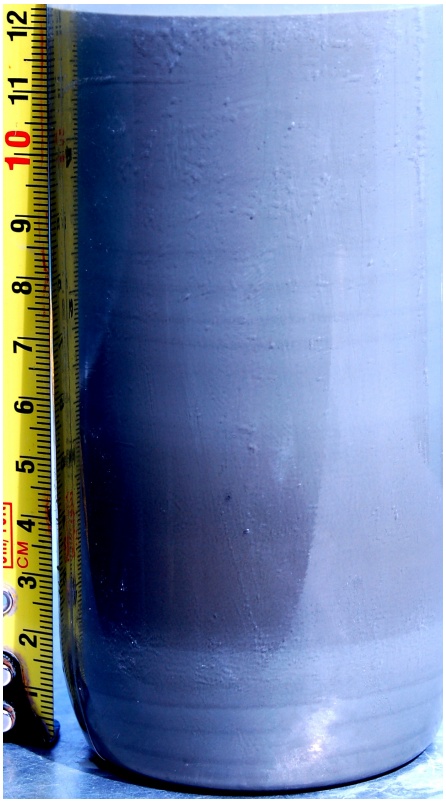

Figure H.1 Photograph of sediment trap immediately after removal from mooring C. Trap was deployed 0.5 m from the lake bottom from June 27 to July 12, 2007. For mooring location see Fig. 4.1.

Figure H.2 Photograph of the partially dried sediment surface showing the vertical sequence of accumulation in a sediment trap deployed 0.5 m off the lake bottom at Mooring A from June 27 to July 8, 2007. For mooring location see Fig. 4.1.

Appendix I

Organic matter content in flood deposit

Table I.1 A comparison of the organic matter content in the flood deposit of June 30 to July 1, 2007 with non-flood material in the sedimentary record

Sample	Organic Matter Content (%)
Flood deposit at mooring C	2.66
Non-flood sediment at mooring C	2.34
Flood deposit at mooring D	1.41
Non-flood sediment at mooring D	1.04